UNIVERSITY OF LIVERPOOL

Iceberg distributions in Greenland's fjords

Thesis submitted in accordance with the requirements of the University of Liverpool for the degree of Doctor in Philosophy

by

Connor James Shiggins

May 2023

Declaration

I declare that this thesis has not been presented for an award at any other university and that the research has been conducted by myself.

Abstract. Iceberg calving is currently responsible for half of the mass loss from Greenland's marine-terminating glaciers and could increase well into the 21st century. While dynamically important for the stability of the Greenland Ice Sheet (GrIS), icebergs also have a major influence on fjord circulation and stratification through melting and the subsequent release of fresh and cold water. The ice-ocean interface remains a difficult to access zone and we consequently know little about iceberg distributions in the near-terminus regions of Greenland's outlet glaciers. This is as a result of few observational studies existing which have sought to derive iceberg observations in the fjords of Greenland. This study utilises cloud computing techniques and digital elevation models (DEMs) to automatically detect icebergs around the GrIS and constrain their distributions to interpret the importance of iceberg sizes on calving and fjord dynamics.

This thesis shows cloud computing is a powerful application to automatically identifying icebergs on large spatial and temporal scales using open access DEMs. The approach has been packaged into a graphical user interface to provide an iceberg detection tool for researchers wanting to derive a dataset of icebergs at Greenland's ice-ocean interface. The utilisation of DEMs allows the derivation of a volume for individual icebergs and has allowed this PhD project to provide comprehensive iceberg area-to-volume convertors for studies working with two-dimensional satellite imagery. Greenland-wide analysis has revealed each sector of the ice sheet calves relatively similar iceberg sizes, with pronounced differences in the larger size classes exceeding 10000 m^3. Currently, it is not possible to derive a direct relationship between iceberg sizes and source glacier bed topography, as well as translating a glacier's solid ice discharge into a predicted iceberg volume size due to data availability. When scaling to the largest marine-terminating glacier on the southwest coast of Greenland, Kangiata Nunaata Sermia (KNS) we find a complex fjord environment where iceberg decay is dominated by melt based processes, rather than fracture. These findings have implications for both remote sensing and modelling studies, and suggest icebergs in this region at the ice front are not necessarily best described as the typically assumed power law, rather lognormal is the best suited distributional fit. Icebergs calved at KNS tend to be small in size, particularly in August (2013 to 2017) when runoff is prominent and subglacial channels form, causing localised plume upwellings and enhanced melting of only a few sections of the ice front. For the first time, this PhD has been able to provide an ice-sheet-wide dataset of three-dimensional iceberg outlines which can be used to constrain and infer glacier calving behaviour and the subsequent implications of iceberg sizes on fjord environments.

Acknowledgements

First and foremost, I must thank my primary supervisor Dr James Lea for his continuing support and guidance. I can safely say without James, this PhD thesis would not have been possible. He has guided me through this PhD with professionalism and I could not be more grateful to have been supervised by him and consumed many, many beers together. I think it would be fair to say that James has made me the glaciologist I am today, and to be quite frank a better person. A secondary, but no less important thanks is to Dr Stephen Brough who has mentored me throughout my PhD before formally becoming a member of my supervisory team. Stephen has provided wisdom, advice and guidance that without which I would not have been able to complete this thesis. Like James, Stephen has made me the person I am and I appreciate all the time and effort spent working with me. Both of my PhD supervisors deserve the upmost credit and I am sure we will spend many more evenings in the pub together.

Special thanks are given to a good friend, Dr David Ashmore, who like James and Stephen provided unquantifiable advice and guidance around my PhD, but also life in general. Our boozy and sometimes rather cynical chats will forever make me smile and I will look back on them fondly. I owe a huge thanks to Dr Dominik Fahrner and Dr Grace Skirrow for their friendship during my PhD. Grace, you consistently made me laugh with our never-ending gossiping sessions and your outlook on life. Dom, your help with coding in the early days has always been hugely appreciated, and your friendship supported me through some of the more challenging times of my PhD.

A note of thanks needs to be made to the PhD researchers and graduate teaching assistants I shared every Thursday with teaching on first year labs over the last four years. All of you made me laugh constantly and I think I now fully understand basic statistics as a result.

My final thanks are for my family. As a first-generation student going to university in 2015, we as a family knew next to nothing about higher education, however my parents always supported me, and without doubt, I would not have finished my undergraduate, never mind my doctorate without them. A special thanks to my grandparents for their ever-continuing support. Finally, thanks to my girlfriend Emma who has supported me throughout my entire PhD and made sure life outside of work was enjoyable and easy.

Table of contents

List of figures

List of Tables

Sometimes, science is more art than science Morty. A lot of people don't get that. Rick Sanchez.

Chapter 1: Thesis introduction

1.0 **Thesis introduction**

Icebergs are a direct product of calving from outlet glaciers and ice shelves around the Greenland Ice Sheet (GrIS). However, little is known about how glaciers loss their mass via solid ice discharge. This is because remotely sensed iceberg observations around the GrIS are both spatially and temporally limited to a few fjord locations. These data have been generated from manual delineations and (semi)-automatic workflows in predominately Sermilik Fjord (south east coast) (Enderlin et al., 2016; Sulak et al., 2017; Moyer et al., 2019) and Disko Bay (west coast) (Enderlin et al., 2016; Sulak et al., 2017; Scheick et al., 2019). However, there are some 285 marine-terminating glaciers which drain the ice sheet that have varying iceberg distributions at the ice front and in the fjord. Consequently, to gain a more comprehensive understanding of iceberg distributions around Greenland, a greater amount of work is needed to generate large datasets of iceberg outlines over vast spatial and temporal scales.

Understanding how iceberg calving will evolve in the future under different climatic and glaciological scenarios is one of the greatest uncertainties the scientific community faces to date (e.g. Choi et al., 2021; IPCC, 2022). Consequently, more iceberg observations around the ice sheet are needed to determine how their parent glaciers are calving and whether this varies spatially and temporally.

Currently, there is a significant lack of iceberg observations derived from satellite imagery at the ice-ocean interface around Greenland and those that do exist are often identified from manual (Crawford et al., 2018) or semi-automated approaches (Sulak et al., 2017; Moyer et al., 2019; Scheick et al., 2019). While useful, these approaches are not practical for large-scale iceberg delineations and are therefore limited through both space and time. The only viable approach for ice sheet wide iceberg detection is through the automation of workflows and algorithms which can identify icebergs with minimal user classification as there are millions of icebergs at any one time in Greenland's fjords.

Semi-automated workflows to date tend to utilise optical imagery (e.g. Landsat 8, Sentinel 2, Planet) and typically involves band thresholding on the panchromatic band (Landsat 8) of the satellite to classify icebergs and open water. This can produce high quality data, however this approach struggles with iceberg delineation at the ice front and within ice mélange (matrix of icebergs and sea ice) because of its similar return signal to that of icebergs. Having these kinds of environmental conditions at an ice front is often common in Greenland's fjords and can limit the automation of all of the imagery being processed.

Icebergs detected on two-dimensional imagery can only express a planform surface area and therefore rely on an empirically derived convertor to calculate a respective total volume (Sulak et al., 2017). Iceberg volume is an important characteristic which can be used to help infer the total freshwater potential from an iceberg. However, to date, there is a gap in knowledge of iceberg volume, with very few direct observations. Thus, while deriving volumes using a convertor is a useful tool, being able to directly calculate volume for each individual iceberg based on the specific dataset (three-dimensions) will result in more representative and accurate values.

The volume of an iceberg is a more robust characteristic than the planform surface area that is derived from optical and synthetic aperture radar imagery (SAR). Iceberg volume is three-dimensional and can be used to infer how much freshwater is contained in an iceberg, which coupled with knowledge of the respective iceberg size distributions is important for understanding fjord dynamics (Enderlin et al., 2016). Therefore, using just the area of an iceberg relies on a convertor to calculate a three-dimensional volume estimate (e.g. Sulak et al., 2017). Numerical iceberg-ocean models (e.g. Davison et al., 2020a; Kajanto et al., 2023) which derive freshwater fluxes from two-dimensional satellite iceberg observations have to convert the area to a volume, potentially resulting in over- and/or under-estimations of the true volume. This in turn impacts the amount of freshwater stored and released in each iceberg as the model input (converted iceberg area to volume) may not be fully accurate once converted.

Iceberg-ocean modelling relies on remote sensing techniques to provide empirically derived observations that are used as input for calculating freshwater release and melt rates. These models are imperative to our understanding of fjord dynamics, revealing how iceberg melting and the subsequent release of freshwater can enhance fjord circulation. These changes in fjord circulation have been shown to force warmer water from the deeper parts of the fjord to an ice front, and in turn, enhance submarine melting (e.g. Davison et al., 2020a). Similar modelling work in Greenland's fjords has shown deeper basin water below the keel depth of the iceberg becomes modified because of the forced mixing of fresh and cold water with more ambient warmer waters from below (Kajanto et al., 2023).

While these fjord models are continually providing important insights into iceberg dynamics, they are spatially limited to one specific location and there remains a lack of research in how future iceberg distributions may evolve from a dynamically changing ice sheet, such as Greenland. Numerical ocean modelling has revealed that during the Last Glacial Maximum,

the drift pattern of icebergs discharged into the North Atlantic varied significantly depending on the size distributions of the icebergs (Fendrock et al., 2022). However, our knowledge of the current iceberg distribution discharge from the GrIS is currently unknown. This also has implications for how freshwater is released from different sections of the ice sheet and how this may impact on sea surface temperatures.

Researching Greenland's icebergs is not just of interest to glaciologists, rather the application of such research has multiple implications for stakeholders, including those involved with maritime shipping, infrastructure and coastal communities. The risks posed to shipping and settlements from icebergs are rarely seen today, however considerations regarding their mitigation will become at the forefront of Arctic logistics and livelihoods in the near-future with the (in)stability of the GrIS in question.

1.1 **Research aim and objectives**

The aim of this thesis is to identify the controls on iceberg size distributions across space and time.

This will be achieved through four main objectives, namely:

1) *Generating automated workflows to detect icebergs using cloud computing and open-access digital elevation models (DEMs).* This will be achieved through gauging the feasibility of identifying icebergs from time-evolving ArcticDEM strips and fully automating and validating iceberg detection in Google Earth Engine (GEE).

2) *Packaging the workflow into a graphical user interface (GUI) to provide an open-access tool for the iceberg/glaciological community to derive their own iceberg datasets.* This will be achieved through developing an intuitive, automated user interface that can be executed quickly by users for a region of interest (ROI). Detailed and accessible documentation will also be developed to enable this.

3) *Adapt and apply this workflow to all the marine-terminating glaciers in Greenland to gain understanding of iceberg distributions at an ice-sheet scale.* This will be achieved through modifying the workflow (as used in objectives 1 and 2) to remove the reliance on a user defined ROI. This will allow full automation and upscaling of the pipeline, to enable insight into spatiotemporal variability of calving dynamics at an ice sheet scale.

4) *Explore glacier-specific, seasonal iceberg distribution variability and potential controls.* This will be achieved through applying the workflow (as presented in

objective 3) at Kangiata Nunaata Sermia (KNS) and statistically comparing different distributions (power law and lognormal) to describe iceberg sizes proceeding the terminus. These results will also be explored within the context of potential environmental controls on calving.

1.2 **COVID-19 pandemic and project adaption**

The COVID-19 pandemic changed the entire scope of this PhD project as there was no intention to focus on deriving iceberg observations using remote sensing techniques. Rather, the project had originally planned to adapt a two-dimensional numerical salt marsh model developed by Professor Nicoletta Leonardi at the University of Liverpool into a marine-terminating glacier model containing self-organised criticality (e.g. stochastic), a phenomenon exerted by iceberg calving. Once converted into a full iceberg calving model, the project would use in-situ observations from a time-lapse camera at Narsap Sermia (southwest Greenland) to validate the simulations from real-world calving events. The time-lapse camera at the glacier was already in-situ acquiring data from a previous PhD project led by Dr Dominik Fahrner and the supervisory team.

However, it was agreed in May of 2020 with the pandemic worsening and restrictions taking a tighter grasp on society, the development of the numerical model with remote working was going to pose as a significant boundary for project development and a shift to a new research focus would be beneficial. It was at this time discussions began about experimenting with the feasibility of using open access DEMs (ArcticDEM v3 strip data) to detect icebergs within GEE as it provided the option for easy code/script sharing because of its cloud computing nature and thus accessibility for remote working.

While project migration is indicative of a PhD project, the magnitude of this change was not trivial. Despite this change, the resultant project has developed new approaches to the remote sensing of icebergs and has provided a progressive step forward in the iceberg community. The data generated from the automated workflows have varying applications not just for remote sensing studies, but as well for different numerical models in glaciology, such as input and output validation for iceberg calving models and freshwater/melt flux models (e.g. Davison et al., 2020a). As a result, this thesis provides a framework for showing both the scalability and benefit of utilising cloud computing for iceberg detection at an ice sheet scale.

1.3 **Thesis structure**

This thesis is structured into eight Chapters, with Chapters 1 to 3 providing introductory information and a background into Greenland's outlets and icebergs. Chapters 4 to 6 represent the research Chapters and Chapters 7 to 8 synthesise, discuss and conclude the thesis. The research Chapters (4-6) are formatted as research publications which have either been published or are in preparation to be submitted for journal publication.

Chapter 1 provides a brief introduction and rationale for the PhD project, the thesis aim and objectives, and the impact of the COVID-19 pandemic and subsequent project mitigation.

Chapter 2 provides contextual information regarding the importance of the GrIS for both science and society and how the outlet glaciers which drain it are sensitive to changing environmental parameters. The second segment of this Chapter provides an in-depth review of iceberg science, particularly the remote sensing of iceberg distributions and how icebergs are important for both contemporary and paleo-science, as well as their societal implications.

Chapter 3 discusses the capabilities and potential of both GEE and ArcticDEM. A detailed explanation is also included in this Chapter of how ArcticDEM is constructed and its subsequent advantages and disadvantages in some cases.

Chapter 4 is the first results paper of this PhD thesis and is published in *The Cryosphere*. The research presented here provided the framework for the remainder of the project which developed and validated an automated iceberg detection workflow built in GEE using ArcticDEM v3 strip data. This Chapter later applies the workflow to three marine-terminating glaciers, detecting a total of 163738 icebergs to quantify the success of the approach and infer iceberg distributions in each of the glacier's fjords.

Chapter 5 builds on the fundamental workflow presented in the fourth Chapter by removing the manual aspect of the code (i.e. ROI delineation) to fully automate the approach and allow the upscaling of iceberg detection across the GrIS. This updated pipeline generated a dataset of 1.3 million icebergs from 133 outlet glaciers which was used to infer the probability of iceberg sizes around Greenland.

Chapter 6 later focusses on KNS' iceberg distributions in detail for the months of August, September and October between 2013 and 2017. These results allowed the discussion of whether power law distributions are the best descriptor of icebergs in the near-terminus region

of KNS and how the total iceberg count and size decrease in August of each year when subglacial runoff is close to its peak.

Chapter 7 brings Chapters 4 to 6 into glaciological context, as well as discussing the significance of their findings for the scientific iceberg community. In detail, this Chapter provides information on how the PhD project has been able to contribute to the data gaps as outlined by Chapter 3. Further, recommendations are made for the future scope of the remote sensing of icebergs, but also developments for the iceberg detection presented in this thesis.

Chapter 8 summarises and outlines the key findings of the thesis and how it has contributed to the iceberg community.

Chapter 2: Introduction to Greenland's tidewater glaciers and icebergs

2.0 **Introduction**

The aims of this Chapter are to:

1) Highlight the dynamic nature of Greenland's marine-terminating glaciers and how they are sensitive to boundary conditions.

2) Deliver an in-depth review of iceberg dynamics and distributions which will yield clear and concise research avenues needed to advance iceberg science.

The second aim of this Chapter is especially timely as current review papers have discussed both iceberg calving (e.g., Benn and Åström, 2018) and Greenland's marine-terminating glaciers (e.g., Catania et al., 2020), providing clear research requirements for these research topics, however no similar review exists for iceberg science. Such a review is needed as large uncertainties still exist with regards to both glacier-iceberg and ocean-iceberg dynamics. Consequently, these unknowns raise serious questions and uncertainties regarding the future evolution and (in)stability of Greenland's outlet glaciers, and subsequent changes in their fjords.

Since the late 20th century, the Arctic has warmed twice as fast when compared to the global average, often referred to as Polar amplification (Holland and Bitz, 2003; Stuecker et al., 2018). The GrIS, situated in the Arctic has a total ice volume of 2.74 ± 0.02 10^6 gigatons (Gt), equivalent to 7.42 ± 0.05 m of sea level rise (Morlighem et al., 2017). Between 1982 and 2018, the ice sheet lost 3800 ± 339 billion tonnes of ice, making it the single largest contributor to sea level rise globally (Figure 3.1) (The IMBIE Team 2020). The ice is drained through 285 tidewater glacier calving margins (Bjørk et al., 2015) which terminate into the ocean and account for up to 66% of the mass loss from the ice sheet, resulting in a 9 mm increase in sea level, half of which has occurred since 2011 (Mouginot et al., 2019). These glaciers have experienced widespread retreat since the mid-1990's and has continued well into the 21st century due to pronounced increases in air and ocean temperatures (King et al., 2020; Fahrner et al., 2021). Around 50% (550 Gt) of the total mass loss from the GrIS is through iceberg calving (Enderlin et al., 2014) and by 2100, this figure could increase by 22% to 70% (Choi et al., 2021), however this process is currently poorly constrained and large uncertainties exist.

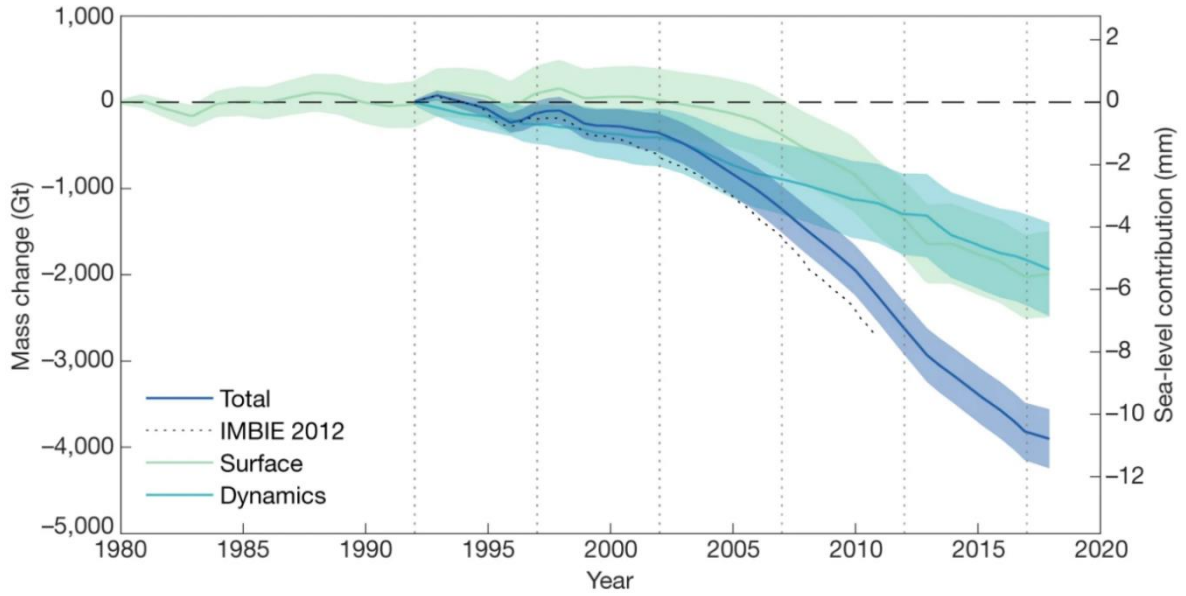

Figure 2.1. Total mass change from the GrIS which is categorised via surface mass balance and iceberg calving with the respective contribution to sea level (mm). The vertical dotted lines represent five-year intervals from when data collection started in 1992 (from The IMBIE Team, 2020).

2.1 **The controls on Greenland's marine-terminating glaciers**

2.1.1 External forcing

The mass balance of an ice sheet is the difference between total mass gain (e.g., rain, snowfall) and total mass loss (e.g., surface melt, iceberg calving). An ice sheet's surface mass balance (SMB) is slightly different which considers the difference between accumulation (e.g., rain, snowfall) and surface melt (e.g., runoff) and does not consider frontal ablation (i.e. calving and submarine melt) in the terminology. SMB is in equilibrium when there is exactly the same amount of snowfall accumulation (typically in winter) and surface melt (typically in summer) (Figure 3.2). However, on the GrIS, surface melt has been fast outweighing accumulation due to increasing summer temperatures, resulting in a SMB decrease of 10.2 ± 2.3 Gt yr^{-2} (van den Broeke et al., 2016). Greenland's marine-terminating glaciers over the last 20-years have shown significant susceptibly to both increasing air and ocean temperatures (e.g. Fahrner et al., 2021). For example, the synchronous retreat of Greenland's southeast tidewater glaciers has been determined to be as a result of both atmospheric and oceanic forcing (Seale et al., 2011; Brough et al., 2023). More broadly, Fahrner et al. (2021) analysed 3801 ice margins from 224 tidewater glaciers, showing retreat across the GrIS is regionally linear with the northwest and southeast sectors being particularly sensitive to annual sea surface temperatures and June-July-August air temperatures.

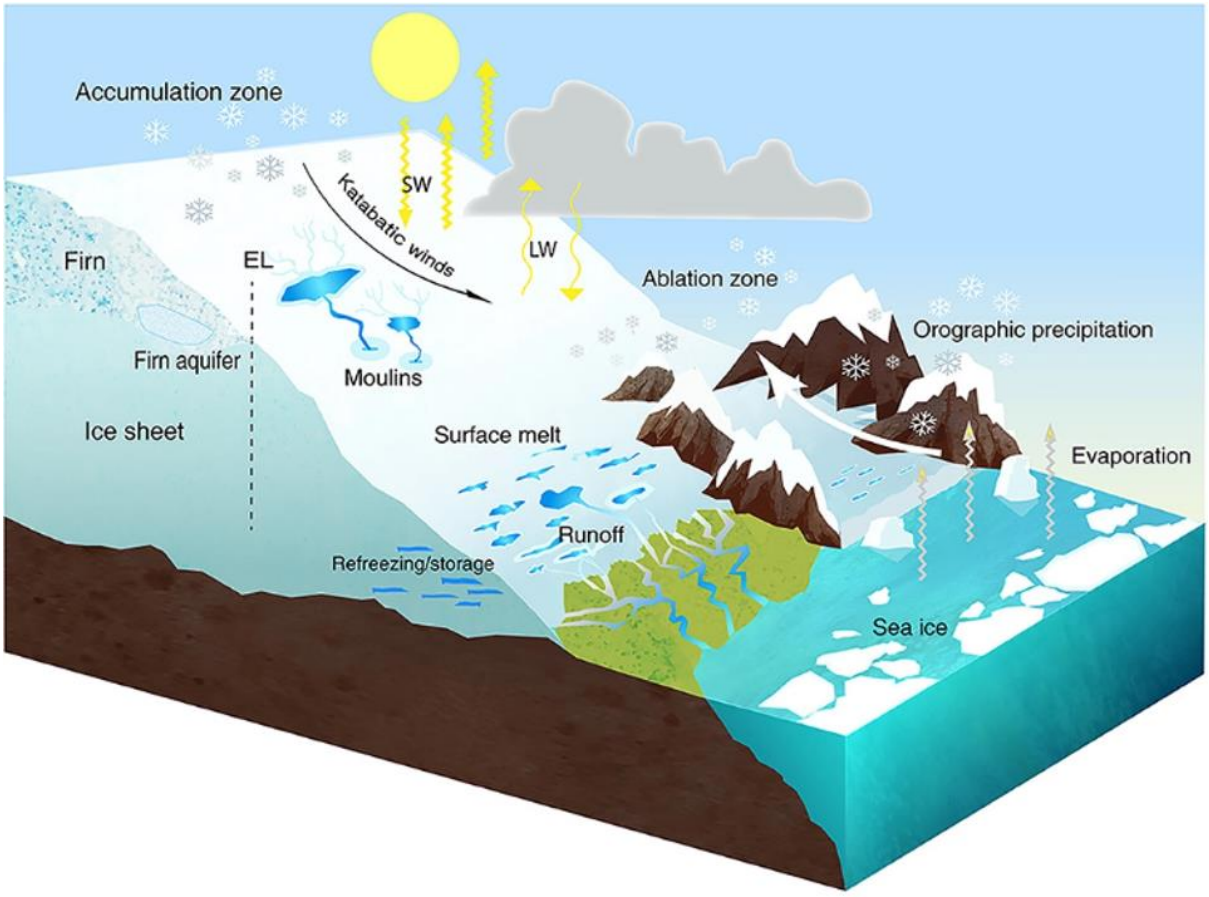

Figure 2.2. Schematic diagram of the surface mass balance dynamics of a typical marine-terminating glacier draining the GrIS (from Lenaerts et al., 2019).

Recent anthropogenic warming since the mid-1990s has shown a step change in exacerbated glacier retreat (King et al., 2020). In 2012, remotely sensed observations revealed up to 98.6% of the GrIS experienced melt, including normally unaffected regions (e.g. higher altitudes) because of a warm ridge of air that stagnated and acted as a heat dome (Nghiem et al., 2012). This system was present in the mid-troposphere over Greenland and has been linked with changes in the summer North Atlantic Oscillation (NAO) and the polar jet stream that encouraged warmer air to be advected along the western coast of the ice sheet (Hanna et al., 2014). Longer, decadal processes may have also contributed to the extreme melt event in 2012, such as the North American drought which was the most extreme since 1895, also coinciding with similar events in Greenland associated with biomass burning (Neff et al., 2014). A continuation of a negative NAO in the 2000s has enhanced melting across the ice sheet through three components: 1) advection of warm air down the western coast, 2) clear sky conditions through high surface pressure and 3) declining summer snowfall, allowing a darker ice sheet surface and thus enhancing melt (Box et al., 2012). Increased surface melt can reach the ice sheet bed through surface pathways (e.g. moulins) and contribute to increased subglacial water

pressure which can influence ice dynamics (see section 2.1.3). Consequently, larger atmospheric systems which influence how the ice sheet melts will fundamentally influence downstream dynamics and calving at the ice-ocean interface.

The modelled reconstruction of submarine melting between 1979 and 2018 has shown that without atmospheric warming, the retreat and dynamic loss from Greenland's outlets would have been suppressed by a third, and even up to half in the northern sector of the ice sheet (Slater and Straneo, 2022). These findings suggest that while ocean temperatures have an annual force on the glacier termini, the first order control on submarine melt rates come from above the ice, in the form of atmospheric warming (Slater and Straneo, 2022; see section 2.1.3).

While submarine melt rates appear to be primarily influenced by atmospheric forcing, persistently warm ocean temperatures can have major implications at the ice front. Atlantic Water (AW) is present in many of Greenland's fjords and has the capabilities of significantly altering a glacier's terminus through submarine melting because of its warmer continental shelf origin (Figure 3.3) (Straneo et al., 2012). For example, glaciers north of 69^{o}N on the east coast remained stable during the 2001 to 2005 synchronous rapid retreat of the southeast glaciers because their fjords are less exposed to the inflow of subtropical, warmer waters (Seale et al., 2011; Brough et al., 2023). Similarly, 35 of 37 analysed glaciers in northwest Greenland retreated significantly between 1985 and 2015 because of ocean warming below 200-m and the two glaciers which remained stable were grounded on shallow sills in colder water (Wood et al., 2018). Thus, the above highlights the significant role of ice-ocean interactions and how atmospheric and submarine forcing can alter glacier dynamics.

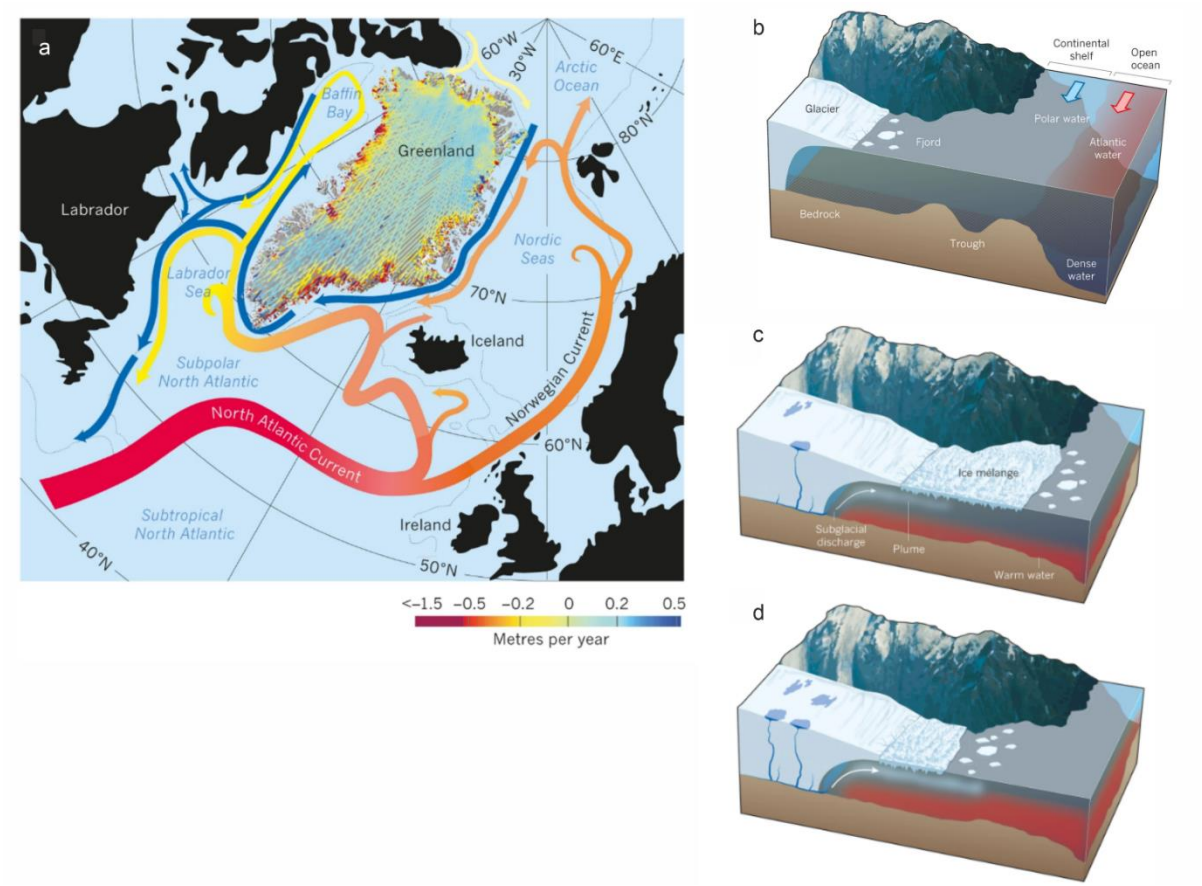

Figure 2.3. a) Schematic of ocean circulation around the GrIS with AW origin shown in reds to yellow and AW trajectories shown in blue, b) schematic of fjord dynamics and how AW can infiltrate into fjords at depth once the continental shelf has been surpassed, c) schematic of how AW may manoeuvre within the fjord with a thick and rigid mélange, whereas d) shows how AW may have an increased presence and influence in retreated conditions with increased subglacial discharge and a weaker mélange (modified from Straneo and Heimbach, 2013).

Warm, AW has also been shown to contribute to the retreat of the Disko and Uummmannaq palaeo-ice streams after the last glacial maximum (ca. 16.2 cal ka BP, ca. 17.1 cal ka BP, respectively) (Jennings et al., 2017). The influence of ocean forcing continues into the present day and model forecasts suggest they can trigger the destabilisation of a glacier and result in a potentially catastrophic ice frontal retreat, depending on the bed topography (Morlighem et al., 2016). The terminus of Sermeq Kujalleq (also known as Jakobshavn Isbræ) is at present in close proximity to its Holocene minimum position and one of the ways to allow the ice front advance in the future is through a substantial cooling in fjord waters (Khazendar et al., 2019) which could endure longer than the Little Ice Age (~300 years) (Kajanto et al., 2020).

2.1.2 Bed topography

The morphology underlaying the GrIS and its outlet glaciers are a key control for velocity, iceberg calving and the grounding line position. Furthermore, different water bodies, some of which contain warmer water (e.g. AW; Section 2.1.1) will be able to reach and undercut greater

regions of glacier termini depending on the fjord geometry (e.g. Porter et al., 2014). However, basal topography is notoriously difficult to access, meaning datasets can still be relatively data poor and large uncertainties exist, e.g. BedMachine (Morlighem et al., 2017).

Subglacial bed topography can act as a fundamental stabiliser to a glacier through sills and ridges which can halt grounding lines in-case of rapid-retreat (Schoof, 2007; Nick et al., 2009; Durand et al., 2011). Likewise, deeply grounded glaciers which have no 'pinning points' (e.g. sills) and/or continue to be positioned upon deeper bedrock on reverse bed slopes when undergoing retreat can contribute directly to the processes of both marine ice sheet instability (MISI) and marine ice cliff instability (MICI) (Figure 2.4) (DeConto and Pollard, 2016). These two concepts are more concerned with the stability of the Antarctic ice sheets and shelves; however, they have relevance to Greenland. The main premise of both instabilities is when a grounding line (i.e. where a glacier becomes buoyant) becomes positioned in a subglacial basin with a reverse bed slope (i.e. one that deepens moving inland), the glacier cannot stabilise and the grounding line position becomes deeper causing further instability (Durand et al., 2011). Subsequently for MICI, the ice cliff above the water line becomes unstable and begins to collapse, resulting in a runaway retreat until the ice margin can be stabilised further upstream on a shallower bed and/or pinning point. This concept has been shown to potentially occur at the well-known glacier, Thwaites in West Antarctica (Rignot et al., 2014; Seroussi et al., 2017).

Between 2000 and 2015, 99% of glaciers on the northwest coast and 96% on the southeast cost of Greenland retreated, with glaciers which retreated more than 200 m a^{-1} being situated on reverse bed slopes (Bunce et al., 2018). Glaciers which are grounded and continue to retreat onto deeper basal topography will result in a reduction of basal stress and encourage dynamic thinning (Hill et al., 2018). Numerical modelling results at Store Glacier suggest while ocean forcing may trigger a grounding line positional retreat, the bed topography will dictate the magnitude of retreat, in this case, the only way of stabilising the terminus is 27 km upstream where it will become land-terminating (Morlighem et al., 2016). Recent work has suggested two future scenarios for marine-terminating glaciers which are grounded on the most elevated (less deep) part of their bed: 1) they continue at the peak of their bed indefinitely, prolonging changes in the local climate or 2) they remain at their peak and continue to lose mass directly related to the local climate and result in rapid retreat once the terminus surpasses the peak (Robel et al., 2022).

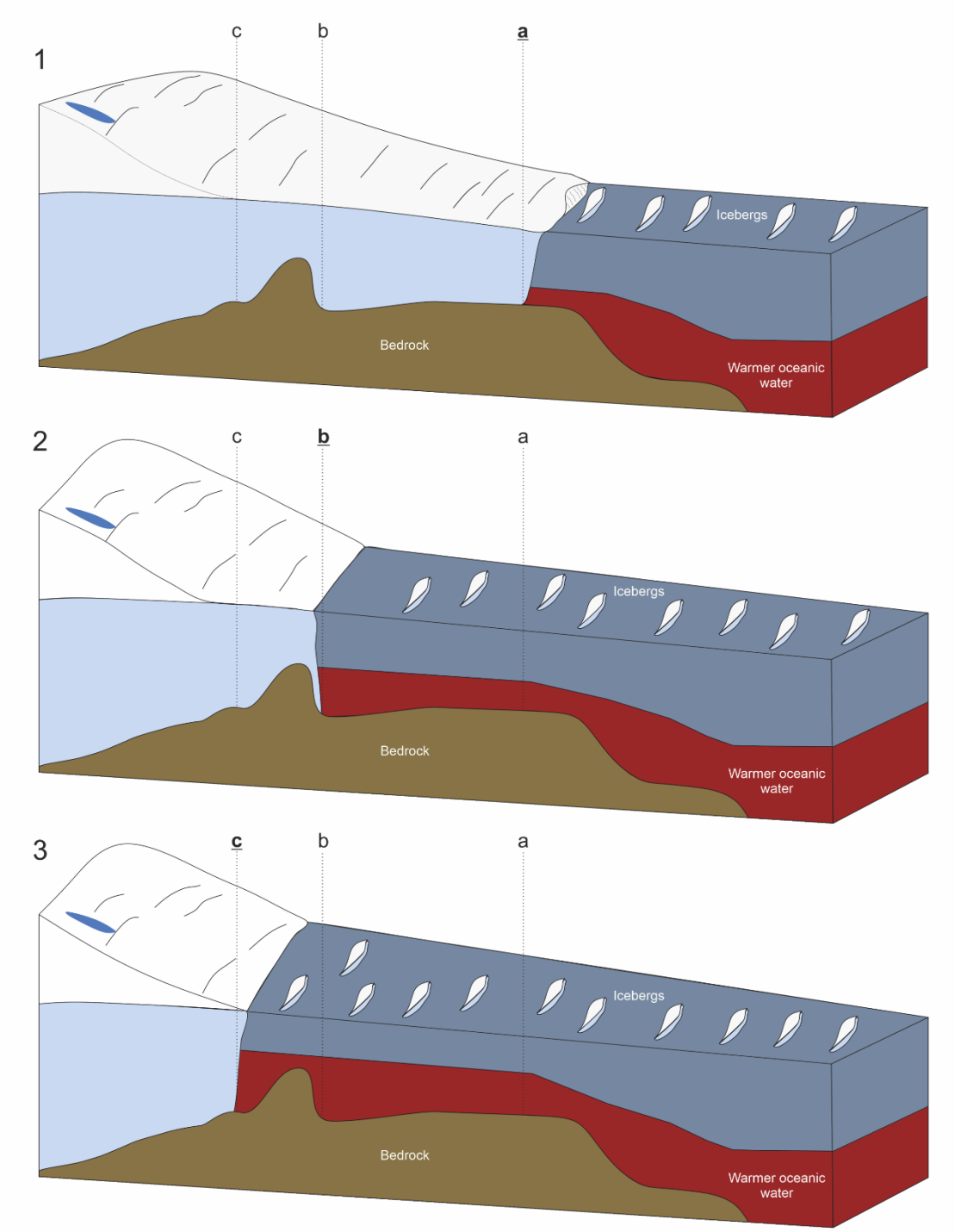

Figure 2.4. Schematic example of different grounding line positions for an idealised outlet glacier from Greenland. 1) shows the most advanced grounding line position on a flat stable bed (a), 2) shows a retreated position proceeding a sill which will act as a pinning point for the ice front (b) and 3) the most retreated grounding line position and is situated on an adverse (or retrograde) bed slope with no topographical features to halt a runaway retreat (c).

Groundling line depths are not only important for the transitional stability of the glacier, rather, the positional depth can influence the magnitude of iceberg calving events. Sermeq Kujalleq retreated significantly in the mid-to-late 2000's (Rosenau et al., 2013) which resulted in

changing grounding line depths and a transition from large icebergs being calved to much smaller ones (Scheick et al., 2019). Iceberg sizes calved will in part depend on the depth of the grounded terminus. For example, a more deeply grounded glacier (i.e. one grounded deeper than 250 m) is more likely going to calve larger and more tabular icebergs because of the potential for full thickness calving via basal crevasse propagation (Bassis and Walker, 2012). Such a scenario has been observed at Helheim Glacier (James et al., 2014) which has an ice depth of 1000 m across the ice front (Kehrl et al., 2017).

The depth of a fjord which an ice front terminates into has the ability to either restrict (e.g. sills blocking) or allow AW, typically >300 m deep (Holland et al., 2008; Wood et al., 2018) to reach the front of marine-terminating glaciers. These waters are warm and consequently melt an ice front at depth, undercut and contribute to the rate of calving (Rignot et al., 2015). If subglacial discharge emerges at the terminus in parallel with warm oceanic water present, there is potential to exacerbate submarine melting significantly (Motyka et al., 2013; Fried et al., 2015).

2.1.3 Subglacial hydrology

Meltwater produced by the melting of the ice sheet, predominately in the summer months is able to reach the bed of the ice sheet. This water at the ice/bedrock interface is able to significantly alter glacier dynamics, which has implications for ice velocity (Davison et al., 2020b) and iceberg calving processes (Bunce et al., 2021). The influence of subglacial water on glacier motion has been well-known in glaciology for over thirty-years (Kamb, 1987). The influence of subglacial water is seasonal and can vary across large spatial scales at both land- (Mair et al., 2002; Mair et al., 2003) and marine-terminating glaciers (Bartholomew et al., 2011) and impact ice dynamics. Recent work at three outlet glaciers has shown more water at the glacier-bed interface can significantly increase glacier velocities during the peak of the melt season (Davison et al., 2020b).

At the ice front of tidewater glaciers, we have since noted two types of hydrological system which form underneath the ice: 1) distributed and 2) channelised, both of which provide pathways for the routed water (Figure 2.5). A distributed system forms when there is less water at the bed (e.g. winter months) and is classed as ‘inefficient’. Whereas an ‘efficient’, channelised system forms when subglacial water is greater during the summer months (e.g. because there is more ice sheet melt). It has since been suggested that if meltwater exceeds the capacity of a channel at the terminus, the system will revert back to that of a distributed one

because it has become overwhelmed and is therefore unable to route the subglacial water in an efficient manner (Slater et al., 2015).

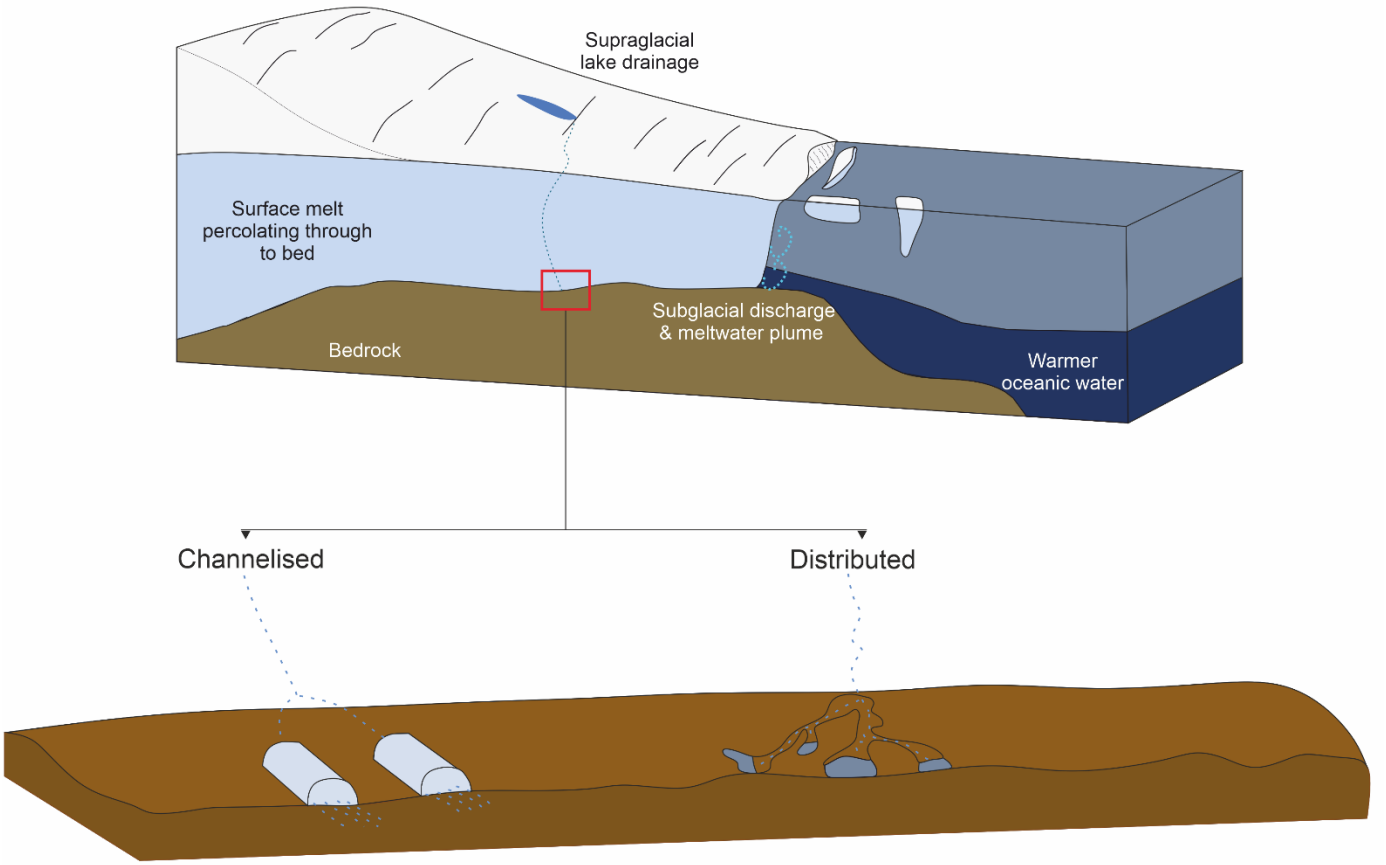

Figure 2.5. Schematic diagram showing the difference between a channelised and distributed subglacial hydrological system at the ice-ocean-bedrock interface. Channelised is considered an 'efficient' system, whereas distributed is 'inefficient'.

While it may just seem important for the routing of subglacial system, the upwelling of plumes entrains ambient water from below which can enhance submarine melting and alter the geometry of the ice front which will impact how the glacier calves. If the pressure from the subglacial water system at the ice front exceeds the pressure exerted by the ocean, the freshwater will exit the outlet glacier in the form of a 'subglacial plume' and can enhance submarine melting as it entrains ambient, warmer water during its ascent (Jenkins, 2011). Melt rates from subaqueous discharge can be in the order of meters per day (Xu et al., 2012). During times of a distributed system, the total melt volume can increase by a factor of five when compared to a channelised system (localised melting) because subglacial water is able to upwell alongside the entire ice front (Slater et al., 2015). Subglacial discharge has the ability to undercut an entire terminus and can therefore interact with surface crevasses and enhance calving (Fried et al., 2015).

Recent work at three of Greenland's southwest outlet glaciers revealed a relationship between increased subglacial water and changes in seasonal velocity accelerations, followed by decelerations to below pre-accelerated speeds due to the development of subglacial channels (Davison et al., 2020b). In 2012, a year of record surface melting (Nghiem et al., 2012), modelling and remote sensing observations at Saqqarliup Sermia (west Greenland) identified that due to increased subglacial discharge, the fjord became more stratified, which subsequently prevented subglacial plumes from upwelling and emerging at the ice front (Andrés et al., 2020). Whereas, when runoff was reduced in 2013, a greater number of subglacial plumes surfaced at the ice front, therefore posing the question of whether subglacial plumes will surface to a greater extent under increased meltwater predictions and thus increased subglacial discharge which can further stratify the fjord and inhibit plume upwellings (Andrés et al., 2020). Furthermore, remotely sensed and time-lapse imagery at Rink Isbræ revealed the lack of seasonal velocity speed ups and relationship with runoff and plume emergence when the subglacial system undergoes inefficient drainage (Schild et al., 2016).

As plumes upwell and undercut the ice front as a result of entraining warmer water from below and exacerbating submarine melting, stress fields above change and impact how a glacier calves (O'Leary and Christoffersen, 2013). These upwellings localise melting at the terminus and can impact the magnitude (Cook et al., 2021) and frequency (Bunce et al., 2021) of calving events. While it is known the morphology of the ice front can impact glacier calving (O'Leary and Christoffersen, 2013; Slater et al., 2015), we do not fully understand how subglacial hydrology impacts the size distributions of icebergs being calved.

2.1.4 Strain rate and velocity

There are two types of crevasses at marine-terminating glaciers: surface and basal; both of which are a response to stress within the glacier. When these crevasses propagate and fracture, they detach ice from the glacier and an iceberg is calved. There are three main forms of fracture propagation as described by Benn et al. (2007b) (see Figure 2.6). Tensile crack (Figure 2.6a) occurs when the walls of the fracture are pulled apart and develop a fracture plane which is normal to the maximum extension axis. With sliding (Figure 2.6b), the walls continue in contact with one another, and fracturing develops along a shear plane. Tearing (Figure 2.6c) includes fracture propagation at right angles in the direction of shearing (Benn et al., 2007b).

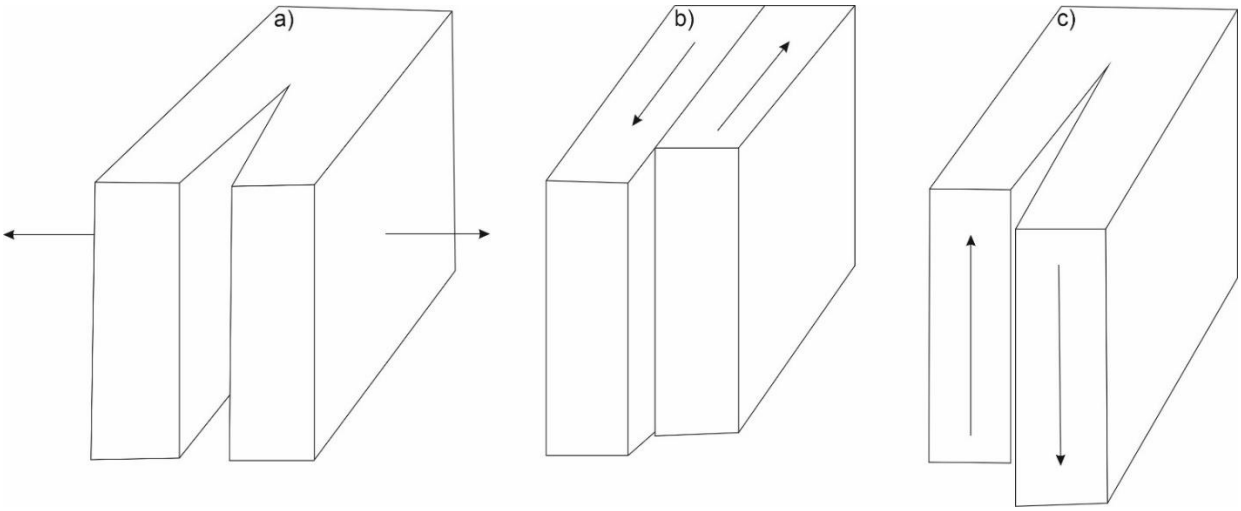

Figure 2.6. Three mechanisms of initiation ice fractures at glaciers: a) tensile crack, b) sliding and c) tearing (modified from Benn et al., 2007b).

The depth of surface crevasses are controlled by longitudinal stress and whether they penetrate the waterline and has therefore been considered a first-order control on calving (Benn et al., 2007a; Benn et al., 2007b). This first-order control has been parameterised with longitudinal strain rates, ice thickness and water depth within the crevasse (Benn et al., 2007b). Numerical calving simulations at Helheim Glacier showed the two-dimensional flowline model was particularly sensitive to water filled crevasses, e.g. larger water depths result in deeper crevasses and resulting in more frequent calving events (Cook et al., 2014). High resolution photogrammetry over the terminus of Store Glacier revealed that while water-filled crevasses existed, they did not act as a mechanism for calving (Ryan et al., 2015). After applying the crevasse depth calving model (Benn et al., 2007b) to 50 of Greenland's marine-terminating glaciers, Amaral et al. (2020) found accurate calving conditions which led to accurate frontal positions (within 10 m d^{-1}) temporally when compared to observations, however the water depth parameter was referred to as redundant because there was no correlation between increasing water depths during the summer and a latitudinal gradient.

Strain rate is primarily controlled by the velocity of a glacier which in turn dictates the location and extent of surface crevasses (Benn et al., 2007b). Ice velocities at the terminus are typically faster than ice velocities up-glacier which results in high longitudinal strain rates which can control when and where icebergs are calved (Benn et al., 2007b).

Greenland's marine-terminating glaciers are fast flowing bodies of ice which can reach speeds of up to 12 km/yr (Moon et al., 2012). Seasonal velocity patterns have been able to categorise Greenland's outlets in to three types of behaviour (Table 2.1) (Moon et al., 2014). Type 1's

behaviour sees a relationship between velocity and terminus position, type 2 glaciers have correspondence between faster velocities and an increase in meltwater runoff, and type 3 a decline in velocity with an increase in meltwater runoff (Moon et al., 2014).

Table 2.1. Description of velocity differences and behaviour between the three-outlet glacier 'types' presented by Moon et al. (2014).

Glacier Type	Description
Type 1	A speedup between late spring and early summer.
Type 2	Velocity is stable from late summer through spring with a string early summer speedup and midsummer slowing.
Type 3	Midsummer slowdown with late summer minimum and rebounds over the winter.

Faster flow is imperative to glacier and calving dynamics for three main reasons: 1) faster ice tends to become more 'damaged', meaning an enhancement in crevassing (altering iceberg calving), 2) faster ice results in higher longitudinal strain rates (altering iceberg calving) and 3) faster ice flow tends to lead to overall thinning (altering iceberg calving). In turn, thinner ice promotes stresses due to increased surface slope and is fundamentally easier to fracture and subsequently calve at the ice front. Recent work on the east coast of Greenland (except Kangerlussuaq) has suggested despite sector-wide terminus speedup, there is no evidence of upstream (or inland) acceleration in ice flow and therefore glacier retreat maybe more sensitive to basal topography and ice geometry (Williams et al., 2021).

2.1.5 Supraglacial lakes

Increases in meltwater runoff can contribute to variations in seasonal ice-flow because of hydrological forcing subglacially (Zwally et al., 2002; McMillan et al., 2007; Davison et al., 2020b; Ashmore et al., 2022). The presence of surface features on the ice sheet, such as surface crevasses and moulins provide pathways for surface meltwater to percolate to the basal zone and contribute water to the subglacial system, potentially impacting on glacier velocities and subglacial plume upwellings (which in turn can vary iceberg calving dynamics; Section 3.1.2).

In the melt season when supraglacial lakes are at their most expansive, they have the capability to reduce the albedo of the ice sheet (Lüthje et al., 2006) with their location and extent often being controlled by elevation, bed and surface topography (Joughin et al., 2013; Sergienko, 2013; Pope et al., 2016). They are significant features of the GrIS surface which can drain rapidly or slowly (Miles et al., 2017) with in-situ observations revealing their depths can exceed 10 m (Legleiter et al., 2014) and drain entire ice thicknesses which approach 1 km within two hours (Das et al., 2008). Observations on the floating ice tongue of Petermann Glacier reveal lakes develop in early-to-mid June and reach total volume by the end of the month, while this peak is never recovered in the higher temperature months of July and August because of drainage events and/or transportation by a river and therefore may reduce the risk of the tongue breaking up (Macdonald et al., 2018).

It has been considered that Arctic warming is resulting in more supraglacial lakes forming and subsequently draining at higher elevations (Leeson et al., 2015). Cooley et al. (2017) identified lakes at elevations exceeding 1600 m are able to drain just as frequently as lakes at lower elevations. Observations reveal that there is up to a three-week delay in total supraglacial evolution between northern Greenland when compared to southwest coast (Sundal et al., 2009). Between 1985 and 2016, supraglacial lakes in northwest Greenland have reached higher elevations (+299 m) and the overall coverage has increased by 2750% during this period (Gledhill and Williamson, 2018). In the southwest sector of Greenland in 2015 (a year with a relatively cold melt season), 21% of supraglacial lakes (>1600 m elevation) drained into moulins, highlighting the relationship between high-elevation surface-to-bed connections even in colder years (Yang et al., 2021). In higher melt years however, lakes on the west coast drain more frequently and earlier in the melt season, therefore implicating the surface-to-bed relationship under a warming climate (Liang et al., 2012).

Supraglacial lakes are not just important and visible during the melt season, rather they have been detected in the winter months, buried on average 1.9 m below the surface across the entire ice sheet and can therefore be a source of meltwater all year round (Koenig et al., 2015). Several lakes in winter draining have also been detected at 79° North Glacier and Zachariæ Isstrøm using Sentinel-1 (Schröder et al., 2020).

It has been forecasted that between 2070 and 2099 meltwater stored in supraglacial lakes could be in the order of 9.8 ± 3.9 km^3 and 12.6 ± 5 km^3 under representative concentration pathway

4.5 and 8.5, respectively, which is between a 113% and 174% increase on 1980-2069 storage (Ignéczi et al., 2016).

Increases in the spatial extent of supraglacial lakes across Greenland has significant implications for iceberg calving as there is a greater potential for more water to reach the bed of the ice sheet through surface and englacial networks. More water in the subglacial system has been shown to impact glacier dynamics (Davison et al., 2020b), the geometry of the ice front (Slater et al., 2015) and the frequency of iceberg calving events (Bunce et al., 2021). Consequently, the expansion of lakes on the surface of the ice sheet will undoubtedly impact on glacier calving regimes, however the extent of this significance remains unknown.

2.1.6 Ice mélange

Ice mélange (matrix of icebergs and sea ice) is a proglacial phenomenon which provides backstress to the glacier and can reduce the amount of warmer oceanic water reaching the ice front. Time-lapse imagery at Sermeq Kujalleq suggested the backstress needed to prevent iceberg calving events at the ice front is in the order of 10^7 N m^{-1} (Amundson et al., 2010). Later work at Sermeq Kujalleq has shown immobile mélange halts iceberg calving (Cassotto et al., 2015), even without a binding matrix of sea ice (Cassotto et al., 2021). This backstress not only implicates calving (Brough et al., 2023), but a subsequent impact on varying ice flow velocities depending on mélange conditions, e.g. rigid (Cassotto et al., 2015; Moon et al., 2015).

Kangerlussuaq experienced a dramatic 5-kilometre (km) retreat between 2016 and 2018 (Brough et al., 2019) because of the presence of a non-rigid mélange which ensured the glacier calved all year round for the two-year period, increasing velocities by 35% and thinning by 35 m (Bevan et al., 2019). During 2019, a rigid mélange formed and allowed the glacier to readvance by 3.5 km (Bevan et al., 2019). Likewise, a full-Stokes 2-D model of Store Glacier showed rigid mélange was a primary control for the seasonal advance of the terminus, with future simulations under a warming climate suggesting that reducing the buttressing provided could hinder ice front advance into a floating ice tongue during the winter months (Todd and Christoffersen, 2014).

Sediment cores in Sermilik Fjord (which Helheim Glacier drains) revealed the Great Salinity Anomalies between 1965 and 1972, the early 1980's and 1990's were associated with reduced calving events through increased ice mélange stability and reduced AW penetration at the ice front (Andresen et al., 2012). Recent work by Wehrlé et al. (2023) has shown 75% of all calving

events in the fjords of Kangerlussuaq, Helheim and SKJI are preceded by episodes of extensive ice mélange weakening. Glaciers south of 69° N on the east coast of Greenland underwent continuous retreat from 2016 as a result of repeated winter calving events and mélange break-up (Brough et al., 2023). Consequently, it is well documented that backstress on a calving margin has the ability to inhibit calving and changes in ice mélange integrity can have important implications on the frontal dynamics of an outlet glacier.

2.2 **Icebergs**

The remainder of this Chapter will focus upon the calving, dynamics and distributions of icebergs, both in the contemporary and paleo-context. Icebergs are blocks of ice comprised of freshwater and are a direct result of glacier and/or ice shelf calving (Figure 2.7). They contribute to the mass balance of glaciers and/or ice shelves (Bigg et al., 2014), impact fjord dynamics through the release of freshwater fluxes (Enderlin et al., 2016; Davison et al., 2020a), and pose current and future challenges to offshore infrastructure (Eik and Gudmestad, 2010), shipping, tourism (Bigg, 2015), ecological habitats (Laidre and Stirling, 2020) and biogeochemical cycling (Lin et al., 2011; Duprat et al., 2016). Icebergs have played a pivotal role when influencing the global heat distribution in the past (Heinrich, 1988), and potentially could again under a deglaciating GrIS (Lenaerts et al., 2015).

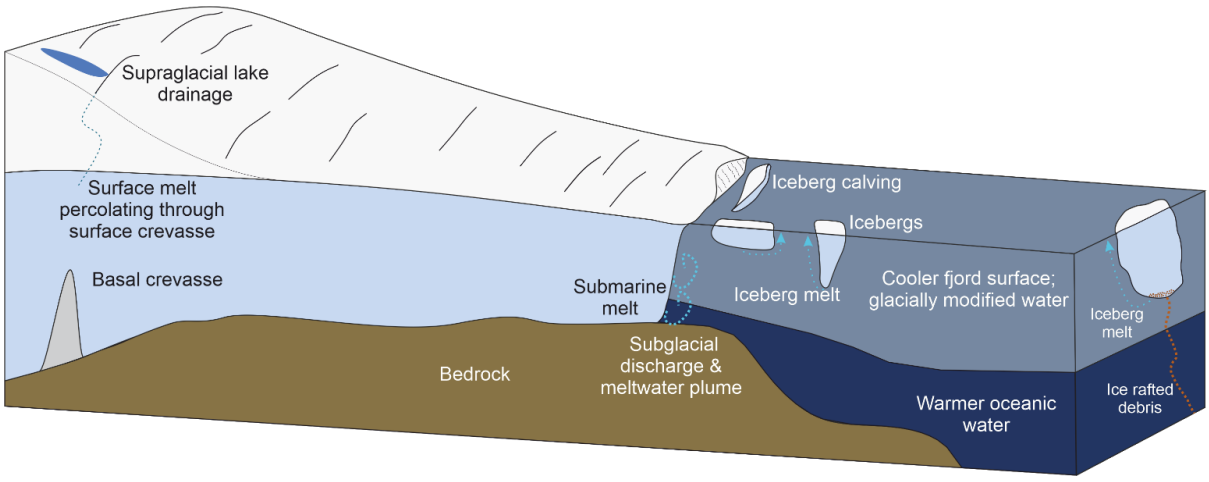

Figure 2.7. Schematic of a typical Greenlandic grounded marine-terminating glacier and the respective ice-ocean interface.

The word ‘ice-berg’ has been traced back to as early as 1773 in the English language since Captain Cook’s voyages where icebergs would be broken down for water supplies (Bigg, 2015). Later in the 19th century, icebergs were towed onshore from the Chilean Andes to be broken-up and used as coolant for the local beer brewery (Riffenburgh, 2007). The idea of iceberg towing led to considerations in the latter stages of the 20th century and resulted in a

conference discussing the feasibility of iceberg towing to water poor regions (Bigg, 2015). The feasibility of the application was somewhat challenging due to complications, including cost, strategic iceberg choice and the incorporation of cold meltwater into environments which are not acclimatised to such conditions (Bigg, 2015).

While icebergs are a direct result of calving, little is known about iceberg size distributions and their relationship with glacier processes. However, in depth investigations about iceberg size, shape, typology, magnitude and frequency may help bridge this research gap. Iceberg area distributions have been shown to provide proxy information about the different calving dynamics between floating and grounded terminus positions at Sermeq Kujalleq (Scheick et al., 2019). Nevertheless, these works are isolated to a handful of glacier sites and no ice sheet wide categorisation has been formulated to constrain relationships between iceberg sizes and glacier processes.

Such relationships are of paramount importance as over half of the mass lost from Greenland is from iceberg discharge (Figure 2.1). Consequently, there needs to be some effort to quantify direct relationships between the size of icebergs and the dynamics of the glaciers calving them (e.g. terminus depth and width, glacier velocities, subglacial discharge values). Once these relationships have been identified, there will be an opportunity to understand the dynamics between iceberg sizes and glacier processes. This is imperative as there is currently no research investigating the physical controls on the size of icebergs, only the rate of ice being calved and where the terminus will be subsequently situated. Our understanding of iceberg calving has hugely progressed in the last two decades, however calving parametrisations of calving rate and terminus position (Benn et al., 2017) have dominated research interests and understanding the size of the icebergs has been subsequently neglected.

Understanding the evolution of iceberg size production under a changing climate is not just important glaciologically speaking, but also for human safety and logistics. Local people who rely on the resources of Greenland are also being adversely affected because of a changing climate, for example, changes in iceberg sizes could have implications for local fishing routes (e.g. different fjord ice cover). We currently do not understand how iceberg calving will evolve into the 21st century and beyond (Choi et al., 2021), however it has large-scale, global implications from climate regulation, to small-scale impacts of local fishing communities (Straneo et al., 2022).

Iceberg sovereignty has been noted as somewhat of a political consideration with uncertain climatic changes into the 21st century as there are currently no international laws that are in place that provide icebergs a political status (i.e. all icebergs calved from Greenland are owned by them and Denmark) (Wood-Donnelly, 2022). Rather than a permeant sovereignty, Wood-Donnelly (2022) suggests icebergs should be considered as a transboundary water resource due to freshwater insecurity and a regulatory system should be put in place to avoid potential conflicts from stakeholders who may harvest their ice and gain economically as a result.

While the scope of this review is focused upon Greenland's icebergs, investigations in the Antarctic and Southern Ocean are also noted to highlight potential research opportunities in the Northern Hemisphere which has occurred in the Southern, as well as demonstrating the centennial to millennial timescale importance of icebergs through Heinrich Events and deglaciating ice sheets.

2.2.1 Iceberg data and detection

2.2.1.1 Remote sensing techniques

Iceberg outline data through both automated and manual identification in the near-terminus regions of outlet glaciers across Greenland are limited to a handful of fjord locations, e.g. Sermilik Fjord (Enderlin et al., 2016; Sulak et al., 2017; Rezvanbehbahani et al., 2020), Disko Bay/Ilulissat (Enderlin et al., 2016; Scheick et al., 2019), Kangerlussuaq (Rezvanbehbahani et al., 2020), Kangerlussuup and Rink Isbræ (Sulak et al., 2017). While these works are incredibly useful and have provided new insights, further research and data is needed at much higher spatial and temporal scales across the ice sheet to understand iceberg dynamics and distributions at a greater range of marine-terminating glaciers with different calving styles and behaviour. To attain this level of data at high spatial and temporal resolution, workflows which are able to automatically detect icebergs are required as manually delineating icebergs during the satellite era is impossible at an ice sheet scale as there are millions of icebergs in the Arctic at any one time.

Manipulating optical imagery data has emerged as the most common technique to (semi-)automatically detect icebergs in Greenland's fjords (Sulak et al., 2017; Scheick et al., 2019; Rezvanbehbahani et al., 2020). However, open-access optical imagery can be spatially and temporally limited through the effect of cloud cover and shadow, limiting the amount of image data for further processing. Likewise, optical imagery (Landsat, Sentinel 2) are often too coarse (10 – 30 m resolution) to identify icebergs below a size threshold as they are too small, yet

equate to significant contributions to the freshwater budget of fjord environments (Rezvanbehbahani et al., 2020). Satellite image availability can also lead to sporadic data coverage in the Arctic.

Automatically detecting icebergs is extremely difficult because of varied data quality and quantity, image storage and processing, and subsequent workflow development. Approaches to automated iceberg detection typically involves band thresholding (Sulak et al., 2017; Moyer et al., 2019) which differentiates between iceberg and ocean. These techniques fundamentally assign pixels different values and if they surpass a given threshold, they will be considered an iceberg. Figure 2.8 illustrates that while these approaches can suitably detect icebergs in open water fjord conditions, they struggle to delineate icebergs in ice mélange due to the same signals returned by the icebergs and mélange to the satellites. This is problematic for obtaining temporally continuous observations because fjord conditions alter seasonally from a fully frozen ice-covered fjord in the winter to open water in the summer. Furthermore, some Greenlandic fjords are affected by temporal changes in ice mélange extent throughout the year (Brough et al., 2023). These dynamic and ever-changing fjord environments result in these simple remote sensing techniques being limited to analysis on appropriate images (e.g. Figure 2.8a), in turn hindering the automation process at scale.

Investigations are needed to automatically delineate icebergs within sea ice dominated fjords because they are still important for spatially and temporally evolving fjord dynamics and freshwater release. One such potential avenue to be investigated could be using a surface roughness parameter to determine differences in sea ice coverage and icebergs and/or elevation if the available dataset has such metadata (e.g. digital elevation models (DEMs); airborne Light Detection and Ranging (LiDAR)).

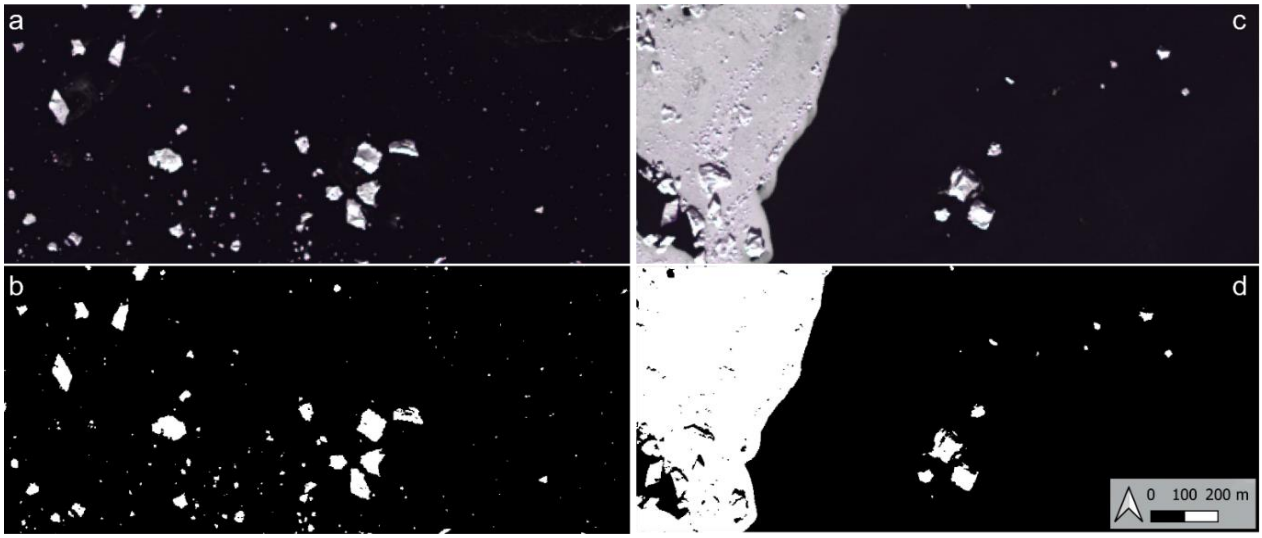

Figure 2.8. Example of simple, automated band thresholding (band 8) on Landsat 8 imagery in the fjord of Rink Isbræ (entering the mouth of Uummannaq Bay) in the same location, but a month apart: a) Landsat 8 image (16th August 2020), b) subsequent binary image of detected icebergs, c) Landsat 8 image (15th September 2020) and d) subsequent binary image of detected icebergs. The scale used in (d) is the same for each panel (a, b, c).

Nevertheless, many works typically avoid iceberg detection in the presence of rigid ice mélange by only selecting the summer months where open water is more likely to occur in Greenland's fjords (Sulak et al., 2017; Moyer et al., 2019). However, some outlet glaciers have continuous ice mélange at the ice front through the summer months which limits these thresholding approaches (Figure 2.8d). Optical imagery is more likely to be available in the summer months due to longer daylight hours and can capture fjord environments which are not densely covered by ice. However, optical data sources cannot provide observations over all parts of the year due to the polar night in winter and continuous cloud cover throughout the year.

Other remote sensing datasets such as synthetic aperture radar (SAR) and DEMs provide alternative options for the detection of icebergs to circumvent obstacles faced by optical imagery. SAR data is derived from an active sensing platform utilising radio waves, meaning SAR satellites can observe the surface of the earth even with dense cloud cover. SAR derived data therefore have the benefit of continuous image coverage compared to optical data as they are not impacted by cloud contamination and have the ability to detect icebergs all year round (e.g. Soldal et al., 2019). Open-access SAR imagery, most notably Sentinel 1 (up to 5 m spatial resolution) is temporally limited when compared to the optical record (e.g. satellite launched in 2014), and coverage over certain parts of Greenland (northwest sector) is spatially poor, particularly in its primary years. However, the platform does return imagery every 6 to 12 days

and provides a high-resolution temporal record when data is available. With Sentinel 1B being deactivated in 2022, due to an anomalous problem resulting in the inability to deliver radar images, there will be a reduction in the temporal frequency with which images are collected until a replacement satellite is operational.

Like optical imagery, when only a single scene is used, SAR data can only express a planform surface area (A) of an iceberg because they do not contain a Z dimension (e.g. elevation) which DEMs are able to provide (i.e. three-dimensions). Being able to derive an iceberg in three-dimensions (i.e. a volume) can provide insights into size distributions and freshwater capacity. Optical and SAR data are limited to identifying icebergs in two-dimensions (i.e. an area) and can only provide information into area size distributions (e.g. Scheick et al., 2019). Consequently, remote sensing and modelling investigations will convert a two-dimensional surface area to a three-dimensional volume (V) using an area-to-volume convertor (e.g. Sulak et al., 2017) (Equation 2.1)

$$V = 6.0A^{1.30} \quad (2.1).$$

DEMs on the other hand are able to calculate each icebergs volume because of the XYZ dimensions they contain and do not require a convertor. As some openly accessible DEMs (e.g. ArcticDEM) are derived from optical imagery (in this case WorldView), they can be contaminated with cloud cover, resulting in sporadic data spatial and temporal coverage over the Arctic. DEMs have been used previously to estimate iceberg volume change through time (Enderlin et al., 2018), and the data can provide key characteristics and relationships between area and volume (Sulak et al., 2017). However, DEM observations tend to only provide a snapshot of icebergs in a fjord at any one time and is reliant on high spatial resolution imagery (Enderlin et al., 2018).

Satellite altimetry also has the potential to calculate iceberg volumes by deriving iceberg area and thickness which can then be used to determine iceberg disintegration through time as the altimeter overpasses (Braakmann-Folgmann et al., 2022). Such techniques have been used to determine and track volumetric change for large, tabular icebergs A68 (5800 km^2) (Braakmann-Folgmann et al., 2022) and B30 (1500 km^2) (Braakmann-Folgmann et al., 2021). These works have provided the scope to use such satellite data, however the outline delineation of the icebergs required to determine these volumetric changes are completed manually using Sentinel 1 and 3 and MODIS (Moderate Resolution Imagery Spectroradiometer) imagery (Braakmann-Folgmann et al., 2022). This limits the identification of the original iceberg

because of user workload, and makes scaling to clusters of target icebergs time-consuming and impractical. Nevertheless, there is scope for deriving iceberg volume change temporally using satellite altimetry on larger spatial scales if the outline delineation was (semi-)automated, but only for large tabular icebergs calved from Antarctica as altimetry is not suitable for smaller icebergs.

The identification and tracking of icebergs are performed for logistical safety and fjord dynamics (Moyer et al., 2019). However, automating iceberg tracking is notoriously difficult for two main reasons: 1) originally and automatically identifying a target iceberg which is of a size large enough to survive through collections of images acquired from satellites and 2) defining the same iceberg in a later image because of a continually changing geometry due to melting, disintegration, and potentially overturning. Having the ability to track a designated iceberg from a glacier terminus, through the fjord and/or ocean automatically, researchers would be able to determine: 1) drift trajectories from parent glaciers, thus inferring fjord and/or wind circulation and identifying hazardous areas around the ice sheet, 2) identify any stranded (grounded) icebergs as they have not drifted for a period of time, 3) calculate iceberg area/volume loss during drifting, identifying disintegration processes (e.g. calving or melting) and as a result 4) constrain the meltwater fluxes.

Across Greenland, obtaining iceberg drift trajectories through tracking is limited to manual identification from satellite imagery (Scheick et al., 2019), in-situ global positioning systems (GPS) (Sutherland et al., 2014; Yulmetov et al., 2016; Carlson et al., 2017) and drone autopilots (Carlson and Rysgaard, 2018). Similar research has been conducted in the Southern Ocean, however the iceberg tracking using satellite imagery has been semi-automated (Lopez-Lopez et al., 2021). Identifying the same iceberg in Antarctica through different images is more feasible when compared to Greenland because of the former's greater surface area (that are typically more tabular) which take longer to melt, calve and disintegrate, making their definition that bit easier through continuously acquired satellite imagery. Some larger icebergs have been successfully tracked using semi-automated approaches based on their shape, e.g. A-68 (Lopez-Lopez et al., 2021) and B43 (Figure 2.9) (Koo et al., 2021). While the tracking maybe automated in some cases (Koo et al., 2021), the original delineation of the iceberg is manually defined to allow identification through continuous satellite images, thus the scalability of such techniques remain limited. Scalable tracking methods are important because small icebergs can account for a significant proportion of total volume, fjord freshwater budget

(Rezvanbehbahani et al., 2020) and therefore require automated identification and monitoring of their drift patterns.

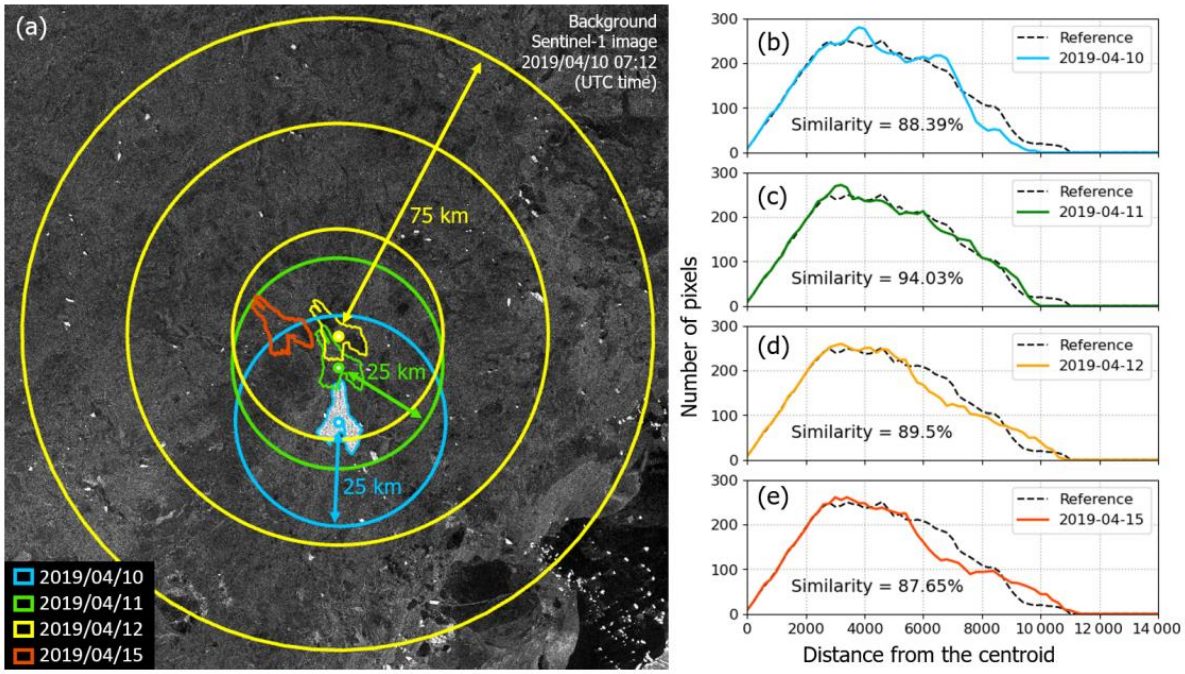

Figure 2.9. Semi-automated tracking of iceberg B43 in Antarctica from Sentinel 1 imagery between the 10th and 15th April 2019 within a search radius with reference to centroids. The original outline of B43 was manually digitised to allow the iceberg to be tracked through images (from Koo et al., 2021).

There are fewer iceberg databases in the Northern Hemisphere than those in the Southern Ocean, however they do exist. A few examples include Greenland's iceberg positions via the Polar Portal website (available at: http://polarportal.dk/en/sea-ice-and-icebergs/icebergs/), the Canadian Ice Island, Drift, Deterioration and Detection database (CI2D3) developed by Crawford et al. (2018) and ALTIBERG which covers the Arctic (Tournadre et al., 2021). These works are incredibly useful for iceberg positions and drift locations, however the databases often do not provide data in the near terminus region of marine-terminating glaciers and therefore determining iceberg distributions and thus calving styles is not applicable to date. Moreover, the iceberg positions via the Polar Portal website does not detect icebergs in areas of sea ice, thus limiting the dataset to mainly open water sections around the ice sheet.

While satellite imagery of varying quality, regularity and spatial coverage has been available for over half a century, we are in an era of relative infancy of returning consistently high-quality imagery from satellites in the Arctic. Using the Landsat programmes, we realistically only have consistent coverage from 2013 through the launch of Landsat 8 and the most recent launch of Landsat 9 which should secure coverage in to the next decade. However, earlier Landsat

satellites, namely Landsat 7 has sparse temporal coverage and poor image quality due to the failure of the Enhanced Thematic Mapper scan line corrector in 2003 (Scaramuzza and Barsi, 2005). The Sentinel 1 and 2 programmes have a higher spatial resolution with more frequent return days, however they only began acquiring data in 2014 and 2015, respectively. Consequently, there is less than 10 years of consistent data coverage over the Arctic regions with high enough spatial resolution (10-30 m) to identify icebergs. Sentinel 1C and 1D are due for launch in 2023 and again, hopefully securing our coverage security (i.e. data coverage every three to six days). As we increase our temporal resolution into the future, we can develop long-term trends of iceberg distributions through novel detection algorithms which should help us better understand the calving behaviour of Greenland's outlets (and other calving ice masses across the globe) and what that may mean for the stability of the ice sheet.

2.2.1.2 Field-based observations

Iceberg tracking in Greenland has often come in the form of field-based measurements through the use of GPS. These systems can be placed on the top of an iceberg, transponding data and geographical locations which can be used to infer iceberg thickness, drift and speed. GPS' were placed on ten icebergs in Baffin Bay with six losing signal within the first 23 days, but one system transferred data for over five months and measured a maximum drift speed of 68 cm s^{-1} and a mean speed of 10 cm/s^{-1} for the sampled icebergs (Larsen et al., 2015). In Sermilik Fjord (SF), five icebergs were tagged with GPS' and showed they generally conformed to circulation driven by along-fjord and along-shelf winds, with the icebergs often recirculating in and out of the fjord (Sutherland et al., 2014). Carlson et al. (2017) deployed a low cost ($300) satellite-tracked GPS beacon, EXpendable Ice TrackEr, in Nuup Kangerlua (Godthåbsfjorden) which transforms into a surface drifter upon capsizing, finding eddies and wind-driven reversal can impact iceberg transport (Figure 2.10). Recent work utilised geodetic GPS units which recorded the absolute height of the iceberg, rotation, deterioration and tipping on two large icebergs in SF (Schild et al., 2021). These data were used to calculate melt rates based on surface lowering and found that melt rates were lower than previous studies in southeast Greenland due to the iceberg geometry below the waterline (Schild et al., 2021).

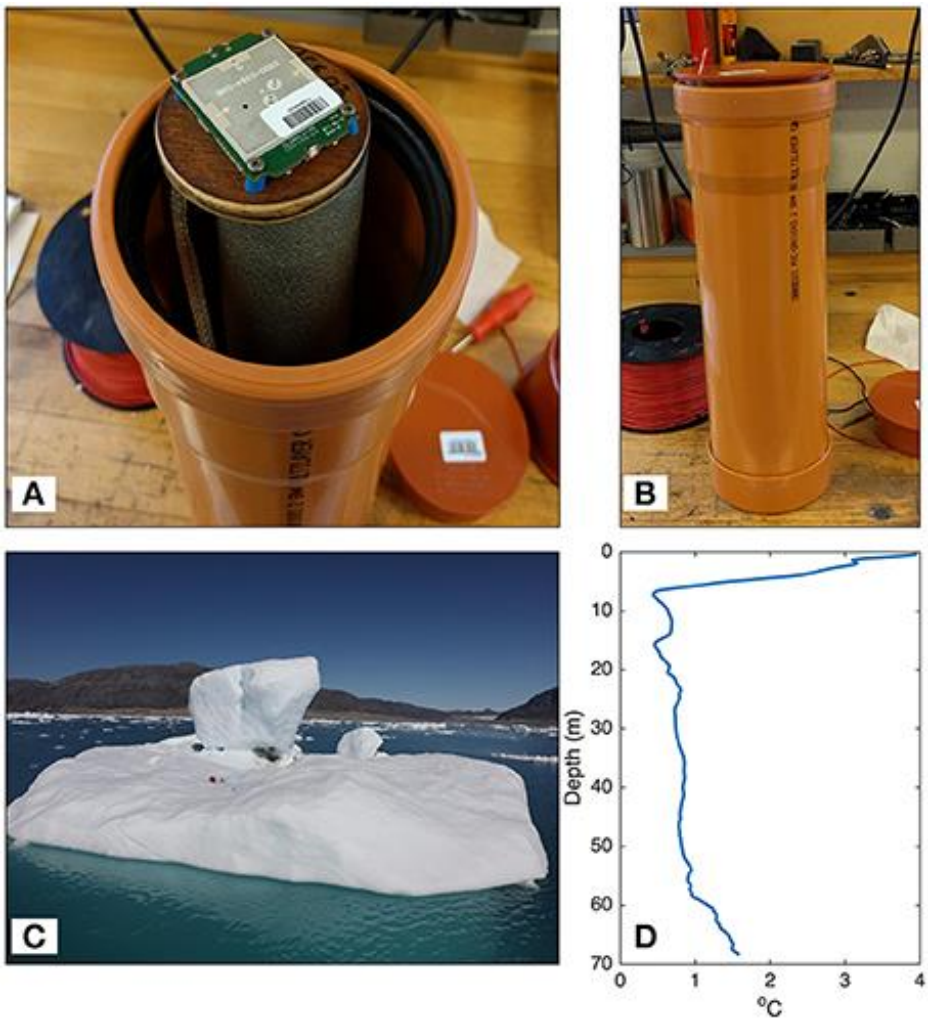

Figure 2.10. Example of a low-cost tracker on the iceberg surface in Nuup Kangerlua (a fjord in southwest Greenland) within a PVC drain pipe and a respective conductivity, temperature and depth probe suspended in close proximity to the iceberg. This equipment was able to provide information about iceberg movement in the fjord and the fjord characteristics close to the iceberg (from Carlson et al., 2017).

Calculating accurate melt rates from icebergs are challenging as we know very little about the basal geometry below the waterline which can therefore limit freshwater flux estimates from remote sensing studies alone. To circumvent this using remote sensing techniques, Enderlin and Hamilton (2014) idealised a subsurface geometry in the shape of cones and cylinders to calculate their melt rates, but this led to large uncertainties in their calculations (8-100%). Melt models also parametrise the basal geometry of icebergs, but it theorises the base of the iceberg far down fjord of the parent glacier where it will have stabilised in equilibrium (Wagner et al., 2017). Schild et al. (2021) utilised sonar scanning to delineate the sub-surface geometry of two icebergs in SF, finding melt rates (01.0 to 0.27 m/d^{-1}) were lower than previously published values because of the idealised parametrisations of the iceberg base (Figure 2.11). These findings highlight the need for 1) more in-situ observations to determine the subsurface

geometry of the iceberg and 2) when these observations are across a greater spatial range, incorporate their geometries into iceberg models and remote sensing studies to ensure melt rates are calculated as accurately as possible. This is a problem which can only be solved with field data because even with high resolution DEMs and satellite images, it is not possible to fully infer the basal geometry which is key for determining how icebergs melt through the fjord.

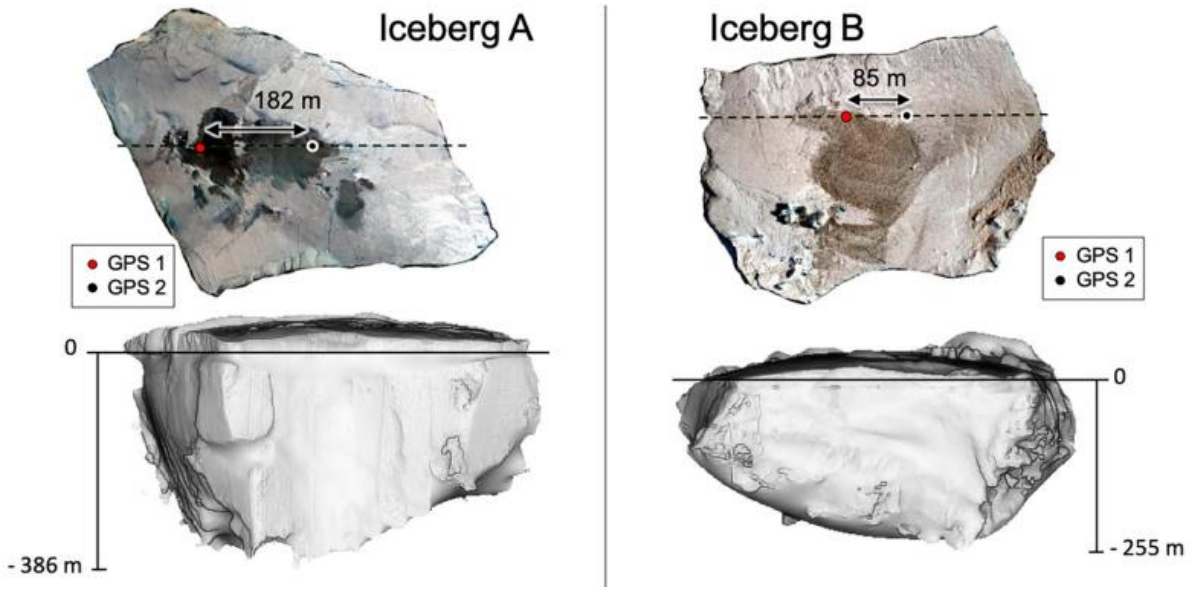

Figure 2.11. Two iceberg geometries scanned by Schild et al. (2021) in Sermilik Fjord constructed from multibeam and drone surveys with the location of two GPS locations noted by the black and red points (from Schild et al., 2021).

2.2.2 Iceberg area size distributions

Iceberg distributions can be used as a proxy to infer glacier calving styles through both space and time (e.g. Scheick et al., 2019), as well as constraining how icebergs disintegrate (Kirkham et al., 2017). There is an assumption that at the time of calving and in the near-terminus region, icebergs will follow a power law distribution (Sulak et al., 2017), but transition to a lognormal distribution down fjord and into the open ocean. This transition is thought to occur because melting is the main process controlling iceberg disintegration and thus the best description of the distribution (Kirkham et al., 2017). Rather, power laws indicate fracture and the subsequent calving is the predominant method of controlling iceberg distributions. Recent research however has suggested power law distributions at the time of calving could be too simplistic to describe the complexity of the iceberg distribution. High temporal resolution radar sampling at Store Glacier showed a bimodal iceberg distribution between meltwater plume surfacing and the frequency of calving events, suggesting there is no relationship between iceberg size and frequency (Cook et al., 2021). Work such as these highlight the need for higher spatial and

temporal resolution field-based observations to identify the detail needed to capture complex distributions which remote sensing approaches cannot.

It is possible to observe iceberg distributions as proxy data to infer changes in glacier calving style. Scheick et al. (2019) utilised this technique to determine iceberg size variability through time as a result of the frontal retreat of Sermeq Kujalleq, which changed from an annually floating terminus calving larger icebergs, to a seasonally grounded terminus, causing much smaller icebergs to be calved.

Power laws are heavy tailed distributions where the probability of the distribution decreases as a power of its magnitude (Clauset et al., 2009). To fit power law distributions, an x_{min} must be defined, which removes values beneath a given threshold value. These distributions have been used across a handful of fjord environments in Greenland to infer calving dynamics by deriving alpha values (power law slopes) to describe iceberg sizes (Table 2.2). Power law slope values reported for Greenlandic glaciers range from -1.23 to -2.89. More negative values are indicative of smaller icebergs in the distribution (e.g. -2.89), whereas less negative values (e.g. -1.23) suggest the presence of larger icebergs. These values can help us decipher iceberg distributions and the behaviour of their parent glacier, i.e. iceberg sizes can change through time due to glacier calving styles (Scheick et al., 2019) and therefore provides opportunities for remote sensing methods to infer the behaviour of calving across the ice sheet.

Table 2.2. Comparison of power law slope values reported for different marine-terminating glaciers across Greenland. Under each study, the defined x_{min} value is noted to show how it can vary spatially and to highlight these iceberg distributions are therefore not directly comparable.

	Sermilik	**Kangerlussuaq**	**Kangerlussuup**	**Rink**	**Disko Bay/Ilulissat**
Enderlin et al. (2016) *(x_{min} = not disclosed)*	-1.90 to -2.10				-2.10 to -2.30
Sulak et al. (2017) *(x_{min} = 2000 m^2)*	-2.00		-1.62	-1.87	
Scheick et al. (2019) *(x_{min} = 1800 m^2)*					-1.89 to -2.89
Rezvanbehbahani et al. (2020) *(x_{min} = 288, 387, 3200, 12000 m^2)*	-1.27 to -1.29	-1.23 to -1.24			

Handling the iceberg data correctly is crucial for deriving power law distributions and the subsequent slope values (α exponent). There are a few key definitions which require careful attention to fit the distributions, mainly the x_{min}. This value is a threshold which removes icebergs below a certain size because smaller icebergs result in less robust fits because they do not follow the same size distributions when compared to their larger counterparts (Scheick et al., 2019), therefore skewing the α value and potentially misinterpreting the data. If the x_{min} is defined too low, the α exponent will be influenced and skewed, yet if the value is defined too high, especially at glaciers which calve smaller icebergs, there will be significant data loss. If users are wanting to compare iceberg distributions temporally at the same glacier, the x_{min} value needs to be defined equivalently across all images. It is also important that the data from each individual image is handled exclusively and not just amalgamated into one sample to infer a single α value. Rather, it is more effective to handle each iceberg dataset from each individual image, e.g. 17 images results in 17 exponents being derived to provide a range of values to be used to help infer iceberg characteristics, constraining calving dynamics.

2.2.3 Iceberg freshwater flux

Icebergs contain and release significant amounts of cold, freshwater into a fjord environment, influencing circulation, stratification and salinity (Moon et al., 2018; Davison et al., 2020a). They are responsible for 60% of the total freshwater fluxes from the GrIS (Bamber et al., 2012). A global circulation model has shown freshwater contribution from the West Greenland Shelf has gradually freshened the surface of the Labrador Sea, but is yet to have a significant impact of the Atlantic Meridional Overturning Circulation (AMOC) (Böning et al., 2016). Icebergs calved in the western sector of Greenland usually enter Baffin Bay and drift south because of the Labrador Current, however eastern icebergs rarely do so, instead the southeast sector account for 60% of all the icebergs which cross the Labrador Sea (Marson et al., 2018).

In SF, icebergs contribute to 85% of the freshwater flux, 65% of which was from Helheim Glacier alone (Mernlid et al., 2010). Just over three-quarters (78%) of iceberg melt is released beneath 20 m of the ocean surface, with up to 100% of the melt continuing at depth in SF (Moon et al., 2018). In SF, 91% of the total iceberg volume is melted and released as freshwater before exiting the fjord, meaning only as much as 15% of all ice calved leaves as a solid ice flux (Moyer et al., 2019). These freshwater flux values have been calculated for June (1270 ± 735 $m^3 s^{-1}$), July (1200 ± 700 $m^3 s^{-1}$), August (3410 ± 1975 $m^3 s^{-1}$) and September (1150 ± 670 $m^3 s^{-1}$) in SF (Moyer et al., 2019). Davison et al. (2020a) found modelled submarine iceberg melt in SF cools the fjord waters by up to 5ºC and this release of freshwater drives a 10% increase in net up-fjord heat flux, thus forcing warmer water to the glacier front, altering the geometry and influencing calving through submarine melt (Section 3.1.3). Ice mélange water fluxes dominate the freshwater budget in Illulissat Isfjord (678 – 1346 $m^3 s^{-1}$) and SF (126 – 494 $m^3 s^{-1}$) (Enderlin et al., 2016). Recent work by Rezvanbehbahani et al. (2020) has shown small icebergs in SF, which may have been undetectable previously from satellite imagery, contribute significantly to the total freshwater budget (melt rate of ~2020 $m^3 s^{-1}$).

Between 2009 and 2013, Ilulissat Isfjord's mean freshwater flux was calculated at 70.6 ± 4.2 km^3, 85% of which was because of icebergs calved from Sermeq Kujalleq (Mernild et al., 2015). At seven of Greenland's marine-terminating glaciers, iceberg melt rates tend to be low and uniform until 200 m depth, but steadily increase to 350 m (Enderlin et al., 2018).

2.2.4 Iceberg modelling

2.2.4.1 Ocean-iceberg modelling

As shown previously, solely deriving datasets from remote sensing and/or in-situ observations alone is extremely challenging and therefore ocean-iceberg modelling can be used to assess iceberg drift (Smith, 1993) and distributions (Bigg et al., 1997), as well as meltwater fluxes (Davison et al., 2020a). One such model is the Nucleus for European Modelling of the Ocean (NEMO) (e.g. Marsh et al., 2015). Ocean-driven retreat of Greenland's marine-terminating glaciers constitute one of the greatest uncertainties in forward-looking sea-level rise models (Edwards et al., 2020) because of limited observational data at calving fronts across the ice sheet (Sutherland et al., 2019).

Iceberg modelling of the 20th century has shown changes in the calving regimes of Greenlandic marine-terminating glaciers corresponding to declining sea ice cover and warming sea surface temperatures in the Labrador Sea and Baffin Bay, which in turn increases calving rates (Bigg et al., 2014).

Modelling of icebergs within the ocean has predominately occurred in the Southern Ocean, rather than icebergs calved from the GrIS. Modelled motion in the Weddell Sea found the Coriolis force keeps icebergs contained in the coastal current around Antarctica and topographic features actually allow icebergs to leave these coastal regions (Gladstone et al., 2001). Simulations of drift trajectories of iceberg C-7 suggest dense sea ice (concentration less than 90%) coverage can trap icebergs and enhance their movement as it creates momentum of the wind over a large area (Lichey and Hellmer, 2001). Stern et al. (2017) found tabular icebergs are forced from the ice shelf because of ocean currents, wind and the Coriolis force, with melt motion upwelling along the sides of icebergs, entraining ambient water and therefore warming the surface water. Modelling studies are increasing their scale with increasing complexity, for example, England et al. (2020) simulated large tabular icebergs which were 1000 km^2 in area size, this being 400 times larger than previous work.

2.2.4.2 Glacier-iceberg modelling

Having the ability to model glacier calving events is somewhat challenging and has been for decades. Glacier calving dynamics are poorly implemented in ice sheet models and represent one of the major uncertainties in the future behaviour of ice sheets (Edwards et al., 2020). Two general 'calving laws' currently exist in glaciology: 1) *calving rates* which are based on model derived stress or strain rate of the glacier itself at its calving front, e.g. von Mises (Morlighem

et al., 2016) and 2) *calving position* which infers calving loses from the depth of both surface and basal crevasses from stresses, ice geometry and water pressure (Benn et al., 2007b).

As numerical modelling of calving events is computationally expensive (Åström et al., 2013; Åström et al., 2014), it is difficult to incorporate them into larger scale, ice sheet models. Despite a substantial community effort to derive a calving law (Brown et al., 1982; Van der Veen, 1996; Vieli et al., 2001; Benn et al., 2007; Nick et al., 2010; Levermann et al., 2012; Morlighem et al., 2016; Mercenier et al., 2018; Schlemm and Levermann, 2019), not one is able to be universally applied across different glacial environments (e.g. outlet glaciers, unconstrained ice shelves). Calving laws are parameterisations (i.e. a physical approximation of real-world processes), whereas particle modelling (e.g. Åström et al., 2013; Åström et al., 2014) attempts to actually model the real-world processes (and is therefore computationally heavy), but are spatially and temporally limited in application.

Choi et al. (2018) modelled four calving laws at nine marine-terminating glaciers in Greenland: height-above buoyancy (e.g. Vieli et al., 2001); crevasse-depth calving (Benn et al., 2007; Benn et al., 2017); eigencalving (Levermann et al., 2012) and von Mises tensile stress (Morlighen et al., 2016), finding the von Mises most appropriate because 67% of the modelled flowlines were within 500 m of empirical observations. Wider modelling of 50 Greenlandic marine-terminating glaciers using six calving laws (Table 2.3) found the crevasse depth calving model (Benn et al., 2007b) was the most accurate deriving calving conditions temporally (Amaral et al., 2020). However, it suggested the crevasse water depth parameter in the model is redundant because there is no correlation between increasing water depth during the summer months and a latitudinal gradient (Amaral et al., 2020).

Table 2.3. The six models used by Amaral et al. (2020) that applied two calving laws (calving rate and calving position) to identify the success of these approaches at 50 tidewater glaciers around Greenland.

Calving model type	Calving model	Author(s)
Calving rate model	Eigencalving	Levermann et al. (2012)
	Von Mises	Morlighem et al. (2016)
	Surface stress maximum	Mercenier et al. (2018)
Calving position model	Height above floatation	Van der Veen (1996)
	Fraction above floatation	Vieli et al. (2001)
	Crevasse depth criterion	Benn et al. (2007b)

2.2.5 Biogeochemical cycling

Icebergs are not only a source of freshwater, they are also carriers of sediments and nutrients because glacier activity promotes the erosion and weathering of rocks in their environment. Again, there is a greater abundance of research when assessing the influence and delivery of biogeochemical cycling from Antarctica's icebergs to the Southern Ocean when compared to our current knowledge across the GrIS. Biogeochemistry cycling research in Greenland predominately focuses on glacial meltwater and the subsequent impacts (Hopwood et al., 2015; Cape et al., 2019; Hendry et al., 2019; Seifert et al., 2019). Despite icebergs accounting for a significant influence of freshwater in Greenland's fjords, our understanding of the impacts on biogeochemical cycling is much more limited. In Nuup Kangerlua, icebergs contribute to 22% of the total meltwater flux (Van As et al., 2014) and have a large variety of dissolved silica concentrations which are as high as 18 µM in debris-rich samples (Meire et al., 2016). It has been suggested similar processes of iceberg upwelling of nitrate from meltwater which will stimulate biological activity as seen in the Southern Ocean, probably occurs in Arctic and sub-Arctic waters (Smith et al., 2013). Recent work by Bigg et al. (2021) suggested it is feasible that iceberg-delivered iron can contribute to enhanced productivity and it would be worth quantifying across greater regions of the northwest Atlantic.

A large proportion of iceberg biochemistry research in the Southern Ocean is owed to iron fertilisation (e.g. Raiswell et al., 2008; Pollard et al., 2009; Shaw et al., 2011; Duprat et al., 2016; Wu and Hou, 2017). Icebergs provide a similar amount of bioavailable iron to the Southern Ocean (0.06 – 0.12 Tg yr^{-1}) when compared to aeolian dust deposition (0.01 – 0.13 Tg yr^{-1}), which was originally thought to be the primary source (Raiswell et al., 2008).

It has been proposed that giant iceberg fertilisation could be responsible for a fifth of the Southern Ocean's downward carbon flux and can enhance chlorophyll levels up to ten times the length of the original iceberg which continues for over a month (Dupart et al., 2016). Iceberg enhancement of carbon can result in a higher abundance of diatoms, zooplankton, higher predators and macronutrient nitrate (Lin et al., 2011). The presence of smaller icebergs results in greater net primary productivity rates when compared to areas of iron deficient sectors in the Southern Ocean: 21% higher in the seasonal ice zone, 16% in the permanent open ocean zone and 12% in the polar front zone (Wu and Hou, 2017). Similar processes are likely to occur around Greenland and in the fjords, however little research has constrained the influence of iceberg size distributions on biogeochemical cycling.

2.2.6 Icebergs as habitats

Different habitats utilise icebergs for breeding and denning sites. For example, there have been six den observations in north and northeast Greenland of polar bears (20 adult females and 35 cubs) in snowdrifts around grounded icebergs frozen in sea ice and in close proximity to the Northeast Water Polynya (Laidre and Stirling, 2020). In 2014, a colony of Ivory Gulls were identified breeding on an iceberg 70 km from Northeast Greenland, again in close proximity to the Northeast Water Polynya (Nachtsheim et al., 2016). However, it is completely unknown whether changes in iceberg distributions from an ever-evolving GrIS can impact on the potential for habitat location in the Arctic.

2.2.7 Icebergs as risks

Icebergs populate fjords, seas and oceans which all host shipping lanes and coastal communities. Logistically, icebergs pose as a significant risk to shipping and coastal infrastructure and it is therefore imperative to constrain the extent of iceberg risk in a changing Arctic climate with increased human exposure in the polar regions (e.g. shipping, tourism). While 26% of the 371 recorded ships colliding with icebergs were abandoned or sank (Hill, 2005), understanding the future evolution of iceberg distributions are important for established (oil and gas) and continually developing industries (e.g. potential for expanding offshore windfarms). Bigg (2015) suggested undersea cables (communications) and pipes (oil / gas) could be at risk from icebergs, depending on their keel depths which could rupture the in-situ infrastructure.

Recent research has shown icebergs do not just present a risk to humans, instead submarine landslides can be caused from grounded icebergs, resulting in marine-geohazards

(Normandeau et al., 2021). When icebergs 1) calve from a glacier and/or 2) calve into smaller icebergs, tsunami waves will often result and pose hazards to local communities and/or tourists in nearby localities (e.g. tours, kayaking and/or local coastal communities). A large calving event at Eqip Sermia, west Greenland caused a tsunami wave as high as 50 m, travelling at 25 – 33 m s^{-1} (Lüthi and Vieli, 2016). In 1995, an iceberg calved in close proximity to a coastal community and caused a tsunami wave, toppling boats (Mendsonboaz, 2009). In 2018, residents of a small settlement on Innaarsuit Island were evacuated to higher ground due to the risk posed from a 100-meter high iceberg which threatened subsequent fracturing and calving, thus the production of tsunami waves (The Guardian, 2018). The underwater sound (acoustic energy on the order of 0.1 to 7.6 tonnes TNT-equivalent) of iceberg calving events proceeding the ice front of Bowdoin Glacier have been suggested to cause mechanical hearing damage to marine mammals (narwhals and seals) in the fjords across Greenland (Podolskiy et al., 2022).

While increasing Arctic tourism (e.g. Bislev and Smed, 2018) provides wider public engagement with 40% of tourists (from a 25-sample group) choosing to visit Greenland to see icebergs (Leoni, 2019), people entering these pristine environments is somewhat controversial and results in a greater risk to human safety.

2.2.8 Paleo-iceberg importance

While the scope of this Chapter is to review the contemporary understanding of Greenland's icebergs, it would be remiss to neglect the paleo-importance of the Northern Hemisphere ice sheets as they provide insights into potential outcomes of a melting Greenland. Icebergs are not only significant in the contemporary context, rather they have influenced the global climate in the past, noticeably Henrich Events (Heinrich, 1988). These occurrences were as a result of the catastrophic release of icebergs from the Northern Hemisphere ice sheets into the North Atlantic during the last glacial maximum (Heinrich, 1988; MacAyeal, 1993) and correspond with the cooling stadial of Dansgaard-Oeschger cycles (Dansgaard et al., 1993). This enormous iceberg discharge overwhelmed the AMOC, a distributor of global heat, and led to the near and/or complete shutdown of the system, cooling the Northern Hemisphere (McManus et al., 2004).

These events can be traced through the sediment records in the form of ice-rafted debris (IRD) which constitute glacial sediment layers (Bond et al., 1992), resulting in the six most recent Heinrich Layers (HL1 – HL6) (Grousset et al., 1993). HL3 and HL6 display different IRD characteristics, suggestive of a European Ice Sheet origin, compared to those of HL1, HL2,

HL4 and HL5 derived from the Laurentide Ice Sheet (Grousset et al., 2000). HL3 and HL6 are dynamically different or 'atypical' to the other layers because less IRD was deposited during these events from the Laurentide Ice Sheet when compared to the 'typical' layers (HL1, HL2, HL4, HL5). Each layer has their own individual distinction and thus could be important when constraining their origin (Jullien et al., 2006). Evidence from 17 cores surrounding the northern part of the Atlantic revealed European Ice Sheets may have surged before the Laurentide and suggests the North American Ice Sheets were not solely responsible for the Heinrich Events (Snoeckx et al., 1999). IRD from both HL3 and HL4 in the Norwegian sea has Scandinavian origin, revealing the Laurentide Ice Sheet was not the sole cause of the iceberg discharge (Snoeckx et al., 1999).

Recent work by Condron and Hill (2021) suggest HL3 and HL6 originated from the Laurentide Ice Sheet and could be characteristically distinct from the other layers because icebergs were transported by large meltwater floods making their IRD dynamically different after identifying iceberg scours as low as 24^{o} N in Florida Keys (Figure 2.12). Iceberg scours found 39^{o} N on the modern sea floor near New Jersey are related to the four most recent Henrich Events with H1 and H2 eroding scours made by H3 and H4 (Goff and Austin, 2009). Modelling of icebergs in the North Atlantic during the last glacial maximum has revealed that while total iceberg volume can remain the same, parametrising different iceberg sizes can result in notably varied drift patterns (Fendrock et al., 2022).

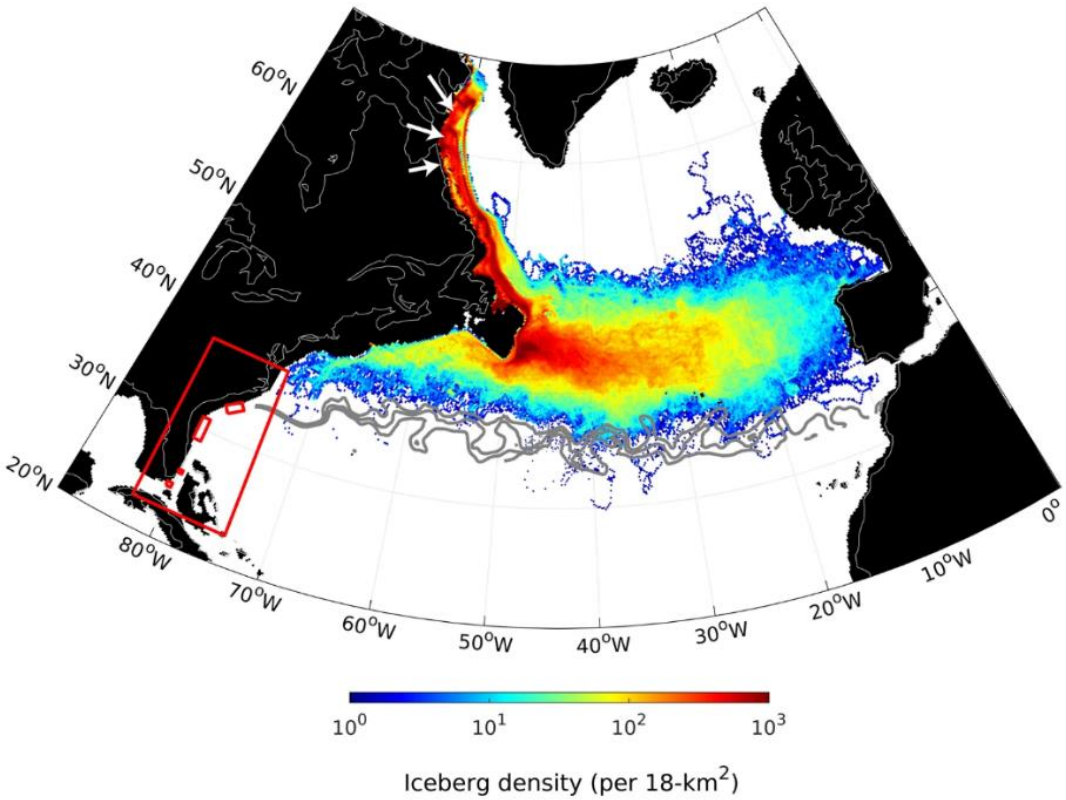

Figure 2.12. Simulated iceberg trajectories during the last glaciation with the calving margin situated in close proximity to the Hudson Bay highlighted by white arrows. The red box (and insets) show the latitudinal limit of where icebergs reached during the simulation with the lowest icebergs being shown to drift to as low as 24° N (Florida Keys) (from Condron and Hill, 2021).

3.3 **Conclusions**

This Chapter has provided an in-depth review of the icebergs calved by the GrIS. Observations of icebergs have increased from both remote sensing and in-situ measurements in the last ten years, however they remain spatially and temporally limited at an ice sheet scale. This is in part due to the difficult nature of observing the ice-ocean interface due to spatiotemporal coverage and accessibility to these environments (Figure 2.13).

There is an identifiable lack of available three-dimensional (i.e. volume) iceberg data derived from satellite imagery which can provide information regarding an iceberg's melt rate and freshwater capacity. Studies convert their two-dimensional iceberg datasets (planform surface area) to a volume using an empirically derived equation (Equation 3.1) which is formulated from 712 icebergs with no statistical uncertainties. Future work should look to datasets that have the capability of deriving volumes (e.g. DEMs) directly from iceberg observations. This is particularly important for numerical models having to currently convert iceberg input from two-dimensions to three-dimensions. If the newly calculated volume from their surface area is

over- or under-estimating the volume of the iceberg, the subsequent output of melt rate/freshwater flux will be fundamentally flawed in a model's domain.

Automating iceberg detection is difficult, however it is the only realistic approach to increasing the quality and quantity of iceberg observations at an ice sheet scale. Workflows need to be continually developed using a range of different datasets (e.g. optical, SAR, DEMs) to provide new insights into glacier calving styles and fjord dynamics. Output from these remote sensing approaches should focus on deriving iceberg trajectories through fjords where possible to better understand how icebergs decay through space and time. This is not just important for those scientifically interested in icebergs, rather logistical stakeholders invested in both tourism and shipping.

By attaining more detailed datasets of iceberg outlines through space and time, opportunities arise to identify underlying relationships between iceberg sizes and glacier processes which has not been achievable to date. This specific rationale provides a strong basis for a large proportion of this thesis (Chapters 5 and 6) to create large iceberg datasets and see how they relate to glacier specific processes at both glacier and ice sheet wide scales.

Field-based observations provide a level of detail that is incomparable to satellite imagery. However, more measurements are required in a range of Greenland's fjords, particularly those looking at the subsurface geometry of an iceberg as the shape of the keel is critical for calculating melt rates. In-situ studies should also analyse when an iceberg does melt, quantify the trajectory of the meltwater and how it interacts with the fjord column.

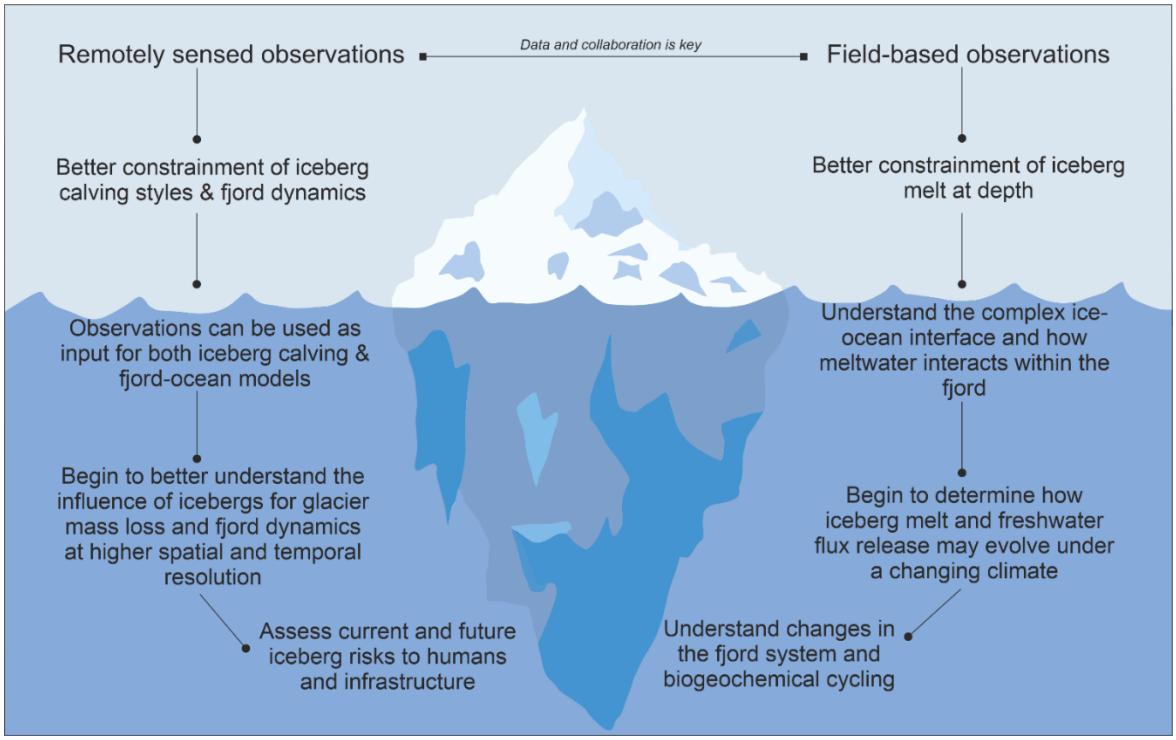

Figure 2.13. Visual workflow of how both remotely sensed and field observations can help scientists better understand iceberg dynamics and subsequent sub-disciplines on both large spatial and temporal scales.

Chapter 3: Google Earth Engine and ArcticDEM

3.0 **Introduction**

This Chapter describes and discusses Google Earth Engine (GEE) and ArcticDEM data to provide a broad overview of their capabilities and potential for academic, non-profit and commercial research. When referring to ArcticDEM strip data, this thesis is specifically referring to the version (v) 3 dataset, unless explicitly mentioned otherwise. The aim of this Chapter is to show the high-level capabilities of GEE and ArcticDEM across a wide range of different research topics. The versatility of ArcticDEM has allowed the development of research projects in both the subglacial (Bowling et al., 2019) and supraglacial setting (Barr et al., 2018; Benedek et al., 2021) on the Greenland Ice Sheet. Transient features such as icebergs at the ice sheet margins are identifiable on time-evolving ArcticDEM strips, but the dataset has never been used to analyse iceberg size distributions and dynamics.

3.1 **Google Earth Engine**

GEE is a cloud-computing platform with petabytes worth of datasets ingested into its catalogue (Gorelick et al., 2017). This platform is free for individual licenses for research, education and non-profit use and allows data to be accessed and analysed via the Google Cloud. Traditional methods of remote sensing would typically involve bulk downloads of huge quantities of data on to a user's local computer and/or an external hard drive where the subsequent images have to be stored and later processed. Storage and processing are both time and computationally expensive. However, GEE's cloud computing nature avoids both of these rather large problems remote sensors encounter.

GEE is used across the geosciences and not just limited to glaciology. For example, the capabilities of GEE have been utilised in numerous earth surface studies, including: glaciology (e.g. Lea, 2018; Smith et al., 2020;), permafrost (Zakharov et al., 2020), coastline variability (Vos et al., 2019), coastal wetlands (Wang et al., 2020), fluvial geomorphology (Boothroyd et al., 2021) and canopy cover (Anchang et al., 2020). These are just a few examples of different ways of using GEE. However, it shows the versatility and potential that cloud computing has to conduct world leading research and highlights the huge potential for its use by glaciological remote sensors, beyond the aforementioned studies. As evidenced in some of the above studies, GEE is able to perform basic land and ocean surface mapping, as well as more advanced technical machine learning approaches utilising algorithms via TensorFlow, for example. Consequently, GEE is able to provide a very high level of remote sensing analysis with varying approaches across the discipline.

GEE is able to access petabytes of satellite imagery rapidly with only a few lines of code. Using Landsat 8 as an example, a user can open the GEE code editor and on the interactive map navigate to a region of interest (ROI) which can be defined onscreen using a geometry tool. From here, the user can then write (or alter the default) code which will obtain every available Landsat 8 tile that intersects the defined ROI (i.e. an image collection). These data are then available for analysis, meaning all data storage and processing occurs within GEE. Once the performed analysis has been completed and if the user requires this data offline and outside of GEE, the resulting output can be exported in various geospatial formats via raster (image), vector (point) or tabular (e.g. csv) data to their Google Drive.

The online GEE code editor utilises the JavaScript programming language, however recently, an Earth Engine Python API has been developed. This allows GEE datasets to be accessed via Python and its syntax, meaning the data is even more accessible as new languages do not necessarily need to be learnt (i.e. if Python is already a known language to the user). Ultimately, it does not matter which route a user decides to take to access GEE, however the main benefit of utilising the Python API is the ability to access built in packages (e.g. Matplotlib, Seaborn etc.) to visualise the derived data as the default plotting in GEE is more limited when compared to Python.

In GEE itself, raster data are stored as image collections, whereas vector data are stored as feature collections. To ensure efficient code development and correct function usage it is important to correctly utilise both image and feature collections. To apply the same analysis on every available image/feature within a collection, mapping functions must be utilised which are fundamentally ‘for loops’ in other programming languages. Mapping functions can be difficult to implement for users new to the GEE platform due to their stylistic differences when compared to a for loop. However, they are a significant component for automating workflow development.

While the advantages far outweigh the disadvantages of GEE, complex remote sensing approaches still require thoughtful and efficient code developments which can be challenging for those new to the platform. Graphical user interfaces are one-way scientists can provide their data as assessable tools which require no coding (e.g. Lea, 2018; Smith et al., 2020). However robust these tools may be, they will only be able to derive the output designed by the operators at their inception. Users wanting to develop new workflows to analyse datasets will ultimately have to write and navigate the somewhat technical code and functions within GEE.

3.2 **ArcticDEM data**

The Arctic Digital Elevation Model (ArcticDEM) is an open access resource developed by the Polar Geospatial Center which is part of the University of Minnesota (Porter et al., 2018). These data are divided into two key resources: 1) ArcticDEM strip data and 2) ArcticDEM mosaic, both of which cover the spatial extent of the Arctic.

ArcticDEM data has been used across the breadth of the Arctic to observe and analyse earth surface dynamics and landscapes including, glaciers (Barr et al., 2018) and rivers (Lu et al., 2020), as well as mapping biomass stocks (Puliti et al., 2020) and lava flows (Dai et al., 2018). These data have also been used to supplement other datasets, for example, assisting the identification and location of subglacial lakes situated beneath the GrIS (Bowling et al., 2019). Research has also been able to utilise the ArcticDEM by differencing the elevation change through time from the strip data to asses supraglacial lake drainages (Benedek et al., 2021).

ArcticDEM strip data is derived from overlapping WorldView (50 cm resolution) image pairs that are captured by the Maxar Constellation satellites. The ArcticDEM strip data have a high, 2 m spatial resolution (10 cm vertical accuracy) and each strip tends to cover 13-17 km width and up to 120 km in length. As a result of being derived from continuous observations, ArcticDEM strip data have the advantage of providing a temporal footprint, thus potentially allowing for time series analysis (e.g. surface elevation change).

ArcticDEM mosaic data is constructed through the stacking of the highest quality strips (v3 n = 9228) to output one digital elevation model (DEM) image that covers the entire Arctic at 2 m to 1 km spatial resolution (depending on which product is required). By amalgamating the data into one DEM, this removes the time-evolving snapshot of the strip data. By combining strip data into the mosaic, this results in an Arctic-wide spatial complete DEM. However, some data gaps can still exist in the mosaic image due to some sporadic strip data coverage. Which dataset to use is fundamentally dependent upon the research question being asked, e.g. determining whether a user requires a snapshot of an area or a time evolving DEM. However, both products provide high spatial resolution opportunities to asses surface elevation change across the Arctic which other products are unable to do.

This thesis utilised the ArcticDEM strip data as it can provide spatiotemporal analysis of icebergs across the ice sheet which the mosaic product cannot provide. The spatial coverage of ArcticDEM data in GEE are comprehensive (Figure 3.1), but only provide very basic metadata associated to each DEM, including, but not exclusive to, the acquisition dates of both stereo

images which constructed the DEMs, the XYZ registration and the DEM ID number. The X and Y axis provide the coordinate position of the DEMs and Z provides the elevation. The Z dimension is determined from altimetry derived ground control points from IceSAT to improve the accuracy of the elevation axis (Porter et al., 2018). The limited metadata associated with each ArcticDEM strip is potentially problematic for automated DEM filtering of cloud contaminated DEMs which are inappropriate for analysis. Cloud is one of, if not the biggest drawback of utilising optical imagery and because ArcticDEM strips are constructed from these data, it is potentially problematic that their metadata does not contain such a property.

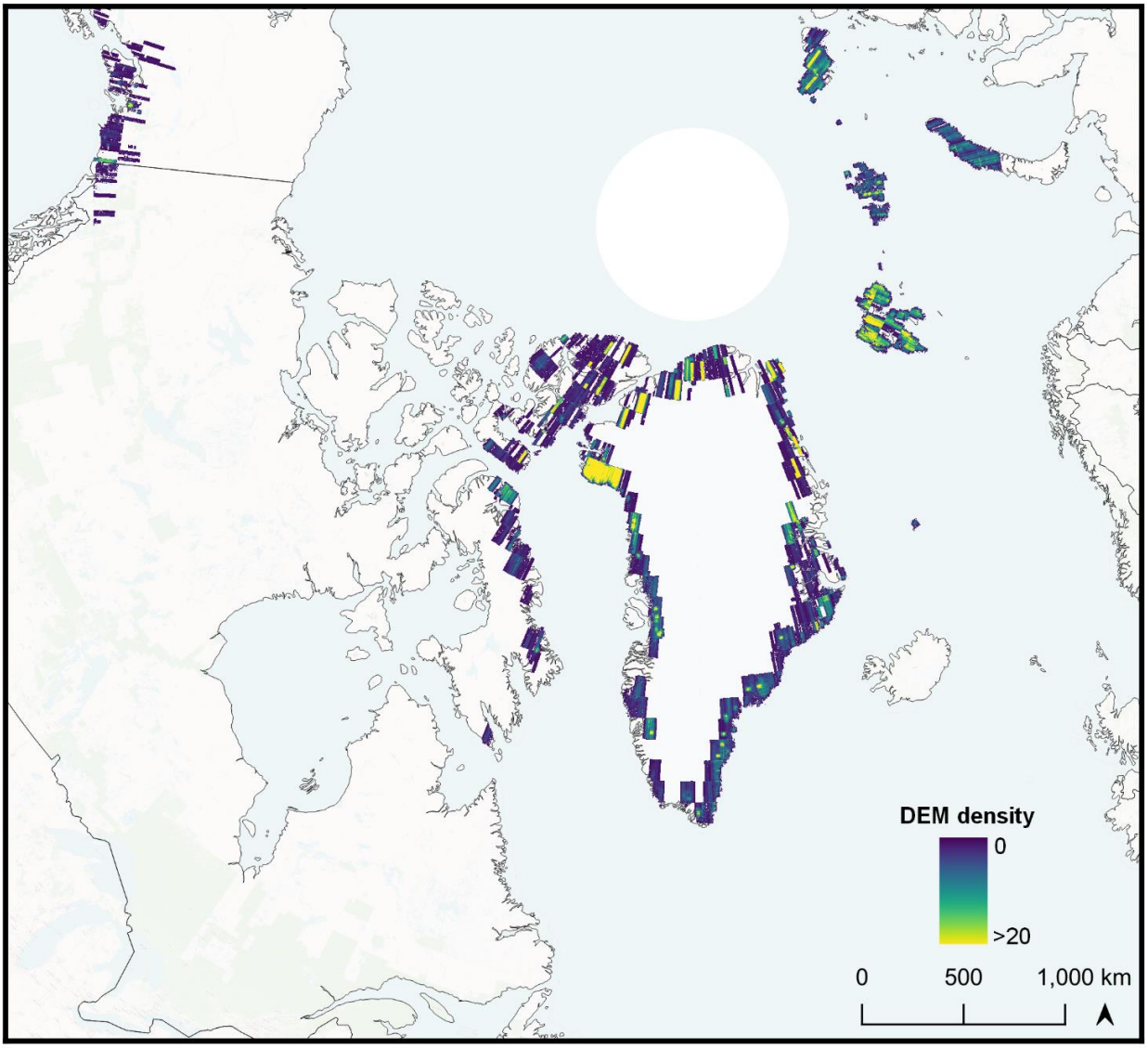

Figure 3.1. GEE ArcticDEM v3 strip data availability (July-October) for Greenland's calving margins and all marine/lake/shelf terminating glaciers extent in the remainder of the Arctic between 2009 and 2017.

ArcticDEM strip data are constructed through stereophotography, e.g., image pairs forming one, three-dimensional DEM output. Both the WorldView images used to construct the DEMs

do not have to be acquired on the same day. However, this poses problems for transient features (e.g. icebergs). Nevertheless, DEMs exist which have image pairs that were acquired on the same day (within seconds) due to forward and back looking sensors. These DEMs are of interest for analysis here as it limits the impact of iceberg drift in the fjord and ensures the most accurate snapshot of iceberg distributions at the time of data acquisition.

ArcticDEM v3 has been available for the last five years and the data spans between 2009 and 2017. The most recent release (v4) will extend the temporal period up to 2021, allowing a decade worth of available surface elevation data across the Arctic. At time of writing, v4 strip data had been released but not the mosaic, explaining why the latest strips have not been ingested into GEE. Assuming ingestion, the available ArcticDEM data within GEE will be comprehensive and for the first time provide open-access, continuous observations of surface elevation change across the Arctic.

3.3 **Summary**

Using ArcticDEM v3 strip data in GEE represents a powerful combination of a large dataset and cloud computing that is capable of dealing with data at scale. Accessing these data without any download requirements is unprecedented in the remote sensing world and provides opportunities for rapid data processing at comprehensive spatial and temporal scales. Time-evolving ArcticDEM strip data are able to provide time-series analysis of surface elevation change across the entire Arctic and is an underutilised, open-access data source. GEE provides a platform for tackling challenges on large temporal and spatial scales the discipline of glaciology currently faces.

Chapter 4: Automated ArcticDEM iceberg detection tool: insights into area and volume distributions, and their potential application to satellite imagery and modelling of glacier-iceberg-ocean systems

Connor J. Shiggins[1], James M. Lea[1], Stephen Brough[1,2].

[1]*Department of Geography and Planning, School of Environmental Sciences, University of Liverpool, Liverpool, L69 7ZT, United Kingdom.*

[2]*Central Teaching Laboratory, Faculty of Science and Engineering, University of Liverpool, United Kingdom.*

Author contributions: Connor Shiggins led the writing and conducted all of the analysis. James Lea and Stephen Brough provided conceptual advice and contributed towards the writing of the paper.

Published in *The Cryosphere*, 2023.

This Chapter is provided as how it was published in The Cryosphere.

Summary: This Chapter characterises the challenges of automating iceberg detection using cloud computing and digital elevation models (DEMs). Identifying icebergs from satellite data has typically occurred on two-dimensional imagery, however DEMs provide a unique opportunity to investigate iceberg volume distributions due to their three-dimensional structure. The iceberg detection method applied here is able to derive iceberg volumes from a substantial number of iceberg observations (Objective 1) that has been packaged into a graphical user interface (Objective 2) for open-access analysis of three-dimensional iceberg data. The subsequent automated output has been validated by a manual operator and found the iceberg observations are applicable for inferring iceberg size (area and volume) distributions in three of Greenland's fjords.

Abstract. Iceberg calving accounts for up to half of mass loss from the Greenland Ice Sheet (GrIS), with their size distributions providing insights into glacier calving dynamics, and impacting fjord environments through their melting and subsequent freshwater release. Iceberg area and volume data for the GrIS are currently limited to a handful of fjord locations, while existing approaches to iceberg detection are often time consuming and are not always suited for long time series analysis over large spatial scales. This study presents a highly automated workflow that detects icebergs and appends their associated metadata within Google Earth Engine using high spatial resolution timestamped ArcticDEM (Arctic Digital Elevation Model) strip data. This is applied to three glaciers that exhibit a range of different iceberg concentrations and size distributions: Sermeq Kujalleq (Jakobshavn Isbræ), Umiammakku Isbræ and Kangiata Nunaata Sermia. A total of 39 ArcticDEM scenes are analysed, detecting a total of 163738 icebergs with execution times of 6 minutes to 2 hours for each glacier depending on the number of DEMs available and total area analysed, comparing well with manually digitised outlines. Results reveal two distinct iceberg distributions at Sermeq Kujalleq and Kangiata Nunaata Sermia where iceberg density is high, and one distribution at Umiammakku Isbræ where iceberg density is low. Small icebergs (< 1000 m^2) are found to account for over 80% of each glacier's icebergs however, they only contribute to 10-37% of total iceberg volume suggesting that large icebergs are proportionally more important for glacier mass loss and as fjord freshwater reservoirs. The overall dataset is used to construct new area to volume conversions (with associated uncertainties) that can be applied elsewhere to two-dimensional iceberg outlines derived from optical or synthetic aperture radar imagery. When data are expressed in terms of total iceberg count and volume, insight is provided into iceberg distributions that have potential applicability to observations and modelling of iceberg calving behaviour and fjord freshwater fluxes. Due to the speed and automated nature of our approach, this workflow offers the potential to interrogate iceberg data on a pan-Arctic scale where ArcticDEM strip data coverage allows.

4.0 **Introduction**

Iceberg production is of critical importance when considering the mass balance of ice sheets and glaciers (Bigg et al., 2014), freshwater fluxes (Enderlin et al., 2016; Davison et al., 2020a), offshore infrastructure (Eik and Gudmestad, 2010), shipping, tourism (Bigg, 2015) and ecological habitats (Laidre and Stirling, 2020). Their area-size distributions can be used to infer glacier calving dynamics (Sulak et al., 2017; Scheick et al., 2019; Åström et al., 2021, Cook et al., 2021) and also estimate freshwater fluxes (Enderlin et al., 2016; Moon et al., 2018; Moyer et al., 2019; Davison et al., 2020a). It has been suggested that icebergs could account for up to 22-70% of the total mass loss by 2100 from the Greenland Ice Sheet (GrIS) (Choi et al., 2021), though how future changes in glacier dynamics will influence iceberg size distributions (and vice versa) is currently poorly constrained.

Multiple different approaches have been taken to iceberg detection, including analysis of optical imagery, synthetic aperture radar (SAR) imagery and digital elevation models (DEMs). Semi-automated and/or automated iceberg detection utilising optical imagery typically involves band thresholding to differentiate ice and water (Sulak et al., 2017; Moyer et al., 2019). However, these approaches often use medium-resolution data (10 – 30 m pixel data, e.g. Landsat and Sentinel-2) that have insufficient spatial resolution to identify the smallest of icebergs or distinguish between larger adjacent icebergs without more complex processing. For example, convolutional neural networks (CNN) have been developed to downsample images, allowing the delineation of smaller iceberg edges at sub-pixel scale (e.g. Rezvanbehbahani et al., 2020). While CNNs provide opportunities, they are often challenging to construct/validate across large spatial scales and require substantial training data that are obtained from user-intensive manual labelling of images.

In optical imagery, the presence of ice mélange (mixture of icebergs and sea ice) in images also proves problematic for automated band thresholding techniques. This arises due to the similar reflectance signal of mélange to that of icebergs, potentially leading to the generation of erroneously large outlines. Additionally, prolonged cloud cover in some parts of the polar regions and polar night can result in large gaps between observations using optical imagery.

SAR data have the potential for more continuous coverage as the active nature of the sensor can penetrate cloud cover, and do not rely on solar illumination to acquire imagery (e.g. Soldal et al., 2019). However, a notable shortfall of both optical and SAR data is that they are only capable of expressing a surface area of an iceberg, with volumes typically estimated using

empirical area-volume relationships derived from DEMs (Sulak et al., 2017; Schild et al., 2021).

Time-stamped ArcticDEM version 3 (v3) (Porter et al., 2018) tiles represent an under-exploited resource that allows the derivation of both iceberg areas and their volumes, providing the opportunity to obtain more complete data than optical and/or SAR imagery. These data are obtained from optical stereo-image pairs acquired between 2009 and 2017 and are available in Google Earth Engine (GEE). These provide high spatial resolution DEMs (2 m posting), though have variable temporal coverage due to cloud contamination and satellite image acquisition tasking. While this archive currently has poor return frequency compared to optical and SAR satellite platforms, its spatial resolution and ability to determine iceberg volumes offers the potential for gaining insights that are applicable to the more frequently acquired optical and SAR derived data.

Due to the significant numbers of icebergs existing at any one time in the polar regions, time-intensive manual delineation is not a practical approach to apply to ice-sheet-wide analysis or even at a single glacier site. However, manually digitising icebergs are viable options for: 1) creating training sets for supervised classification of semi-automated approaches for a selection of image scenes (Sulak et al., 2017); and 2) to generate highly targeted datasets of icebergs, e.g. the Canadian ice island drift, deterioration and detection (CI2D3) database (Crawford et al., 2018).

Iceberg area distributions have previously been used to constrain glacier calving dynamics (Scheick et al., 2019) and determine iceberg disintegration processes (Kirkham et al., 2017). These distributions have previously been described using power laws in particle modelling studies (Åström et al., 2021) and from imagery in areas adjacent to glacier termini, to gain insight into calving dynamics in both Greenland (Enderlin et al., 2016; Sulak et al., 2017; Scheick et al., 2019; Rezvanbehbahani et al., 2020) and Antarctica (Tournadre et al., 2016; England et al., 2020). These relationships describe probability distributions of iceberg size, with Equation 4.1 describing the general form of these relationships,

$$p(x) = Cx^{-\alpha},\ where\ x \geq x_{min} \tag{4.1}$$

where p(x) is the distribution with x representing either area (A) or volume (V), C is a constant and α is the exponent of the power law (or slope value). The value of α (reported hereafter including the negative sign in Equation 4.1) provides an indication of iceberg size distributions at the time of data acquisition with lower values suggesting a higher prevalence of smaller

icebergs, whereas more positive values indicate that relatively larger icebergs dominate. Typical α values for Greenlandic and Antarctic environments have been reported between -1.2 and -3.0. As icebergs drift from Greenland's termini to the open ocean, their distributions have been observed to transition from being best described as power law distributions (suggested to be controlled by calving) to lognormal distributions as melting becomes the primary control on their disintegration (Kirkham et al., 2017).

When fitting icebergs to power law distributions and calculating α, it is important to determine a threshold which removes icebergs below a certain area-size (x_{min}). Where smaller icebergs are included in the distribution, these can result in less robust fits with power laws because they follow different size distributions compared to larger icebergs (Kirkham et al., 2017). Including smaller icebergs in this analysis can therefore skew the α value and potentially misrepresent the data (as discussed in Scheick et al., 2019). Given the larger surface area to volume ratios of smaller icebergs, it is also more likely that their different size distribution arises from more extensive modification by submarine and atmospherically driven melting. Defining the appropriate x_{min} value is therefore critical for investigations that seek to determine how iceberg size is impacted by glacier calving processes.

A further complexity of the x_{min} value is that if the value is defined too high there will be significant data loss that will limit the explanatory value of the distribution. This is especially the case for glaciers where there is a high proportion of small icebergs. For example, at Sermeq Kujalleq (Jakobshavn Isbræ), Scheick et al. (2019) defined an x_{min} value of 1800 m^2 as it improved the fit compared to other x_{min} values tested, appropriately justifying this in terms of both their research question and the glacier being characterised by relatively large icebergs. In other studies, the resolution of imagery available has impacted the range of x_{min} values that can be defined. For example, CNN performed on Planet imagery (3 m optical imagery) resulted in x_{min} values of 288 m^2 and 387 m^2, while Sentinel-2 (10 m optical imagery) required values of 12000 m^2 and 3200 m^2 for Sermilik and Kangerlussuaq Fjords, respectively (Rezvanbehbahani et al., 2020). This demonstrates how the availability of finer spatial resolution data can in some cases also allow the definition of smaller x_{min} values and the retention of more data.

Few studies (e.g. Sulak et al., 2017) have been able to directly estimate iceberg volume, as optical and/or SAR imagery are (without significant further processing) limited to the extraction of iceberg areas only. The three-dimensional shape of an iceberg above the waterline allows its volume to be inferred, though it does not always scale exactly with its planform area.

For example, rafts of icebergs frozen together by mélange/fjord ice that occur at some glaciers will be relatively flatter and have a lower volume compared to single icebergs of the same area that have calved from a glacier. Applying a single iceberg area to volume conversion determined from iceberg data to these rafts would therefore lead to an over-estimation of their volumes.

One of the current difficulties faced by those studying the impact of icebergs on fjords is the lack of available iceberg outline *and* volume data that are suitable for use in numerical models of fjord circulation, stratification and iceberg melting (e.g. Moon et al., 2018; Davison et al., 2020a). Models that include the quantification of iceberg meltwater flux currently assume iceberg area-volume distributions within fjords, though direct observations of these from satellite data are rarely available (e.g. Davison et al., 2020a) This issue is compounded by the time and computational expense involved in the detection of icebergs (e.g. data collection, storage, memory and processing). One solution to this is offered by the GEE cloud computing platform (Gorelick et al., 2017) that provides the ability to rapidly access and process data from multiple different satellites, offering the potential for ice-sheet-wide and global analysis (e.g. Shugar et al., 2020).

This study provides a GEE workflow and easy to use graphical user interface (GUI), using 2-m strip ArcticDEM v3 data (Porter et al., 2018) to automatically detect icebergs at three marine-terminating glaciers on the west coast of Greenland. The aim of this study is to demonstrate the ability of the workflow to automatically generate a large and reliable dataset of icebergs from glaciers of varying size and fjord conditions. In doing so the workflow aims to allow users to gain detailed insight into iceberg area-volume relationships, and identify how these vary between glaciers.

4.1 **Study sites**

Three different marine-terminating glaciers were selected to conduct analysis, identified on the basis of their different fjord environments, iceberg sizes and data availability: (1) dense large iceberg coverage: Sermeq Kujalleq (Jakobshavn Isbræ) (hereafter SKJI); (2) mix of dense iceberg coverage and frequent open water: Umiammakku Isbræ (hereafter UI); and (3) dense small iceberg coverage with occasional open water: Kangiata Nunaata Sermia (hereafter KNS) (Figure 4.1). Regions of interest (ROI) at each glacier were identified to maximise ArcticDEM data availability and reduce the impact of winter/spring seasonal advance of the caving margin during the study period of 2009-2017.

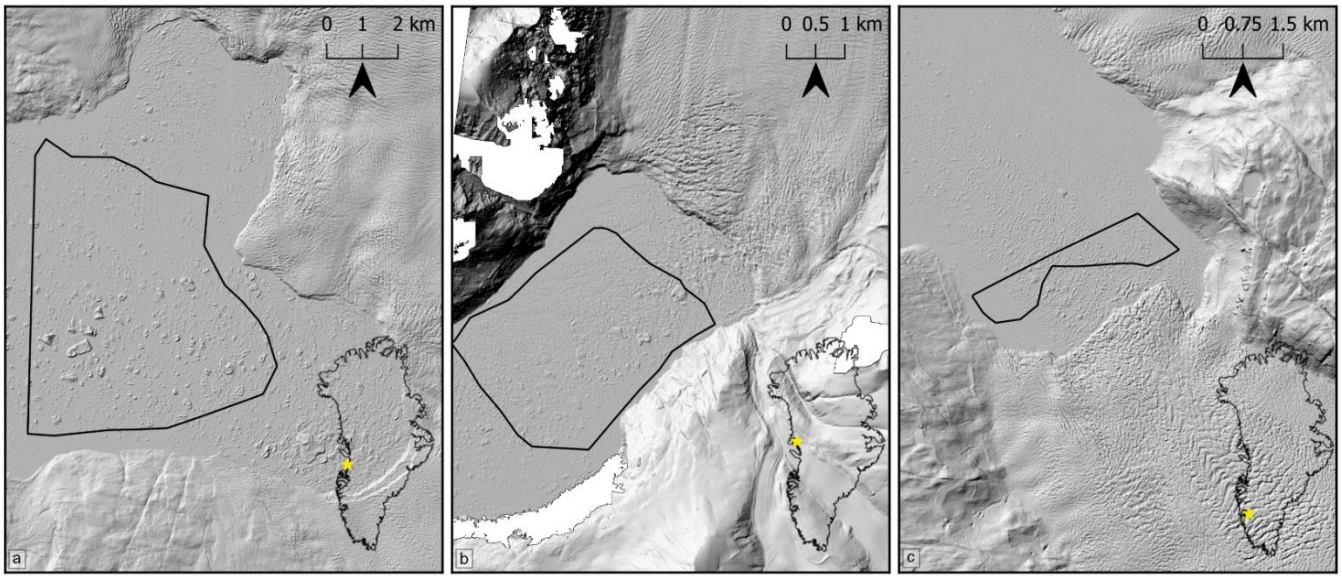

Figure 4.1. ArcticDEM imagery of the near terminus region for a) Sermeq Kujalleq: 69.16° N, 49.91° W, b) Umiammakku Isbræ: 71.42° N, 52.26° W and c) Kangiata Nunaata Sermia: 64.25° N, 49.50° W. The ROIs for each glacier are mapped by black bounding boxes.

SKJI accounts for 45% of the total drainage of Greenland's central west sector, with a mean ice discharge (2010-2018) of 43.64 Gt yr^{-1} (Mankoff et al., 2019; Mouginot et al., 2019) (Figure 1a). Ice mélange buttressing of its terminus can inhibit calving, influence flow and allow advance (e.g. Amundson et al., 2010; Cassotto et al., 2021). Between 2011 and 2017, SKJI experienced a range of grounding line depths varying from 828 m and 980 m (Morlighem et al., 2017; Khazendar et al., 2019), producing icebergs as large as 700-1000 m across, forcing ice mélange down-fjord because of full-thickness calving events (Amundson et al., 2010; Walter et al., 2012). The retreat of SKJI from an annually floating terminus which calved larger icebergs (2000-2002) has led to a seasonally grounded terminus, causing much smaller icebergs to be calved during the summer months (2013-2015) (Scheick et al., 2019).

UI has a mean ice discharge (2010-2018) of 1.36 Gt yr^{-1} (Mankoff et al., 2019) (see Figure 1b), with terminus depths ranging from 230 to 500 m between 2013 and 2015 (Carroll et al., 2016; Morlighem et al., 2017; Fried et al., 2018). Prior to the study period between 2003 and 2008, UI experienced a substantial (4 km) rapid retreat of its terminus (Bartholomaus et al., 2016; Fahrner et al., 2021).

KNS is the largest marine-terminating glacier south of SKJI on the west coast of Greenland with a mean ice discharge (2010-2018) of 4.92 Gt yr^{-1} (Mankoff et al., 2019) (see Figure 1c). It has retreated over 23 km from its Little Ice Age maximum position (Lea et al., 2014a; Lea et al., 2014b), but has remained relatively stable in the last decade (Davison et al., 2020b; Fahrner et al., 2021). The glacier's fjord is typically filled with mélange of small icebergs and brash ice and currently has a relatively shallow grounding line depth of approximately 250 m (Morlighem et al., 2017). While the development of a channelised, subglacial hydrological system at KNS increases localised calving activity due to greater submarine melt and plume surfacing, it decreases terminus-wide calving and suggests high levels of runoff could decrease the number of calving events (Bunce et al., 2021).

4.2 **Data and Methods**

4.2.1 ArcticDEM data

The availability of ArcticDEM within GEE and its high 2-m spatial resolution (10 cm vertical accuracy) is used to create a highly automated workflow to delineate icebergs and derive their individual volumes, which are validated against manually digitised outlines. The workflow is also packaged in a GUI with a respective GitHub page that contains the necessary information on how to access the tool, define an ROI and export the data to a user's Google Drive or GEE asset (see: https://github.com/ConnorShiggins/Google-Earth-Engine-and-icebergs). To ensure a consistent level of high-quality data, analysis is automatically limited to only include DEMs generated from stereopair images acquired on the same day. In doing so, this limits the effect of iceberg drift, ensuring that only the highest quality DEMs are analysed. DEMs acquired between the months of July and October are analysed to avoid the presence of seasonal floating ice tongues that form and persist through winter and spring that could lead to erroneous results. The data availability for each glacier is variable, with KNS having 16 available images from 2013-07-04 to 2017-08-26, SKJI 20 images, ranging from 2011-07-08 to 2017-08 -09 and UI 3 images between 2012-07-04 and 2017-07-03.

4.2.2 Workflow description

The only user defined input required for the code to execute is a ROI (Figure 4.2), the users can also modify other parameters (see below). The workflow dynamically filters the ArcticDEM image collection to retain DEMs with >80% coverage of the ROI, before scenes with low image quality (e.g. cloud affected) are removed by calculating the 90th percentile of a scene's elevation, and ensuring that it is within ± 10 m of the WGS84 geoid.

To allow for potentially poor spatial registration in the Z dimension of the DEM and different tidal states at the time of data acquisition, sea level is automatically calculated for each individual DEM. This is achieved by assuming that when DEM elevation values over the fjord are plotted as a histogram with 0.25 m bin widths, its peak (i.e. the most common elevation in the DEM) represents sea level at the time the image was acquired (Figure S1). This allows each DEM to be registered to a common base level (i.e. 0 m above sea level) for consistent iceberg identification, and calculation of iceberg freeboard height and volume. The results in this study are limited to analysing DEMs acquired between July and October to minimise the likelihood of rigid mélange and sea ice being present at the ice front, though users are able to define any time period of interest. If for any reason this occurs and an erroneous sea level bypasses a filter, the value is appended to each iceberg as metadata and a user can filter any anomalously high values post-processing.

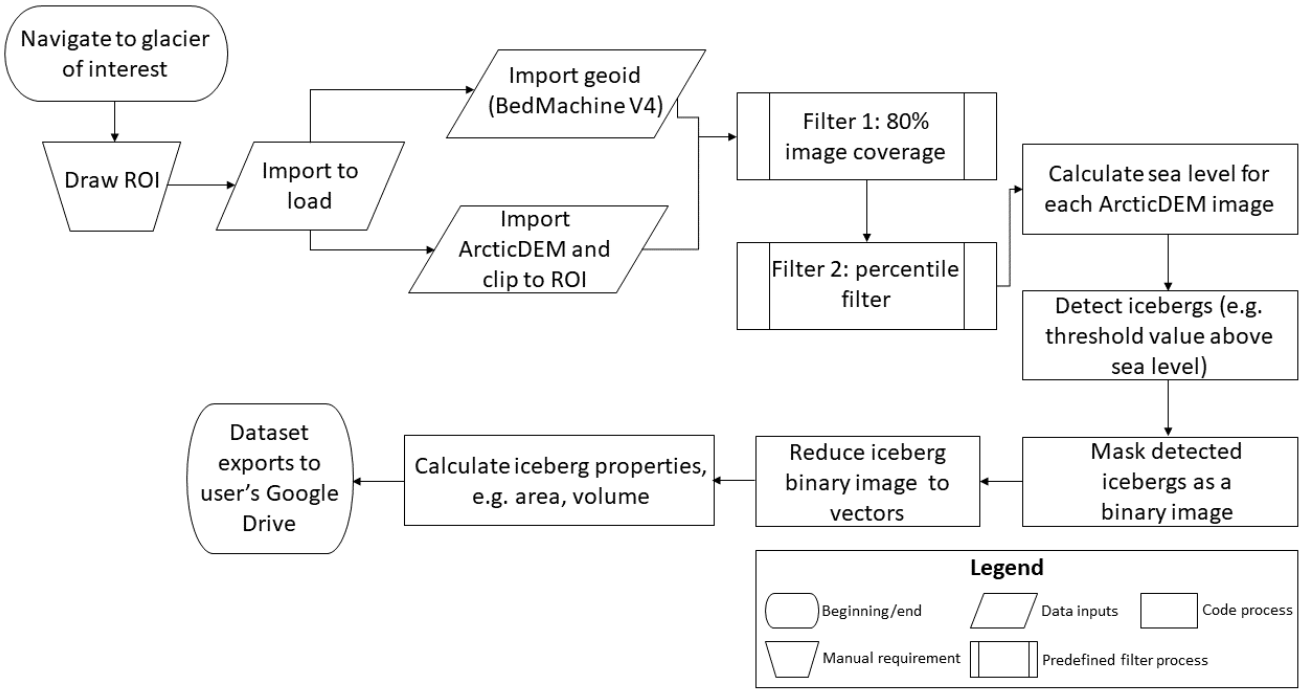

Figure 4.2. Workflow model of the automated iceberg detection in GEE.

To delineate iceberg outlines, it is necessary to separately define a threshold value above sea level where icebergs can be confidently delineated without multiple icebergs being erroneously merged. Consequently, derived iceberg areas and volumes from the workflow represent minimum estimates. Potential threshold values for each glacier were explored, using increments of 0.1 m between 0.1 m and 1.5 m for KNS and UI (glaciers where small icebergs dominate), whereas this was increased to 0.5 m increments between 1.0 m and 5.0 m for SKJI where dense concentrations of large icebergs exist. There are extremely small variations (~0.04) in the power law slopes at SKJI, providing reason for testing the detection threshold increments by 0.5 m. From these results, the most appropriate iceberg detection threshold was evaluated through visual comparison to manually digitised iceberg outlines. From this, the most appropriate threshold was determined to be 1.5 m above sea level for KNS and UI, and 3.0 m for SKJI. The workflow uses the threshold value to identify any area above sea level where it is exceeded as an iceberg. Depending on the type of fjord environment (e.g. densely packed, open water) and the research question being addressed, the user can potentially alter the default iceberg detection threshold of 1.5 m above sea level within the workflow (see GitHub read.me).

Within the workflow, areas of the DEM that exceed the threshold are converted to a binary image (1 = iceberg, 0 = no iceberg) which are then vectorised into iceberg outlines. Iceberg specific metadata (e.g. area, volume) are appended to each outline automatically, using DEM

input data where needed. The final part of the workflow removes any large object (> 100000 m^2) in case of false iceberg detection by erroneously delineating fjord edges and/or the glacier termini before the user can either choose to export results to the Google Drive in their preferred file format (e.g. CSV, Shapefile or GeoJSON) or to a GEE asset.

4.2.3 Iceberg distributions

Once exported from the GUI, iceberg areas and volumes from each glacier are fitted to power law distributions as described in Equation 4.1 using the 'powerlaw' package in Python (Alstott et al., 2014). To allow consistent comparison of how power law distributions evolve through time x_{min} values are kept the same for every image, defined as 500 m^2 for KNS and UI, and 1000 m^2 for SKJI. The lower x_{min} value of 500 m^2 for KNS and UI was chosen as they produce smaller icebergs compared to SKJI, meaning that 1,000 m^2 value would have resulted in significant data loss. Both values assigned for the three glaciers allowed reduced skewing of the α exponent and provided more robust fits to power law distributions. The x_{min} values defined are also within the range used by previous studies and provided internal consistency for each glacier dataset (e.g. Sulak et al., 2017; Scheick et al., 2019; Rezvanbehbahani et al., 2020). The ability to determine iceberg area and volume for each iceberg in the dataset allowed the derivation of an empirical area-to-volume conversion expressed as a power law relationship following Sulak et al. (2017).

4.3 **Results**

4.3.1 Workflow evaluation

The ROI at SKJI was 41 km^2, 9.6 km^2 at UI and 5.3 km^2 at KNS with the number of detected icebergs across all available images ranging from 6973 at UI to 147714 at SKJI (Table 4). For each individual glacier, iceberg distributions obtained from automated and manual delineation methods were found to be qualitatively and quantitatively comparable (Pearson's r value = 0.70 to 0.96) (Figures 4.3 and 4.4; Table 4.1).

Table 4.1. Data from the three glaciers, including the ROI size, the date of the ArcticDEM image which was manually validated, number of images in the entire collection, number of icebergs detected, both automated and manual power law slope values (with one sigma) for area with corresponding x_{min} (total iceberg volume below and above the respective value: SKJI =1,000 m^2, UI and KNS = 500 m^2) and the execution time. The error attached to the automated power law slope is one standard deviation derived in the 'powerlaw' Python package.

	ROI (km^2)	Date	Images	Total number of icebergs detected (icebergs per scene per km^2)	Automated power law slope	Manual power law slope	X_{min} (m^2)	Total iceberg volume below x_{min} value (km^3)	Total iceberg volume above x_{min} value (km^3)	Execution time (minutes)
SKJI	41	2011-09-10	20	147714 (180)	-1.88 ± 0.06	-1.91 ± 0.06	1,000	0.984 (10%)	8.629 (90%)	~120
UI	9.6	2012-07-04	3	6973 (242)	-2.16 ± 0.12	-2.17 ± 0.13	500	0.016 (24%)	0.051 (76%)	6
KNS	5.3	2013-08-21	16	9051 (107)	-2.38 ± 0.16	-2.77 ± 0.16	500	0.021 (22%)	0.074 (78%)	8

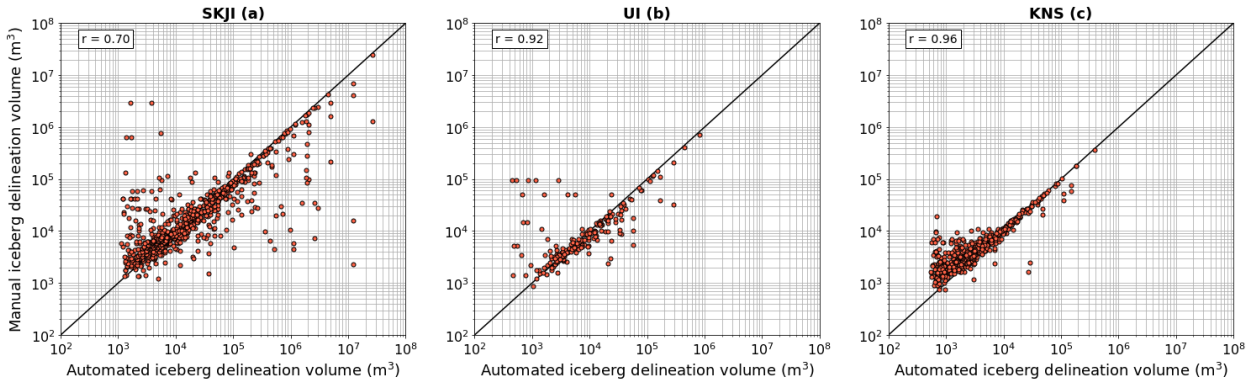

	SKJI (a)	UI (b)	KNS (c)
n	805.0	198.0	507.0
Automated volume sum (km^3)	0.2127	0.0049	0.0045
Manual volume sum (km^3)	0.1065	0.0044	0.0046
Difference (%)	49.0	11.0	2.0
RMSE (km^3)	1.767e-05	6.682e-05	2.437e-05

Figure 4.3. The relationship between the iceberg volume for both the manual and automated delineation methods for each glacier and respective summary statistics. The Pearson's correlation coefficient is also highlighted (SKJI = 0.70, UI = 0.92, KNS = 0.96).

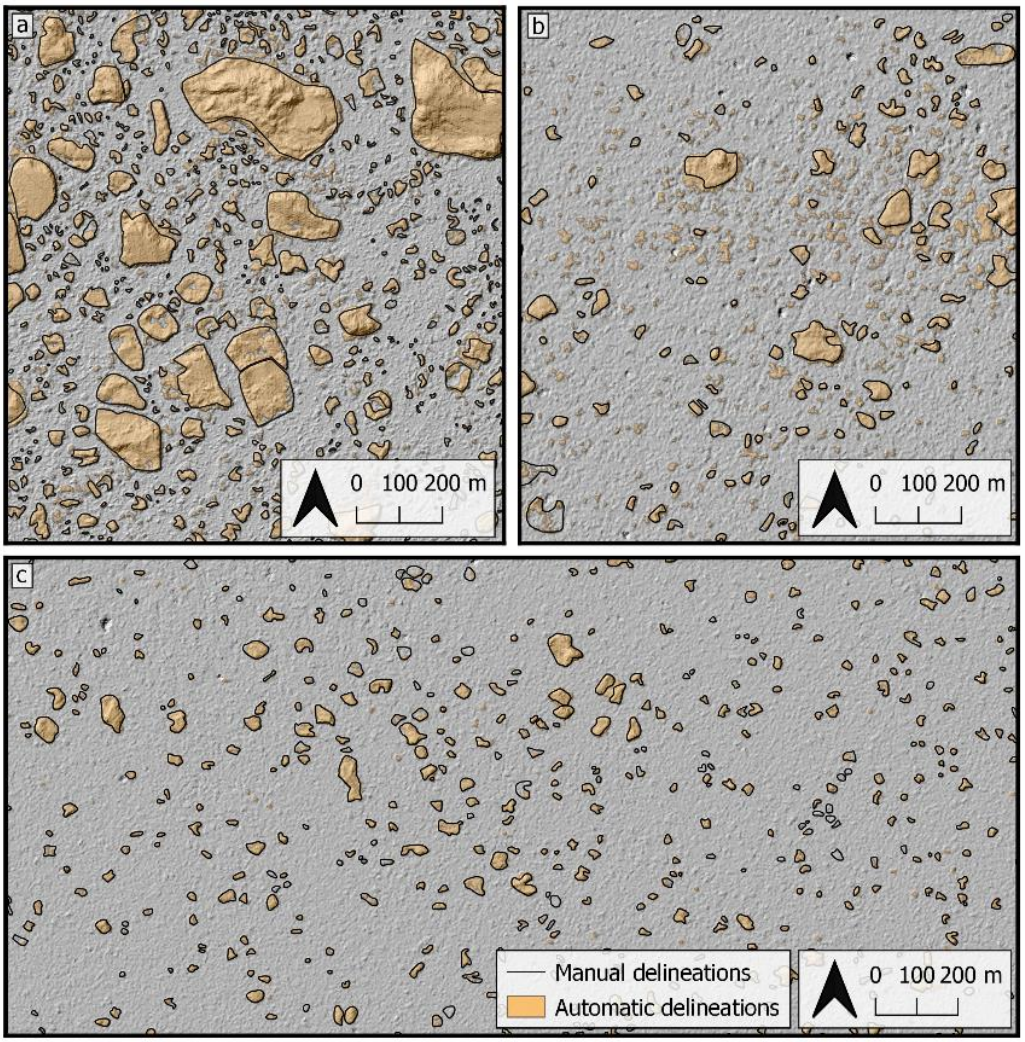

Figure 4.4. Manual (black lines) and automated (orange) delineation of the iceberg subset for a) SKJI (2011-09-10), b) UI (2012-07-04) and c) KNS (2013-08-21) overlaying the hillshaded ArcticDEM v3 strip data for each glacier.

For each ArcticDEM scene throughout the study period at each glacier, sea level ranged from 23 m to 39 m, broadly following the local geoid sea level elevation. Visual comparison between manual and automatically delineated data for each threshold showed that threshold values of 1.5 m above sea level for KNS and UI, and 3.0 m above sea level for SKJI (Figure 4.5) provided the best visual correspondence and provided more concordant power law fits with manually digitised outlines (Figure 4.6; see Methods).

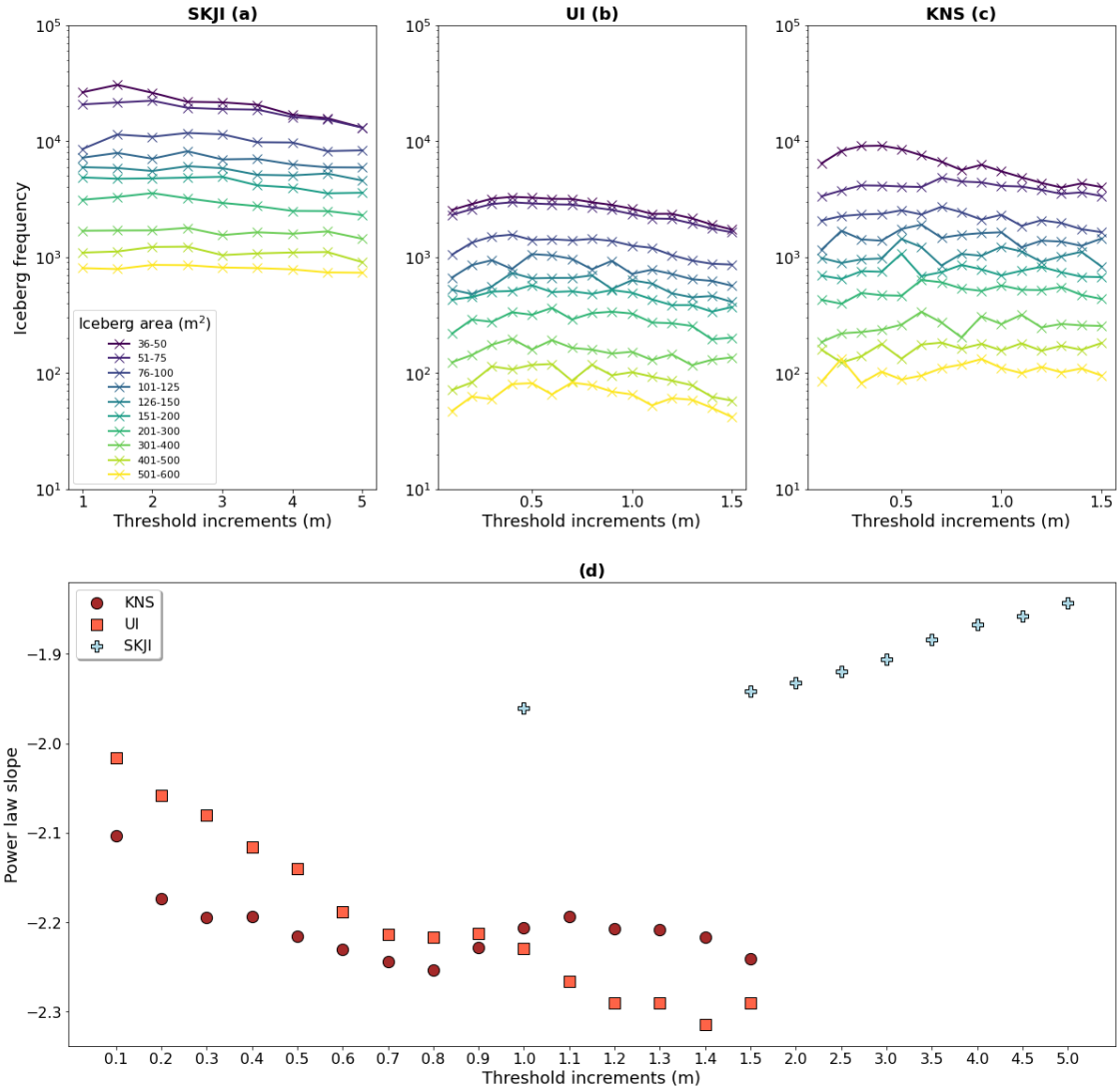

Figure 4.5. Iceberg frequency for each threshold increment tested. a) SKJI's increments were every 0.5 m above sea level between 0 and 5 m above sea level. Increments of 0.1 m between 0 and 1.5 m above sea level were ran for both b) UI, c) KNS. d) shows how the α value for each glacier changes, depending on which threshold increment is chosen to detect their respective icebergs. Note the log-scale on the y-axis in subplot: a, b and c.

Iceberg area-size distributions of both the manually and automated methods are found to follow power law distributions for the x_{min} values applied (Figure 4.6). Results reveal that SKJI has the least negative power law slope (α = -1.88) of the three glaciers followed by UI (α = -2.16) and KNS has the most negative values (α = -2.38), correctly highlighting icebergs at SKJI are generally larger than those at UI or KNS (Figure 4.4). Good correspondence between automatically and manually delineated iceberg area α values were observed for SKJI and UI where they differed by 0.03 and 0.01 for SKJI and UI respectively, though this increased to 0.39 at KNS). Power law relationships applied to iceberg volume distributions for each of the

glaciers showed similar results, however the difference in the α value reduces to 0.02, 0.01 and 0.20 at SKJI, UI and KNS respectively.

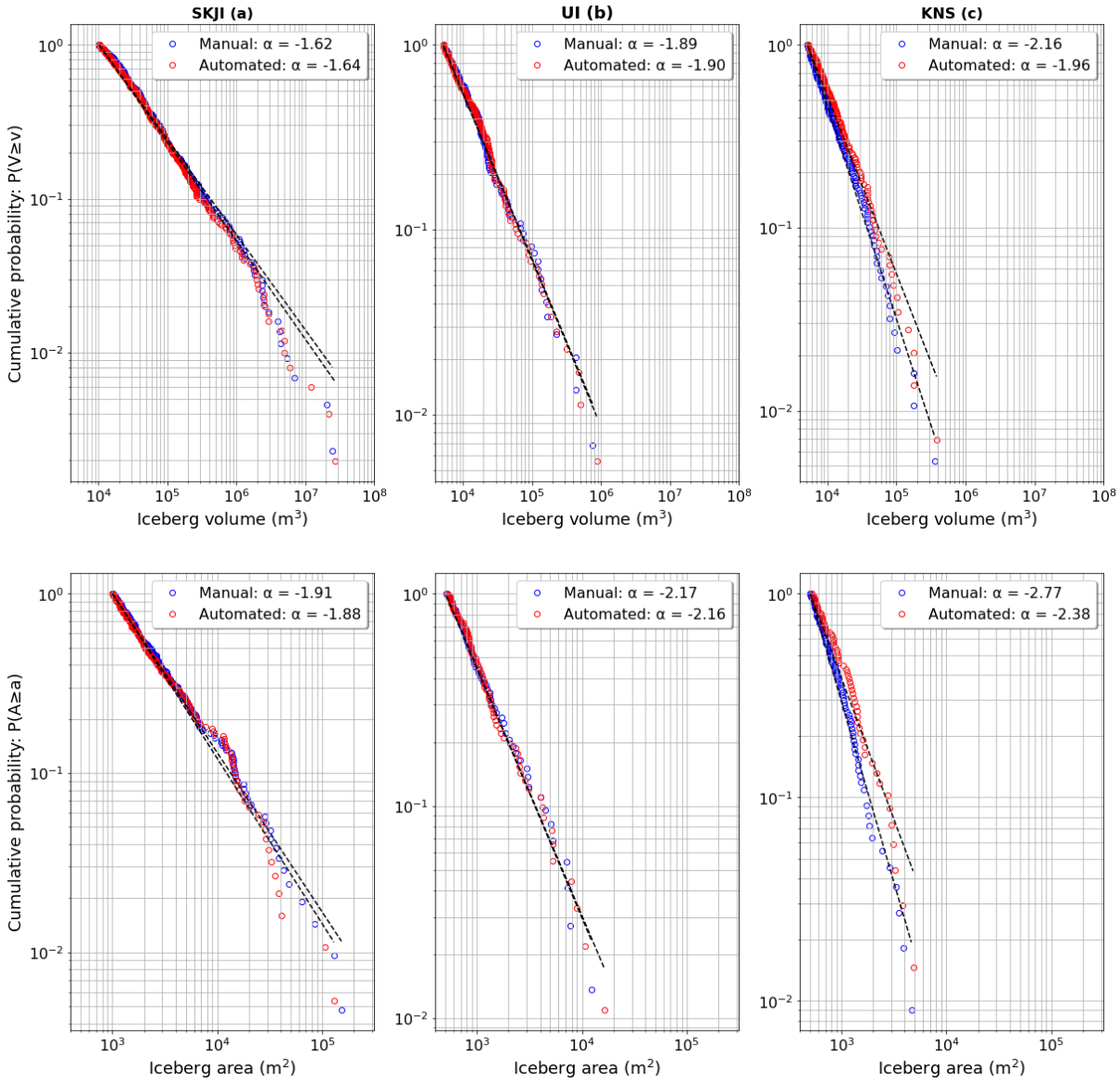

Figure 4.6. Power law plots for the manual (blue open circles) and automatically (red open circles) delineated icebergs. For iceberg area: a) SKJI has an x_{min} value defined at 1,000 m^2, compared to 500 m^2 for both b) UI and c) KNS. For defining an x_{min} for iceberg volume distributions, the respective area x_{min} value was converted using the equation of Sulak et al. (2017; their equation 5) yielding a value of 10,270 m^3 for SJKI and 5,135 m^3 for UI and KNS. The black lines show the line of best fit for the iceberg distributions. Note the y-axis is plotting cumulative probability where alpha equals -1.

4.3.2 Iceberg area and volume distributions

The three-dimensional nature of DEMs allow the volume of each iceberg to be calculated assuming neutral buoyancy, allowing the derivation of the relationship between planform iceberg area (A) and volume (V) (Figure 4.7). To reduce the potential for biasing power law relationships towards more frequently observed smaller icebergs, the relationships reported are

derived from binned means using bin increments of $\log_{10}(A+0.1)$. For the entire iceberg dataset this can be expressed as

$$V = 14.90A^{1.16} \quad (4.2).$$

The large nature of the dataset also allows equations describing the lower and upper confidence bounds to be derived, with the 5th percentile of the distribution described by

$$V = 7.55A^{1.18} \quad (4.3)$$

and the 95th percentile of the distribution described by

$$V = 15.73A^{1.20} \quad (4.4).$$

When compared to the previously published area-to-volume conversion equation of Sulak et al. (2017; their equation 5), their relationship would produce lower volumes for small area icebergs (area = < 1000 m^2; Rezvanbehbahani et al. [2020]), and higher volumes for large area icebergs (Figure 4.7).

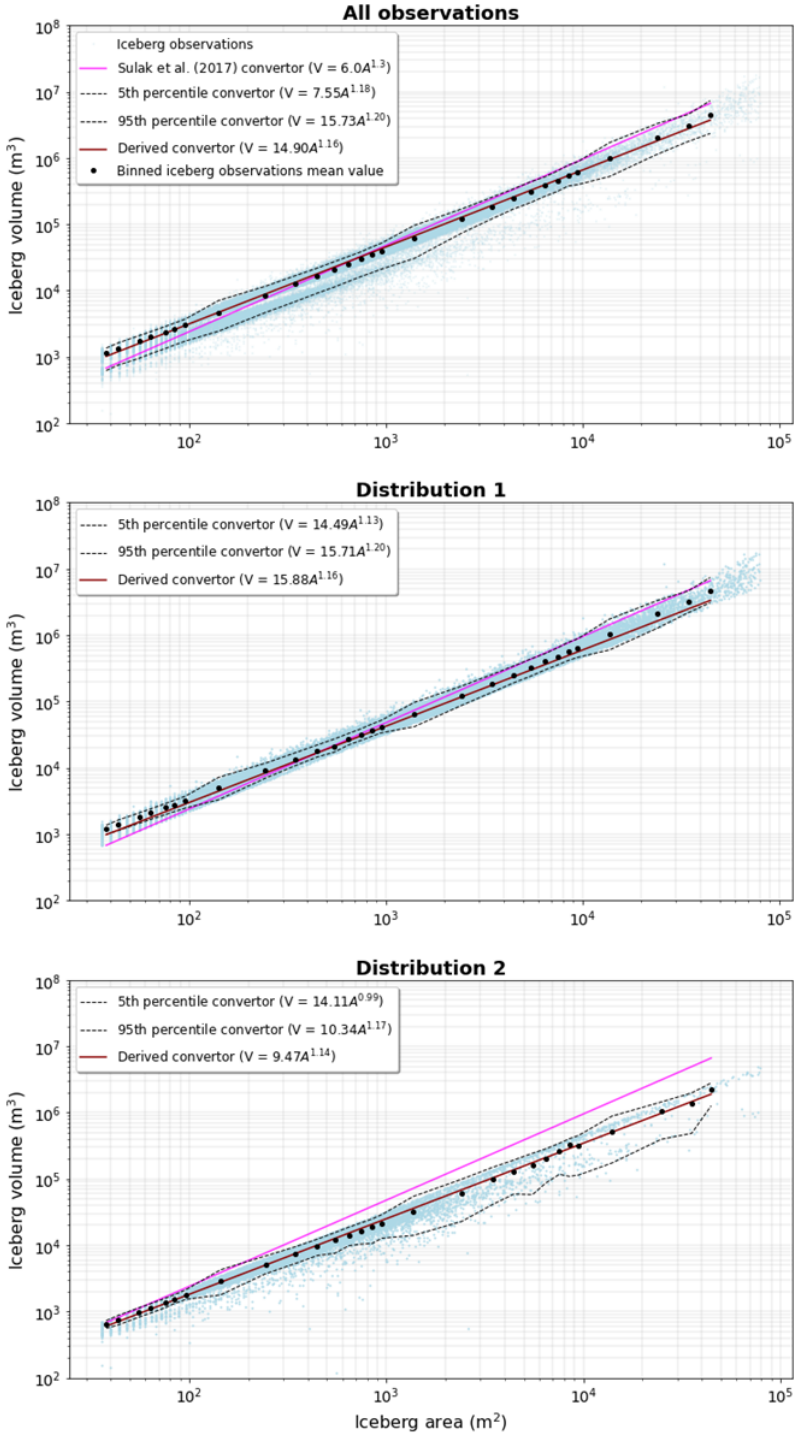

Figure 4.7. The mean iceberg area and volume for each size class (e.g. mean of 30 – 40 m^2, mean of 100 – 200 m^2, mean of 1000 – 2000 m^2, and so on) for the respective glacier, overlaid with the Sulak et al. (2017) conversion (pink) and the one derived here (brown). By calculating mean iceberg area and volume within $\log_{10}(A+0.1)$ binned increments, this reduced the potential for biasing area-volume relationships towards smaller, more frequently observed icebergs. Uncertainty in these distributions is also characterised by deriving similar relationships for the 5% and 95% limits. To note, these limits are derived from the binned mean size classes and are therefore not straight.

When observing how iceberg area scales with volume, two distinct distributions are identified at SKJI and KNS (Figure 4.8; Table 4.2), persisting between individual DEMs throughout the study period. While the lower distribution at both SKJI and KNS accounts for only 7.2% of the icebergs in the population, the divergence between the upper and lower distributions is found to proportionately increase with iceberg area (Figure 4.8 insets). These two distributions can be described in a similar manner to the overall distribution, with the equations for the upper (red) and lower (blue) distributions shown in Equation 4.5 and Equation 4.6 respectively (Figure 4.7b, 4.7c).

$$V = 15.88A^{1.16} \quad (4.5)$$

$$V = 9.47A^{1.14} \quad (4.6)$$

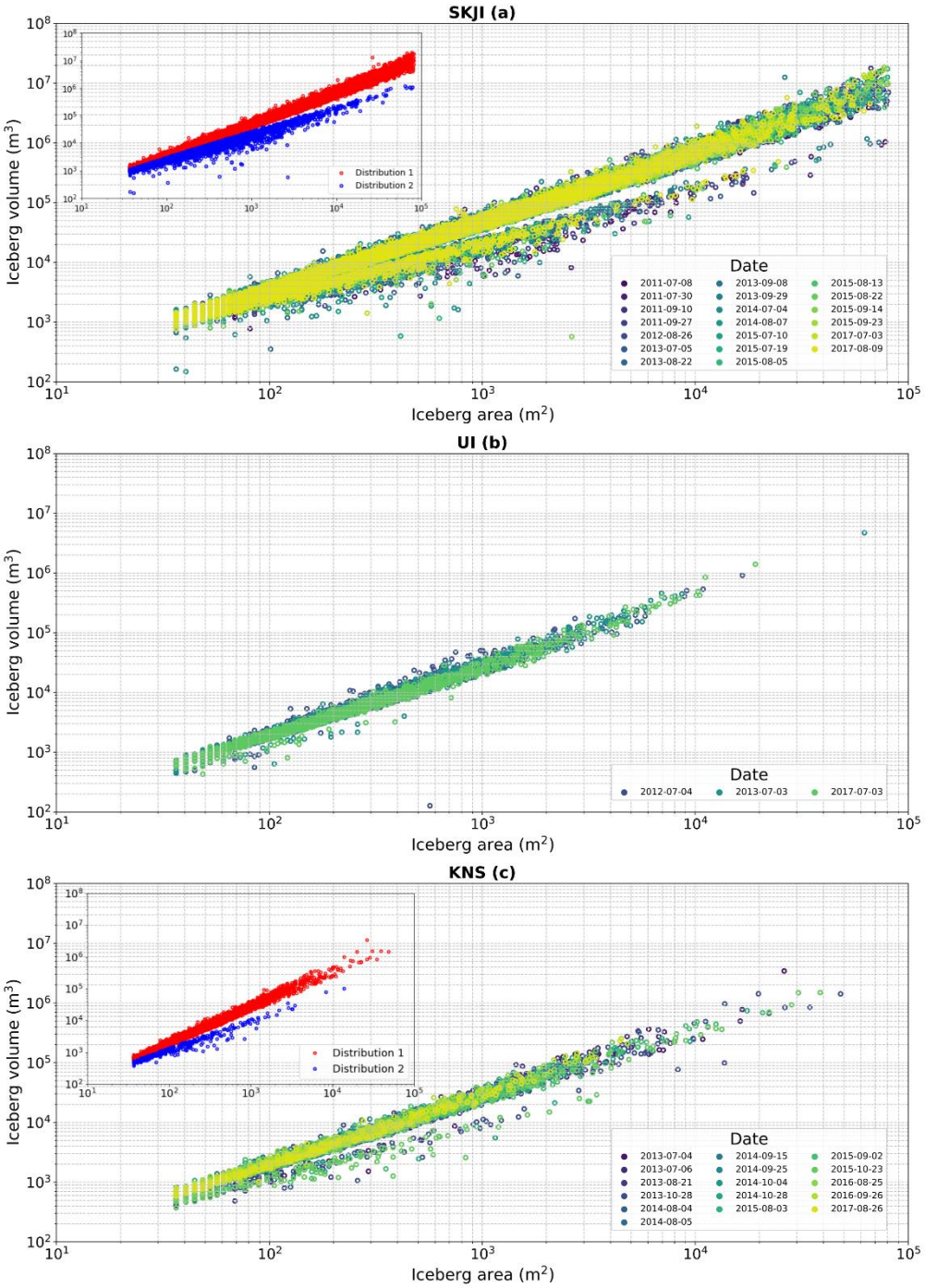

Figure 4.8. Iceberg area versus volume and freeboard height which is colour coded by each ArcticDEM scene date. The inset in both the SKJI (a) and KNS (c) panels show the two distributional branches identified in the data with the respective derived convertors for each distribution. Each distribution is separated by identifying local minima in probability distribution histograms of the entire dataset.

Table 4.2. Summary statistics of the two distributions outlined at SKI and KNS. (1) represents distribution 1 and (2) represents distribution 2. Standard deviation is abbreviated to SD.

	SKJI (1)	SKJI (2)	KNS (1)	KNS (2)
Number of icebergs	136673	11041	8697	354
Mean area (m^2)	1036	434	383	307
Mean volume (km^3)	6.9×10^{-5}	8.0×10^{-5}	1.1×10^{-5}	2.7×10^{-6}
Maximum area (m^2)	79820	77192	47520	13536
Maximum volume (km^3)	0.017	0.001	0.003	9.5^{-5}
Area SD (m^2)	3929	2169	1347	935
Volume SD (km^3)	4.0×10^{-4}	3.3×10^{-5}	5.8×10^{-5}	7.2×10^{-6}

In the entire dataset, small icebergs (area = < 1000 m^2; Rezvanbehbahani et al. [2020]) account for over 80% of the total iceberg count for each glacier, however they only contribute to 10%, 37% and 35% of the total volume at SKJI, UI and KNS, respectively (Figure 4.9). Consequently, while small icebergs dominate the distributions in the fjord of each glacier, compared to larger icebergs they are found to account for a significantly smaller proportion of total iceberg volume.

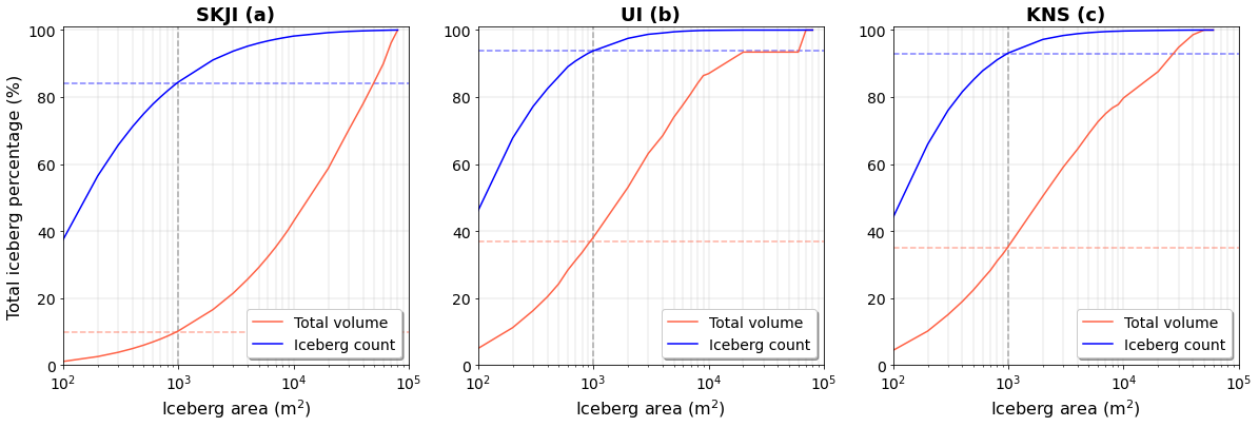

Figure 4.9. Cumulative iceberg volume (orange line) and count (blue line) plotted as percentage with their respective surface area. The small iceberg threshold (< 1000 m^2) is defined by a dashed grey line. The total volume made up by small icebergs is represented by the orange dashed line and the total number is the dashed blue line.

4.4 **Discussion**

4.4.1 Workflow

The workflow presented here allows users to successfully delineate icebergs and capture their area and volume size distributions and assign a range of metadata to each individual iceberg (Figure 4.6). The workflow therefore allows users to rapidly obtain iceberg data to interrogate glacier calving styles and iceberg freshwater fluxes. The application of the workflow to glacier fjords with a range of different iceberg concentrations and sizes demonstrates the utility of ArcticDEM data for iceberg detection and mapping across a range of different fjord environments typical of Greenland and elsewhere. As a result, this approach is suitable for pan-Arctic iceberg detection where availability of DEM data allow (see Figure S2).

This new method is quick to execute and is capable of successfully filtering ArcticDEM scenes by cloud contamination, ROI data coverage, and dynamically defines sea level for each ArcticDEM scene to account for potentially poor image registration and local tidal state. While this results in the rejection of scenes with data gaps and partial cloud contamination where parts of the image may be suitable for analysis, the automated image filtering steps implemented in the workflow removes the requirement for time consuming user-led data cleaning. These thresholds can be manually adjusted by the user if required (see GitHub read.me).

The detection thresholds defined (1.5 m for KNS and UI and 3.0 m for SKJI) are found to be suitable for correctly delineating iceberg outlines and subsequent size distributions (Figure 4.4). Though a mismatch in size distributions are found at KNS where small icebergs dominate, it is likely that this arises from operator bias in the manual delineation of these. This arises due to the manual operator delineating icebergs across pixels in the DEM compared to the

automated approach that only identifies icebergs through whole pixel analysis. y. In this instance, the workflow therefore provides a more complete footprint of small icebergs than a manual digitiser is able. Visual comparison of iceberg outlines produced by the workflow to multi-angle hillshaded DEMs (Figure 4.4) provide confidence that it is able to detect icebergs as small as 40 m^2 (10 pixels). However, larger proportionate mismatches in area are expected between manual and automated delineation methods for smaller icebergs, explaining the mismatch in power law slope values observed at KNS (Figure 4.6).

Exploration of the workflow's sensitivity to increasing the detection threshold above sea level shows that higher thresholds detect only larger icebergs, and will result in fractionally smaller overall iceberg areas and volumes of these (Figure 4.5). The user definition of this detection threshold is dependent on whether smaller icebergs are important to include for the user's research question. Where only the largest icebergs are of interest, a higher detection threshold could therefore be set with relatively little loss in the final iceberg areas and volumes. This is because volumetrically larger icebergs are more likely to have higher freeboard heights, and the iceberg margins omitted due to higher thresholds are likely to be small in terms of their relative area and volume. We show that by defining different x_{min} values between SKJI (1000 m^2) and UI and KNS (500 m^2) can result in the retention of a significant proportion of iceberg data (Figure 4.9). As highlighted by previous studies (e.g. Sulak et al., 2017; Scheick et al., 2019; Rezvanbehbahani et al., 2020) and shown here, the definition of x_{min} is therefore critical for ensuring sufficient data are available for analysis.

As a consequence, those wishing to explore power law size distribution relationships where small icebergs are less important for a user's research question can potentially set a higher detection threshold. Conversely, if a study is wanting to retain the maximum number of icebergs for subsequent analysis, a lower threshold could be defined, though this risks that outlines of neighbouring icebergs being erroneously identified as a single iceberg. This is highlighted by the fact that rafts of small individual icebergs frozen together by mélange are correctly identified by the workflow as single floating bodies of ice, though the individual icebergs that they are comprised of are not separated out by the workflow. If a user's research question requires both iceberg and iceberg raft cover (distributions 1 and 2) within an ROI, the default threshold of 1.5 m above sea level is suitable, as is the 3.0 m threshold for more densely ice-covered fjords such as SKJI. If only iceberg outlines are needed, a higher detection could be defined to remove iceberg rafts (distribution 2). It should be noted that setting a higher detection threshold would result in the potential loss of data relating to smaller icebergs which

have lower freeboard heights, and fractionally lower iceberg volumes obtained from larger icebergs. An alternative approach that would retain smaller icebergs and not result in the minor under-estimation of iceberg volume would be to use a lower threshold (e.g. 1.5 or 3 m), with data from distributions 1 and 2 separated as part of post-processing (e.g. Figure 4.8 insets). While it should be emphasised that all results from the workflow are likely to represent minimum area and volume estimates, it is suggested that for the majority of cases a threshold of 1.5 m should be sufficient.

Choosing different ROIs at the same glacier can result in varying numbers of DEMs available for analysis because of the workflow filters (Figure 4.2) and spatial coverage of ArcticDEM v3 strip data. This is more pronounced at glaciers with longer termini (e.g. SKJI), rather than narrower fjords as data is more likely to cover the terminus (e.g. KNS). For example, by subsetting three ROIs at SKJI, it is apparent the number of available DEMs varies from 4 to 30 across the ice front, and provided different power law slope values (-1.78 to -2.03) (Figure 4.10). Whether these differences in power law slopes are solely dependent on the amount of data available is not currently possible to ascertain, as these may also be a product of variable calving dynamics across the ice front (i.e. different calving styles between northern, central and southern ice front sections at SKJI).

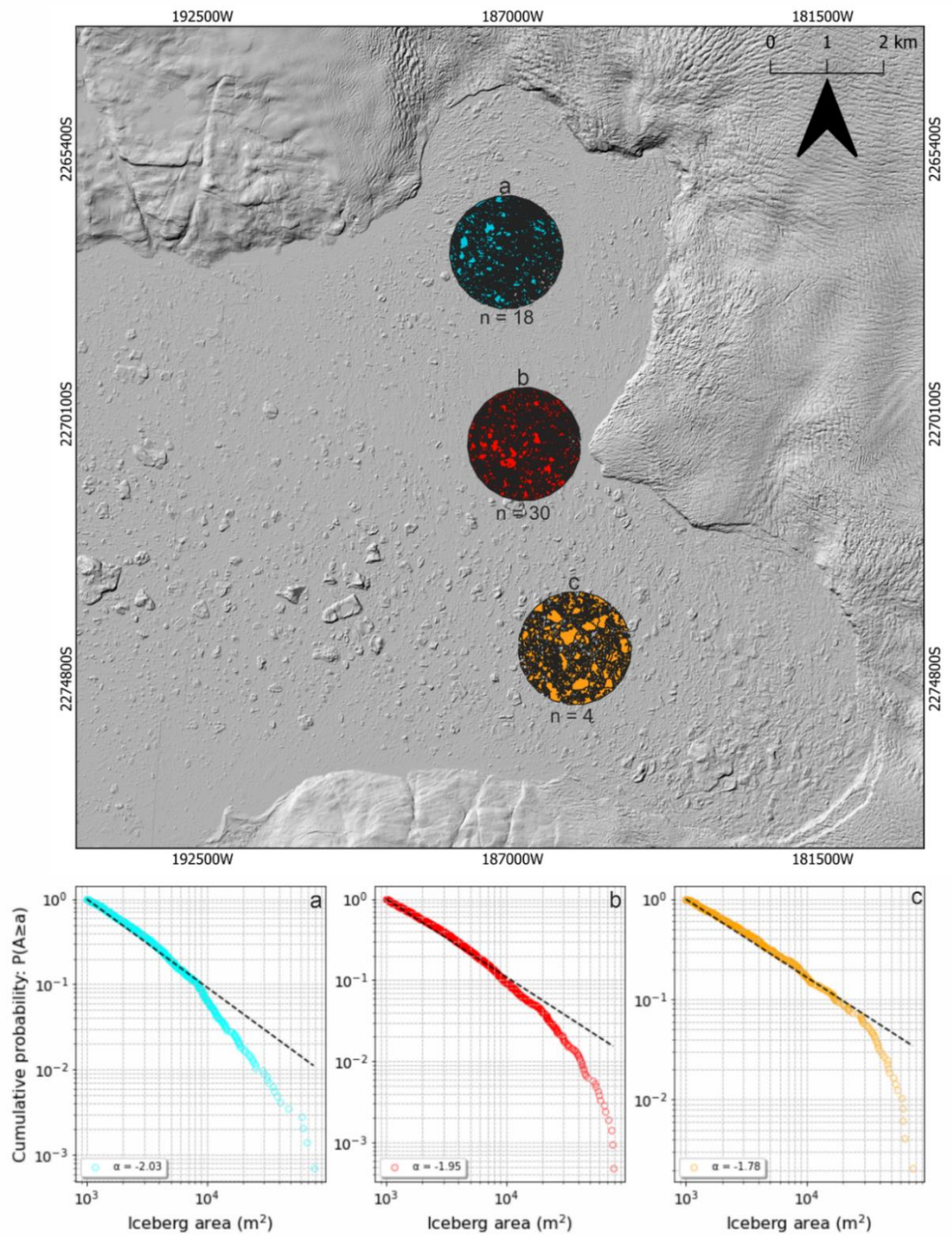

Figure 4.10. Subset sampling across SKJI's ice front to determine how iceberg distributions change spatially. Overlaying the hillshaded ArcticDEM image are the total iceberg collections for each subset with the respective power law slopes beneath, corresponding by both letter and colour. The 'n' underneath each iceberg collection is the number of available DEMs within the subsetted ROI.

4.4.2 Glaciological implications

The new area-to-volume conversions presented offer the potential for wide-scale application to iceberg area outline data that have been derived from optical and/or SAR imagery (Equations 4.2-4.6; Figure 4.7). The large dataset generated also allows for the quantification of uncertainties when scaling area-to-volume (Equations 4.3 and 4.4 for 5th and 95th percentiles

respectively; Figure 4.7). This will allow iceberg volumes to be estimated from data sources that extend beyond the spatial and temporal availability of ArcticDEM and that are more frequently acquired (e.g. Landsat satellites and Sentinel-1 and-2). Improved constraint of uncertainties in iceberg volumes therefore provide new opportunities for temporally and spatially extending studies that seek to model fjord freshwater fluxes (Davison et al., 2020a) and quantify iceberg volume distributions (e.g. Schild et al., 2021). While it should be remembered that the conversion equations result in minimum volume estimates, inclusion of lower and upper limits will assist in better quantification of ranges of potential iceberg volume from iceberg outline data alone.

We find evidence of two iceberg populations at SKJI and KNS across multiple ArcticDEM scenes between 2010 and 2017, though only a single population at UI (Figure 4.8). The DEM surface expression of icebergs identified in the second distribution tend to be flatter than those of distribution 1, resulting in lower overall volumes. Manual inspection of DEMs suggest the majority of those in distribution 2 represent rafts of small icebergs that are frozen together by mélange. Though distribution 1 dominates the total dataset, studies using two-dimensional data (i.e. optical and/or SAR) should be aware that their methods may identify these iceberg rafts as single icebergs. For glaciers where these two iceberg distributions exist using a single area-to-volume conversion will therefore result in an overestimation of total iceberg volume. It may therefore be appropriate for users to separate out these distributions during post-processing and apply Equations 4.5 and 4.6 to obtain complete volume estimates (e.g. Figure 4.7). To identify iceberg rafts from two-dimensional image data it may be required to undertake further analysis (e.g. approaches that go beyond pixel level analysis; for example, incorporating iceberg level image texture as part of machine learning methods (e.g. Rezvanbehbahani et al. 2020)).

The two distributions noted at SKJI and KNS suggest different populations are present in fjords across Greenland, representing icebergs and ice rafts respectively. The evolution of both populations through time is currently challenging as ArcticDEM v3 data at the study sites occur irregularly through seasons and between years. This means that identification of seasonal and multi-annual timescale changes in these distributions cannot currently be characterised with confidence. However, with the recent (October 2022) release of more temporally comprehensive ArcticDEM v4 strip data we anticipate that it will become possible to use the workflow for detailed timeseries analysis on sub-annual to multi-annual timescales. At the time of writing, these data are yet to be ingested into GEE, however if and when they are, the workflow will be updated to be made available within the GUI.

Results show that small icebergs (area = <1000 m^2) account for the majority of those identified (over 80% for each glacier) yet contribute a smaller fraction of the total iceberg volume (10-37% of total volume; Figure 4.9). Consequently, small differences in the number of large icebergs can have a disproportionate impact on overall fjord iceberg volume. At these glaciers, large icebergs therefore represent comparatively larger freshwater reservoirs in their fjords, and account for a more significant proportion of overall ice mass loss from their source glaciers.

Expressing iceberg counts and volumes for each glacier as percentages (Figure 4.9) also offers the potential for empirically estimating the evolution of iceberg populations for individual ice sheet outlets from frequently updated velocity derived glacier discharge data (e.g. Mankoff et al., 2020). Although this would assume a consistent calving style through time, such relationships could assist in estimating how the number and volumes of icebergs have evolved; may evolve in the future (through application to ice discharges from ice dynamic modelling [e.g. Choi et al., 2021]); and assessment of potential iceberg hazards.

4.5 **Conclusions**

This study presents a new workflow and GUI to automatically detect icebergs within Google Earth Engine using ArcticDEM, offering the potential to significantly and rapidly expand iceberg area and volume datasets. Results from the workflow show good agreement with manually digitised iceberg outlines (r-values = 0.70, 0.92, 0.96), with mismatches occurring for the smallest of icebergs where the precision of manual digitisation is poorer compared to that of the workflow. The workflow identifies two distinct iceberg populations at SKJI and KNS and one at UI representing: (1) individual icebergs; and (2) small iceberg rafts frozen together by mélange. – The significantly greater amount of data generated by the workflow has allowed derivation of new area-to-volume conversion equations for each distribution including upper and lower bound uncertainties for the first time. While smaller icebergs at each glacier are found to dominate the distributions (84-94% of the total count), their contribution to total volume and therefore freshwater flux are relatively small (10-37%).

Although ArcticDEM data are temporally and spatially limited relative to those obtained by optical and SAR satellite platforms, the results presented here offer the potential for extending studies into fjord iceberg cover and glacier calving that use iceberg outlines derived from these data. A new approach of expressing relationships between iceberg count and volume will also allow empirical estimation of iceberg size distributions from iceberg discharge observations.

This would have benefits to those investigating iceberg freshwater fluxes within fjords, and who seek to model the evolution of mass loss from the GrIS.

The workflow and user-interface presented here allows users to generate their own large, reliable datasets for their glacier(s) of interest. Consequently, it opens the possibility of extending the results presented here to any location where suitable ArcticDEM data are available.

Chapter 5: Large icebergs dominate Greenland mass loss through calving

Connor J. Shiggins[1], James M. Lea[1], Stephen Brough[1,2].

[1]*Department of Geography and Planning, School of Environmental Sciences, University of Liverpool, Liverpool, L69 7ZT, United Kingdom.*

[2]*Central Teaching Laboratory, Faculty of Science and Engineering, University of Liverpool, United Kingdom.*

Author contributions: Connor Shiggins led the writing and conducted all of the analysis. James Lea and Stephen Brough provided conceptual advice and contributed towards the writing of the paper.

Paper in preparation for submission to The Cryosphere.

Summary: This Chapter modifies the automated workflow presented in Chapter 4 and upscales the approach to all outlet glaciers with available data around the Greenland Ice Sheet (GrIS) (Objective 3). This approach provides the largest dataset of three-dimensional iceberg data in existence. Results have revealed outlet glaciers calve similar iceberg sizes, and that fjords are made up of mainly small icebergs in terms of count. However, their total volume is dominated by larger icebergs. Comparison of iceberg size distributions with glacier boundary conditions (Objective 3) shows that it is currently not possible to constrain systematic relationships between iceberg size, terminus depth and glacier discharge.

Abstract. Remotely sensed iceberg observations in the polar regions are scarce and thus limits our understanding of how icebergs are distributed in glacial fjords that have implications for both glacier and fjord dynamics. Icebergs are a key component of the glacier-ice-ocean interface, owing importance to both the mass balance of the Greenland Ice Sheet (GrIS) and the physical and biological impacts on the fjords in which they reside. We present a modified, fully automated workflow using ArcticDEM v3 strip data in Google Earth Engine (GEE) to detect over 1.3 million icebergs, proceeding 133 marine-terminating glaciers around Greenland. This study has therefore been able to compile the largest ever dataset of icebergs in the near-terminus region at an ice sheet scale for the first time. Smaller icebergs (< 1000 to 2000 m^3) are found to be the most frequently occurring (87%) iceberg size identified in the near-terminus regions of Greenland, but contribute little (12%) to the total iceberg volume in the fjord. Their larger counterparts exceeding 10000 m^3 are relatively rare in abundance, however we observe a closely coupled power relationship ($r = 0.77$) between their magnitude and frequency (i.e. larger icebergs dominate the fjords overall iceberg volume). Results cannot distinguish any discernible relationship between iceberg volume distributions, and the terminus depth of the glacier or the solid ice discharge across each sector of the ice sheet or individual calving margins. These findings are as a result of incomparable temporal footprints between datasets (i.e. varying acquisition of data) and the quality of bed topography data. We have shown the use of three-dimensional iceberg data as a viable approach to ice-sheet wide analysis of calving dynamics. This is the largest dataset assembled in the near-terminus regions across the GrIS and has revealed larger icebergs dominate the total mass loss via calving from outlet glaciers.

5.0 **Introduction**

Icebergs are a by-product of glacier calving which have significant implications for glacier mass balance, but also for fjord freshwater fluxes (Enderlin et al., 2016; Moyer et al., 2019), circulation and stratification (Davison et al., 2020a; Schild et al., 2021). Understanding of calving dynamics is currently poorly constrained, partly due to the lack of widespread iceberg observations from both satellite (e.g. Sulak et al., 2017; Moyer et al., 2019; Rezvanbehbahani et al., 2020) and in-situ observations (e.g. Cook et al., 2021).

Iceberg observations provide unique insights into calving dynamics as their size distributions can be used as proxy data to infer glacier behaviour (Scheick et al., 2019). Nevertheless, previous studies have been limited to only a few sites around Greenland (e.g. Sulak et al., 2017; Moyer et al., 2019; Rezvanbehbahani et al., 2020; Cook et al., 2021). This is in part due to the difficult nature of automated iceberg detection using remote sensing techniques (Chapter 3; Chapter 4) and thus limits the potential for large scale analysis because of highly dynamic fjord environments, such as the seasonal presence of glacier ice tongues, sea ice and ice mélange.

No fully automated workflows exist to detect icebergs on satellite imagery, rather semi-automated classification (e.g. Scheick et al., 2019) or manual delineations (e.g. Crawford et al., 2018) are preferred to generate specific datasets. The workflows which require no manual supervision with regards to the iceberg detection process still rely on a manual operator defining a search window (Chapter 4). The only way to achieve ice sheet wide detection of icebergs is through workflow automation with equally weighted search windows to remove spatial sampling bias.

Currently, estimating how iceberg calving will evolve in the future is uncertain (Choi et al., 2021). To better understand these dynamics, calving laws have been derived which are empirical relationships used to predict the rate of calving and terminus position depending on boundary conditions at the glacier (Brown et al., 1982; Van der Veen, 1996; Vieli et al., 2001; Benn et al., 2007b; Nick et al., 2010; Levermann et al., 2012; Morlighem et al., 2016; Mercenier et al., 2018; Schlemm and Levermann, 2019; Choi et al., 2021). While these laws can provide information regarding the iceberg calving rate, they cannot infer any knowledge into the resulting iceberg size distributions. The differences in dynamics between different glacier calving margins means there is no universally applicable calving law (Benn and Åström, 2018).

The lack of iceberg observations in Greenland's fjords has made it all but impossible to quantify the probability of iceberg sizes being calved which could allow the derivation of a

relationship between glacier dynamics and iceberg size distributions. This has resulted in the reliance of calving laws and numerical models to predict the frequency of iceberg calving events and how it may impact the ice front and thus behaviour of the glacier. Increasing the magnitude and frequency of iceberg observations at an ice-sheet scale will provide greater insights into the dynamics of iceberg distributions in the fjord and how glacier behaviour may impact resulting iceberg size distributions.

To infer the calving behaviour of glaciers through iceberg distributions in the near-terminus region, power laws have often been used. These power laws derive an alpha value (or power law slope) to quantify the type of iceberg distribution calved from a glacier with more negative values (e.g. -2.7) indicating small icebergs dominate and more positive values (e.g. -1.9) suggest larger icebergs dominate the distribution.

While power law metrics have been used to investigate calving behaviour and iceberg size distributions in Greenland (e.g. Sulak et al., 2017; Scheick et al., 2019; Rezvanbehbahani et al., 2020), the resultant alpha value relies on the definition of an x_{min} value that removes a significant proportion of smaller icebergs from a dataset as they may fit a different distribution. This meaning that all iceberg sizes below a certain threshold are not considered as part of the distribution. Values of x_{min} will also depend on the spatial resolution of the dataset being used to detect icebergs and the research question being investigated. For example, x_{min} values have ranged from as low as 288 m^2 to 12000 m^2 using different datasets (Rezvanbehbahani et al., 2020), while different values have been defined for the same glacier (e.g. Sermeq Kujalleq [SKJI], Scheick et al., 2019; Chapter 4). Consequently, the alpha value can vary significantly depending on both the imagery being utilised and the glacier in question, while having to remove large quantities of data to access one value. A further parametrisation of the x_{min} is that the value must be defined equally across all comparable iceberg distributions from every study site.

Here we constrain iceberg probabilities and distributions around the GrIS from an updated iceberg detection workflow developed in Google Earth Engine (GEE) (Chapter 4). The iceberg outlines are automatically delineated from ArcticDEM v3 strip data with associated metadata to allow ease upon post-processing. This study aims to quantify iceberg distributions in the near-terminus regions of Greenland's outlets, constrain the probabilities of iceberg volume sizes calving into the fjords and investigate whether there are any immediately apparent relationships between iceberg sizes and glacier boundary conditions (namely glacier termini

depth and solid ice discharge). It is hypothesised that deeply grounded terminus positions (>230 m) promote the formation of basal crevasses and allow full thickness calving events (Bassis and Walker, 2012) which typically produce large tabular icebergs (James et al., 2014). A second hypothesis which is tested is the concept that glaciers with higher discharge rates could potentially calve large icebergs.

5.1 **Methodology**

5.1.1 Fully automating iceberg detection

Chapter 4 introduced a highly automated workflow that relied on a user defined search window, however this Chapter fully extends the workflow to allow full automation with no user input. The most significant update from the original workflow is that instead of relying on a manual operator to delineate a region of interest (ROI) for an ice front, it is automatically defined with no manual delineation. This additional step has been implemented to fully automate the workflow, as well as providing consistency of the ROI delineation across the ice sheet. However, geographical bias will remain in ArcticDEM imagery because of data availability to derive DEMs using WorldView data (Porter et al., 2018). A temporal bias will also exist in ArcticDEM data depending on the quantity and timing of when the satellite imagery was acquired to generate the subsequent DEMs (e.g. there are more available DEMs in 2015 than 2011 in our dataset). To ensure consistency across the ice sheet and remove the manual delineation of a search window, the ROI is automatically delineated 2 km proceeding every marine-terminating ice front in Greenland.

Automated search window delineation was achieved by importing the TermPicks dataset (Goliber et al., 2022) into GEE which includes 39060 terminus traces for 278 of Greenland's outlets. These data have compiled terminus traces from numerous different authors and have homogenised their geospatial format for ease and subsequent usage. To define an ROI using these traces, we filtered the data to align with the closest ArcticDEM scene to provide an ice front position for each DEM. The selected trace was then buffered by 2 km on to the respective DEM and the ROI was forged (see Figure S3). The automated ROI definition using TermPicks also allows the search window to be dynamic at an individual glacier site. For example, if a terminus had experienced a retreat and/or advance, the ROI also tracks these changes.

Once the ROI is constructed and the ArcticDEM scenes are clipped to it, a 50 m edge buffer then forms, meaning any icebergs overlapping these areas are filtered out, removing the potential for falsely identifying icebergs as fjord walls or erroneous termini. This filter also

ensures entire icebergs are detected and not just remnants of half an iceberg which would incorrectly influence the subsequent distribution analysis.

Further functionality has also been added to the workflow in this study to increase the amount of useful metadata of each iceberg. These include:

1) the mean, median, maximum and standard deviation of a glacier's terminus depth which calved the iceberg (from BedMachine v5; Morlighem et al., 2017),
2) the derived iceberg keel depth,
3) the area of the ROI covered by water and icebergs (km^2),
4) the glacier terminus width (distance between start and end coordinate of terminus),
5) the date of the terminus delineation used for the ROI delineation,
6) the glacier identification number from the TermPicks dataset to allow reference to each glacier name (if applicable) and location.

This new workflow represents a significant extension of that presented in Chapter 4. The new code not only allows fully automated ice sheet wide iceberg detection for the first time, but also information of the parent glacier (e.g. terminus depth) appended as metadata which can provide further analysis when assessing the iceberg dataset and can reduce user time post-processing.

5.1.2 Iceberg detection across the ice sheet

The iceberg data were identified from all available ArcticDEM scenes around the GrIS. The western and eastern coasts had the most readily available data, while the northern section of the ice sheet has sparse data coverage (Figure 5.1). The southwest coast may appear to have limited data coverage, however compared to the remainder of the ice sheet this section does not host many tidewater glacier systems. The glaciers were divided into their respective ice sheet wide sectors in accordance to Mouginot and Rignot (2019) drainage basins (SW = southwest, CW = central west, NW = northwest, NO = north, NE = northeast, CE = central east, SE = southeast). The number of available DEMs for subsequent iceberg detection ranges from 1 to 22 across the ice sheet, varying how many icebergs are identified at each glacier. These data are acquired from 547 individual ArcticDEM scenes across the ice sheet.

The icebergs were identified by the workflow using the same approach as described in Chapter 4 (see section 4.2) where an automated sea level is defined for each ArcticDEM scene. From the subsequent value, any object which is 1.5 m above the calculated sea level is considered an iceberg (see Chapter 4 for the explicit validation of the detection process). The workflow was executed using this detection threshold to ensure the smallest icebergs could be identified (area = 36 m^2). Further to this, analysis is limited to DEMs acquired between July and October as fjords are less likely to be choked with sea ice and rigid mélange conditions, meaning open water will dominate in most fjords and a 1.5 m detection threshold is therefore suitable.

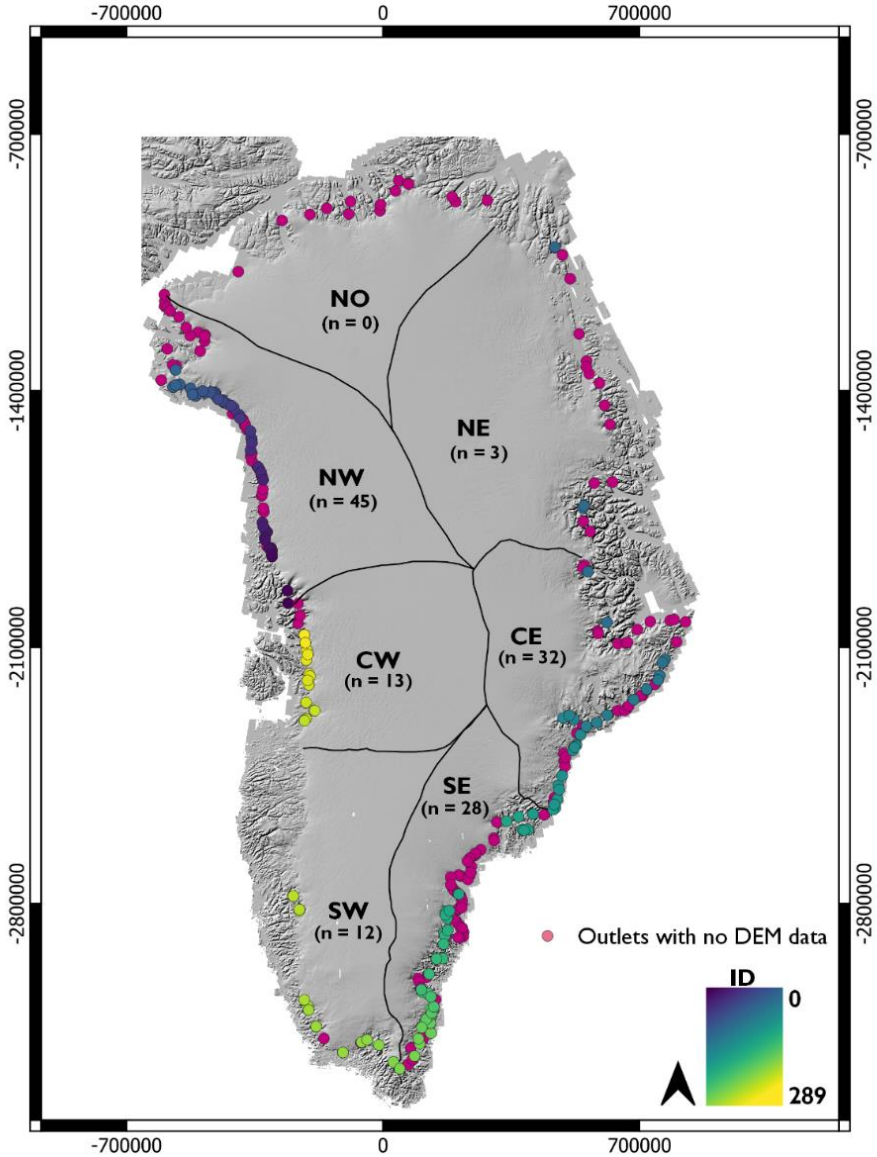

Figure 5.1. Location of all the marine-terminating glaciers around Greenland. Outlets which have ArcticDEM strip coverage (v3) and used in this study are colour coded by their ID (viridis gradient) and the outlets which are not covered by the data are highlighted with purple dots. These data are categorised by region, according to the Mouginot and Rignot (2019) drainage basin dataset. The base Greenland map is the 10 m v3 ArcticDEM mosaic product (Porter et al., 2018).

5.1.3 Terminus depth and discharge

To identify any conditional control on iceberg distributions, we utilised data including glacier terminus depth (Morlighem et al., 2017) and solid ice discharge (Mankoff et al., 2020). The BedMachine v5 data was used to derive the terminus depths (mean, maximum, standard deviation) around the ice sheet in the GEE workflow, whereas the discharge data was generated post-processing. The terminus traces (Goliber et al., 2022) contained identification numbers relating to the Mankoff et al. (2020) dataset.

5.2 **Results**

5.2.1 Identified icebergs

The workflow identifies 133 marine-terminating glaciers around the GrIS with available ArcticDEM strip data, detecting a total of 1,304,288 icebergs between 2010 and 2017. Similar to the findings presented in Chapter 4, the workflow identifies two iceberg distributions: 1) icebergs and 2) iceberg rafts across the ice sheet in the near-terminus region. As we are only interested in the calving dynamics of the glaciers presented here, we filtered distribution two from the analysis as these data points do not necessarily occur as a direct result of calving. By doing so, the final dataset that only contained data from distribution one which was comprised of 1,123,514 icebergs, showing distribution two only accounts for 14% of the total dataset. Furthermore, any erroneous icebergs which have merged to make one larger iceberg will tend to have the same area, but their respective volume will be less and therefore reside in distribution two.

5.2.2 Updated iceberg area to volume conversion

To derive a volumetric capacity from a planform surface area of an iceberg from two-dimensional satellite imagery, a convertor is required (Sulak et al., 2017; Chapter 4). While convertors exist, the magnitude of the dataset produced here (1.1 million icebergs from 133 glaciers) is a marked improvement from previous datasets deriving convertors (163000 from three glaciers and 712 icebergs from one glacier). Consequently, we present an updated iceberg area-to-volume conversion from those presented by Chapter 4 and Sulak et al. (2017) (Figure 5.2). This new conversion can be expressed as

$$V = 7.01A^{1.20} \quad (5.1).$$

As well as equation 5.1, iceberg volumes derived from the conversions presented in Chapter 4 and Sulak et al. (2017) plot in the observed iceberg volumes from around the GrIS (Figure 5.2). The new conversion presented here is derived from the binned mean values for the iceberg

observations (e.g. 30 to 40 m^2, 300 to 400 m^2, 3000 to 4000 m^2 etc.) to avoid bias towards the more abundantly identified smaller icebergs.

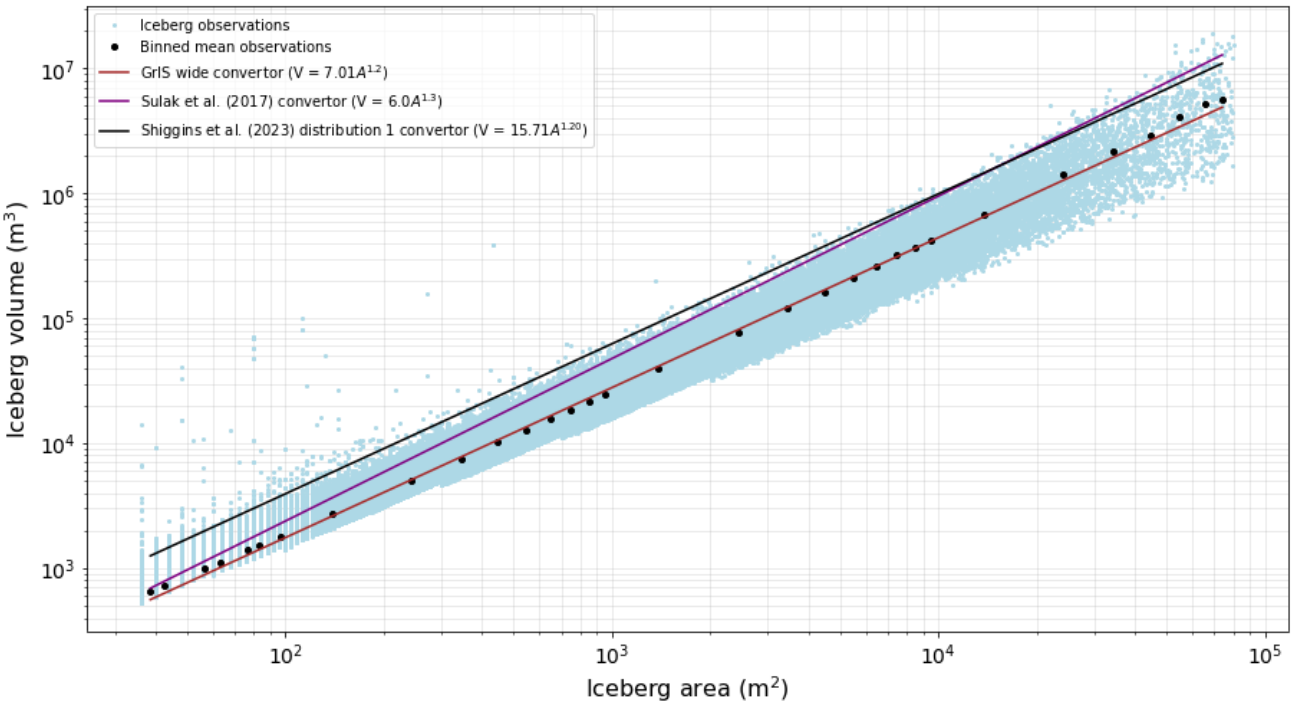

Figure 5.2. The binned mean for each size class for the entire distribution 1 dataset, overlaid with the Sulak et al. (2017) conversion (purple), the one derived here (brown) and the Chapter 4 conversion for distribution 1 (solid black line).

5.2.3 Iceberg probabilities and differences

The most frequently occurring iceberg volume size for each sector across the ice sheet is within the 1000 to 2000 m^3 bin range with probabilities exceeding 0.25 (Figure 5.3). Some glaciers within their respective sectors do deviate from the sector average, however the structure of the probability densities are similar across the ice sheet (Figure 5.4). Nevertheless, the differences of those probabilities within each sector are notable, as are the differences between the sectors and the Greenland average (Figure 5.4). These differences are particularly notable for the sector and Greenland average for icebergs sizes exceeding 10000 m^3. They become even more pronounced when icebergs from each glacier are compared to their sector average, showing significant heterogeneity, which is exacerbated in the larger iceberg sizes (Figure 5.4). These pronounced differences occur due to the high abundance of small icebergs which account for the majority of the total count, however their larger counterparts are rare and may only occur once or twice (if at all) in the larger logarithmic bin sizes.

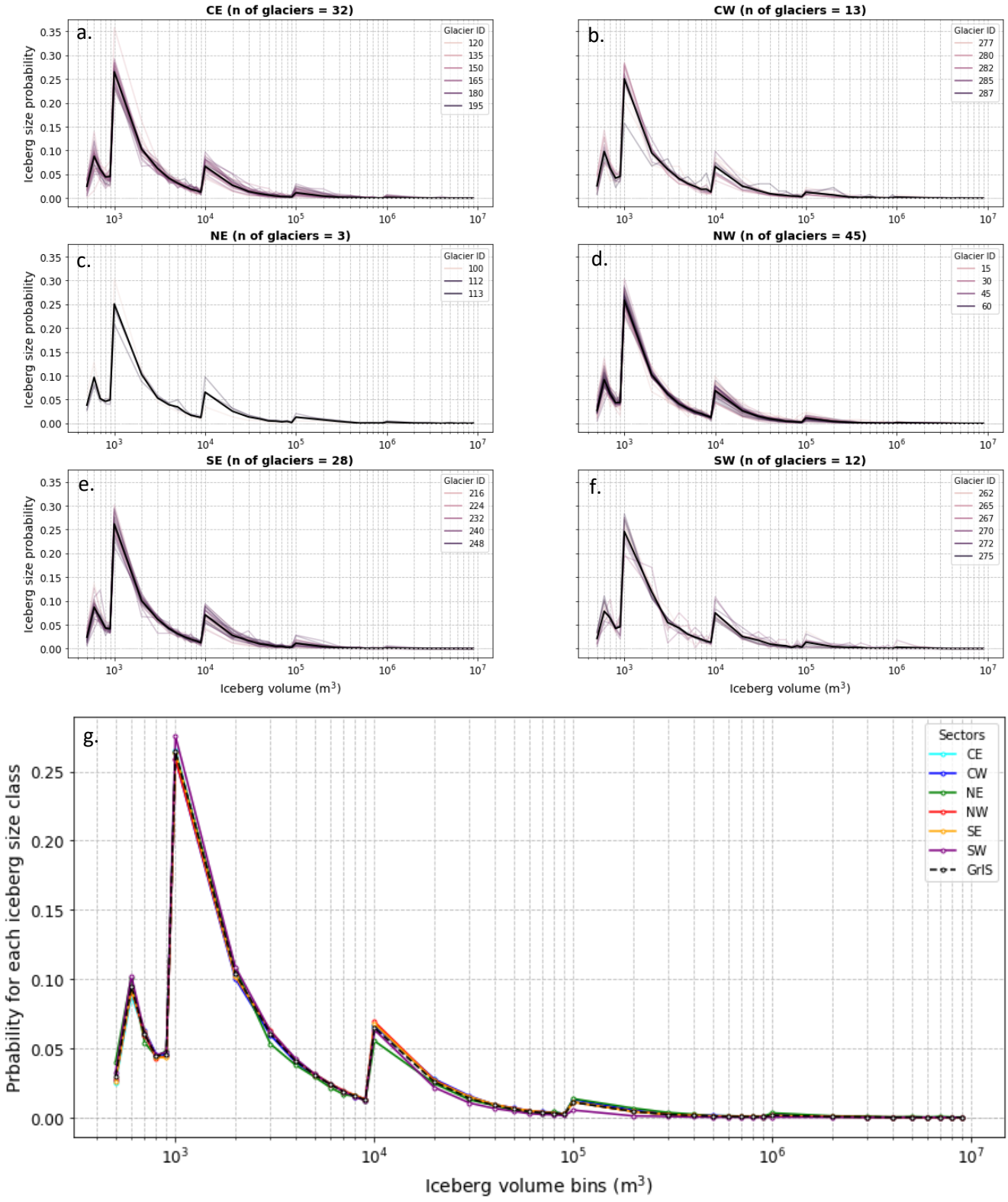

Figure 5.3. Iceberg volume probabilities for the bin value (e.g. 100 to 200 m^3, 1000 to 2000 m^3 etc.) of each sector of the ice sheet and their respective glaciers (a to f). The underlying subplot (g) compares sector wide probabilities to identify any differences across the sectors. The Greenland average iceberg size probability is overlaid to identify any sector divergences. The sector plots have legends which represent the glacier ID range by colour gradient. The black line in each sector plot represents the sector probability average.

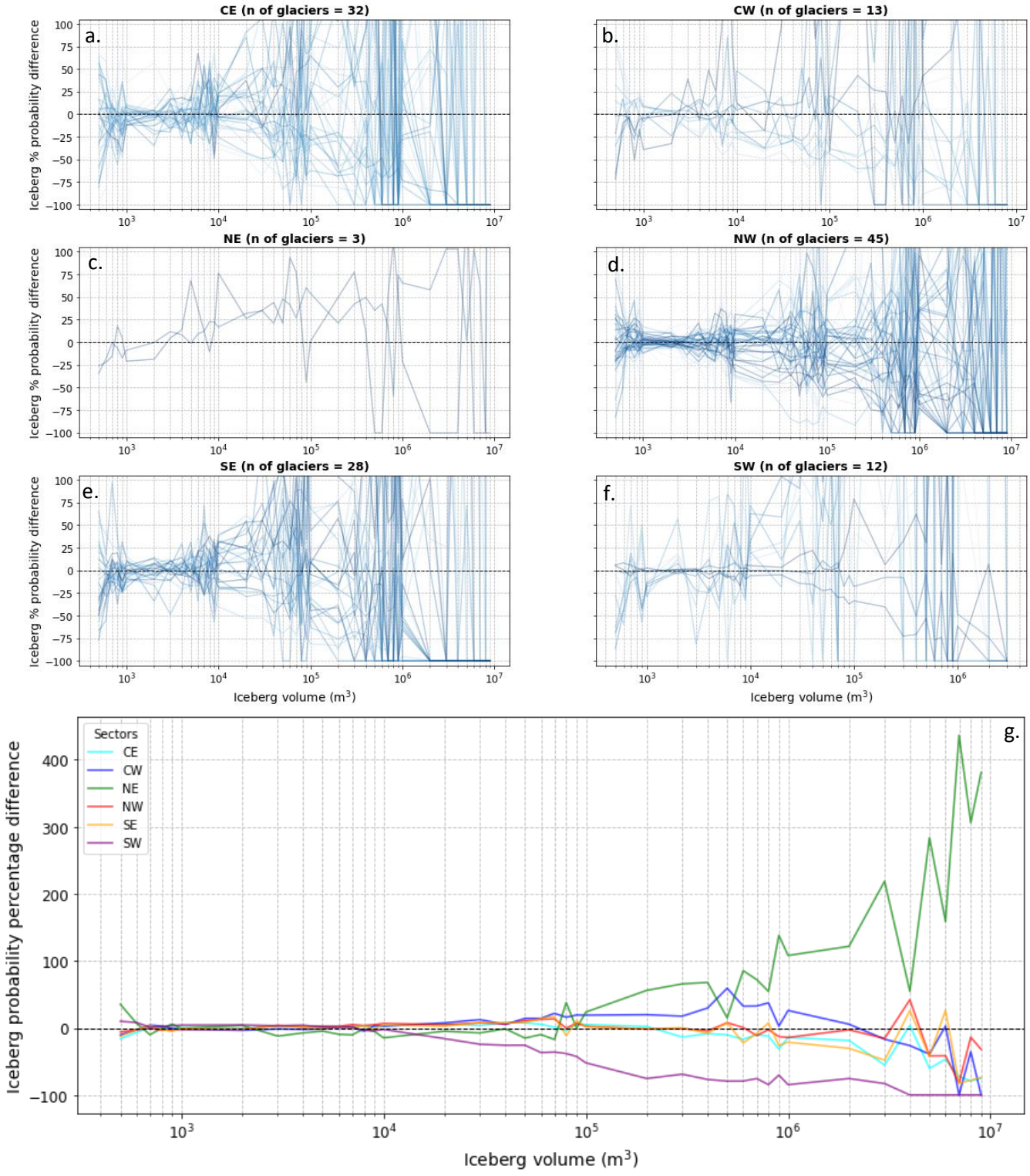

Figure 5.4. The difference of iceberg size probabilities per glacier within their respective sector and how they compare to their sector average (a to f). There is high variability as the deviation of iceberg sizes at one particular glacier can significantly differ to that of sector averages which may contain large and small iceberg producing glaciers. The lowermost subplot (g) compares the sector wide averages against the Greenland average.

5.2.4 Iceberg count and volume

The evident iceberg variability exceeding 10000 m^3 shows a distinct difference in iceberg probabilities (Figure 5.4) and reveals key differences between these iceberg sizes. Icebergs smaller than this value dominate the total iceberg count in Greenland's fjords (median = 87%), but only comprise of 12% (median for dataset) of the total volume (Figure 5.5). Some fjords do deviate from this pattern, whereby their total volume is split relatively evenly between icebergs above and below 10000 m^3, however the majority of the total iceberg volume in Greenland's fjords are dominated by icebergs exceeding 10000 m^3 (57% to 97%) (Figure 5.5).

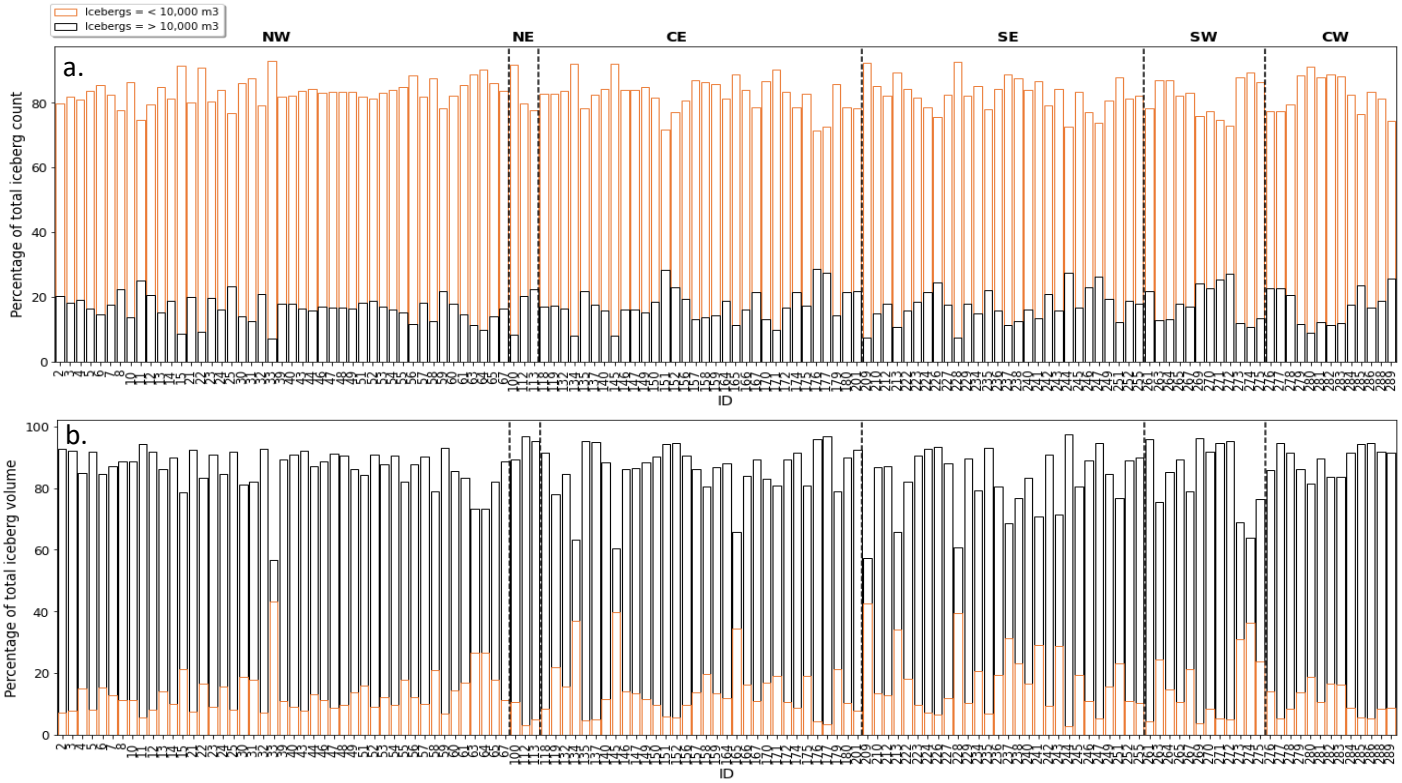

Figure 5.5 Total iceberg count (a) and iceberg volume (b) separated by icebergs preceding (orange bars) and exceeding (black bars) 10000 m^3 for each glacier ID around the ice sheet. Each ID is separated into their respective sector to observe any spatial relationships.

The number and total volume of the fjord made up of icebergs exceeding 10000 m^3 can be described as a power law relationship with higher iceberg counts resulting in a greater percentage of total volume (Figure 5.6). These findings are consistent across the ice sheet, meaning no sector is distinct from the general trend. By observing this across each sector of the ice sheet (other than the NE due to data availability), it is possible to identify strong to very strong relationships between the higher percentage of iceberg count which usually account for a larger percentage of total volume in the larger iceberg categories. Pearson's r-values for the sectors range between 0.69 and 0.91. While the weakest relationship exists in the CW, the total

volume is made up of > 80% of icebergs exceeding 10000 m^3. The stronger relationships in the SE (r = 0.91) and SW (r = 0.90) fjords exist because larger icebergs contribute to 57% to 95% of the total volume.

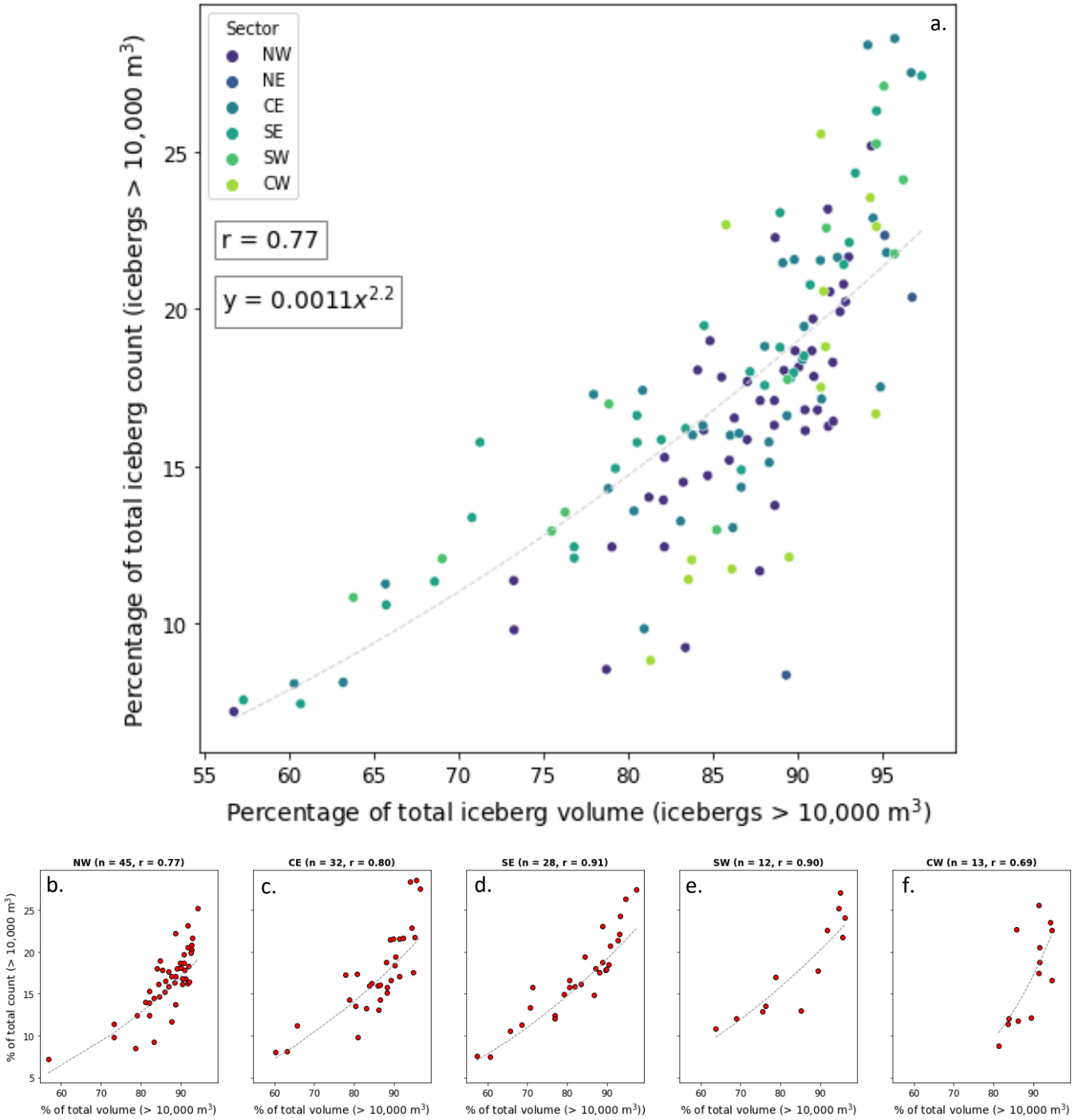

Figure 5.6. Plot of percentage of total iceberg count versus total iceberg volume (icebergs > 10000 m^3), yielding a power law function (a). Beneath are subplots for each sector (excluding the NE due to only containing three glaciers) of iceberg count versus volume (icebergs > 10000 m^3) with respective r-values (b to f). Relationships vary by sector, with r-values ranging from 0.69 to 0.91.

5.2.5 Iceberg distributions and terminus depth

The icebergs were identified in-close proximity to the ice front (2 km) and were fitted to power law distributions to derive alpha values for each glacier. The power law slope value for each glacier were then compared with their respective mean terminus depths (Figure 5.7). However, there is no evident relationship between iceberg sizes and the depth of the terminus which calved them. By conducting this analysis during the months of the study period (July to October), it is not possible to identify clear patterns of variation in iceberg size distributions, discounting any primary control from the melt season (e.g. iceberg size distributions identified in July are not significantly different from those delineated in October). In some cases, deeply grounded termini (> 230 m) calve icebergs that are larger which dominate the distribution (less negative power law slope values), but no meaningful temporal relationship can be derived between the two parameters. There is also no evident metric between iceberg distributions and the glaciers solid ice discharge (see Figure S4 and Figure S5).

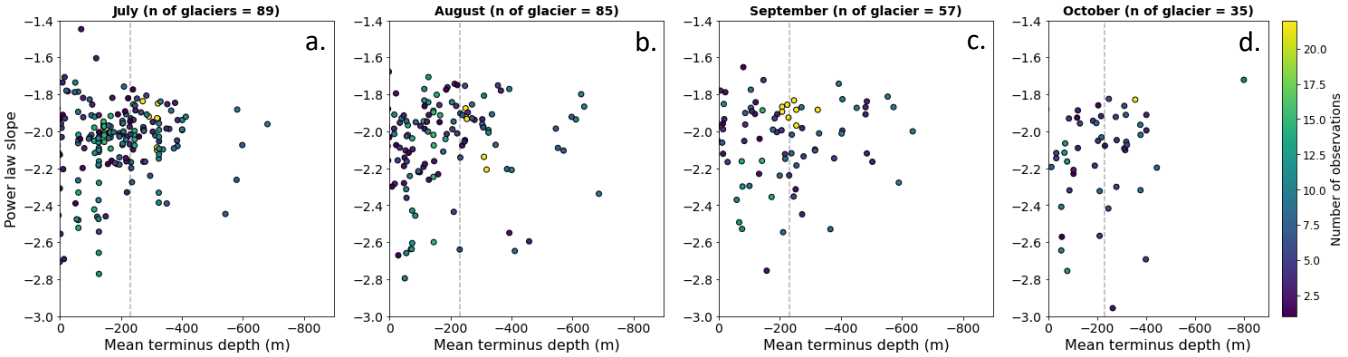

Figure 5.7. Power law distributions (alpha value) for each glacier ID versus their respective glacier's mean terminus depth, separated into the month in which the ArcticDEM data was acquired to observe any monthly divergences in calving style as a result of the melt season. A Greenland wide x_{min} was defined at 1000 m^2 to provide consistency across the removal of icebergs below the defined threshold to fit the iceberg distributions and allows spatial comparisons.

5.3 **Discussion**

5.3.1 Iceberg detection workflow

The combination of ArcticDEM data with data from TermPicks (Goliber et al., 2022) allowed full automation of the workflow presented in Chapter 4, allowing pan-ice sheet scale iceberg detection to be performed for the first time in a methodologically consistent way. The resultant data is high quality and three-dimensional, therefore being able to provide true iceberg volume size distributions in the fjords of Greenland. The modified workflow allowed a time-evolving ROI through the fjord, depending on the terminus position at the time of data acquisition. This ensured the icebergs were identified in-close proximity to the terminus through time and

captured distributions to best describe calving dynamics. The updated workflow has been able to assign a greater quantity of useful metadata to each iceberg, providing contextual information for user post-processing, including the glacier ID, the terminus depth of the glacier, the terminus width, and the fjord area (km^2) covered by water and icebergs.

The iceberg detection workflow has provided new opportunities to gain crucial insights into the size of icebergs and how they are distributed at the front of Greenland's outlets, as well as providing useful supplementary metadata. The technique used to automatically delineate the ROI is transferrable to different iceberg detection workflows as the method does not rely on elevation data for definition. Consequently, the ROI delineation could be applied to satellite imagery (e.g. optical/SAR) with greater spatial coverage and higher temporal resolution to detect icebergs and fully automate the workflow.

5.3.2 Iceberg area to volume conversion

The new iceberg area-to-volume conversion presented here is derived from over 1.1 million icebergs and is therefore comprehensive in its representativeness of ice calved by Greenland's outlets which has not been achieved to date (e.g. Sulak et al., 2017; Chapter 4). While it is true that a new convertor can be derived for every new dataset produced, the one presented here is capable of transforming a planform surface area to a three-dimensional volume and is the most accurate convertor available (Figure 5.2).

It is worth noting that the iceberg volumes derived from the planform surface areas using the new convertor presented here plot below the iceberg volumes derived from the previous convertors (Figure 5.2). This is as a result of the icebergs being delineated within 2 km of every ice front, meaning that their decay (i.e. how an iceberg will be modified through further fracture and melt after calving) will be different to the icebergs identified in previous work (Sulak et al., 2017; Chapter 4). Consequently, the residence time of the icebergs identified in the fjord here is likelier to be much less, meaning that their modification due to melt and fracture will be less significant, particularly when compared to Sulak et al. (2017). The convertor presented in Chapter 4 did delineate icebergs close to the ice front, but not directly proceeding as it was not dynamic through time. While the convertor presented here plots below the previous ones, the iceberg volumes derived from all of the convertors plot within the observed iceberg volumes, showing their versatility (Figure 5.2). These findings highlight the need for using the correct convertor for the research question being addressed. The convertor presented in this Chapter is derived from the largest known dataset created and is well suited for icebergs in

glacier proximal regions. However, it may not be the most approportionate conversion for icebergs identified further down fjord that have been significantly modified by calving and melting.

5.3.3 Iceberg probabilities and differences

Iceberg probabilities are similar in structure across the GrIS with smaller icebergs (< 10000 m^3) being the most frequently identified (Figure 5.3), though key differences exist in iceberg distributions, particularly those exceeding 10000 m^3 for both ice sheet sectors and individual glaciers (Figure 5.4). The variation in the larger iceberg size ranges are as a result of extremely low probabilities when compared to either the ice sheet or sector average. Consequently, these large percentage differences from their probabilities are to be expected. For example, if a glacier in the CW calves no iceberg greater than 1,000,000 m^3, but neighbouring glaciers in the same sector do, then the percentage difference will be significant for that glacier's probability for iceberg sizes in that logarithmic bin range. Such a scenario can be heightened for sectors which contain large iceberg producing glaciers which dominate sector-wide discharge, e.g. SKJI in the CW and Helheim in the SE.

Discussing iceberg residence time in Greenland's fjords, it is apparent larger icebergs are not identified very frequently (5% to 27% of sector iceberg total) when compared to their smaller counterparts, however this does not mean the glaciers around the ice sheet only calve a large iceberg every several days. If the fjord regions close to the terminus are ice free at our study sites during the summer, it is entirely plausible that an iceberg's residence time may be quite low proceeding the glacier. The workflows 2 km search window therefore may not identify particularly large icebergs which may have calved in recent days that have drifted down-fjord out of observable spatial range. This could therefore result in the distributions only containing smaller icebergs in the observable ROI (i.e. bias towards the observation of smaller icebergs), however larger icebergs are calved, potentially just not in the observable search window. Consequently, due to the snapshot nature of our dataset and the current temporal coverage of ArcticDEM it is not possible to quantify the magnitude of this effect.

5.3.4 Disproportionate iceberg count and volume

While icebergs which exceed 10000 m^3 are rare in terms of their overall counts, they are found to dominate the total volume within the ice sheets fjords (Figures 5.5 and 5.6). We therefore divided the data into two segments, those preceding and exceeding 10000 m^3 to see how their distributions alter. Every fjord in Greenland is constituted of >72% of smaller icebergs.

A non-linear relationship (r = 0.77) can be observed between large iceberg count and their respective volume (Figure 5.6). Fjords that have a higher number of large icebergs (~20%) have their total iceberg volume dominated (> 90%) by this size class. However, fjords with less large icebergs identified (~7%) can still have 90% of their total volume made up by these icebergs. Consequently, large icebergs do not necessarily need to be abundant in number to dominate the fjords total volume. These findings reveal that while small icebergs are important for the total iceberg count in the fjord, the mass loss from calving around Greenland's outlets are dominated by large iceberg calving events.

The percentage of larger icebergs can vary by sector, enhancing their importance in glacier mass loss and fjord dynamics. The CW has the weakest relationship (r = 0.69) across the ice sheet, whereby each glacier's fjord volume is made of >80% of icebergs exceeding 10000 m^3. It should be noted that this could be an artefact of the glaciers that are available for iceberg detection (i.e. where larger icebergs dominate fjord cover) due to ArcticDEM coverage.

5.3.5 Difficulty constraining iceberg distributions and boundary conditions

Observing relationships between iceberg sizes, a glacier's depth and solid ice discharge is not currently possible due to data quality and availability. By comparing power law slopes and termini depth has revealed in some cases, deeply grounded glaciers (> 230 m) can have iceberg distributions dominated by larger icebergs, however it is not the case ice sheet wide. Whether a relationship does exist is difficult to quantify because of large uncertainties in the basal topography underlying Greenland's outlets using BedMachine (Morlighem et al., 2017). While a formidable dataset, issues still arise with the data, e.g. many of the outlet glaciers here have positive termini depth which is not possible for marine-terminating environments. Subsequently, if a relationship does exist at such glacier sites, it is impossible to identify as a result of large data uncertainties.

A relationship between iceberg calving and termini depths will exist because of the critical depth theory of propagating basal crevasses (Bassis and Walker, 2012) which will likely result in more full thickness calving events (James et al., 2014). As a result, deep glaciers are more likely to calve larger icebergs which can dominate a distribution when compared to smaller icebergs detached via serac failure. However, uncertainties surrounding the accuracy of the glacier boundary condition data that are currently available mean that it is not possible to decipher relationships with iceberg distributions currently.

With the data available, it is evident that there is no immediately apparent seasonal variation in calving behaviour at an ice sheet scale between July and October (Figure 5.7). We are not suggesting that seasonal variability does not exist in Greenland's iceberg distributions, rather when observations across the ice sheet are combined there are no clear variations. Outlet glaciers encounter seasonal variability in the frequency of their calving events (Bunce et al., 2021) and these findings suggest data may need to be analysed at higher temporal scales to identify seasonality in iceberg distributions. The current temporal coverage of ArcticDEM inhibits the opportunity of identifying seasonality at the majority of Greenland's outlets due to the lack of multiple observations within years.

Translating a glacier's solid ice discharge into predicted iceberg volume sizes is not currently applicable using the temporal snapshots provided by ArcticDEM data (Figure S4 and Figure S5). There is no clear evidence that larger discharging glaciers have larger iceberg sizes. This is partly as a result of monthly discharge data not being transferable to a single snapshot of the fjord environment at the time of data acquisition. For example, if a relationship existed between discharge and iceberg size, by only capturing a snapshot of the fjord for one day, those larger icebergs may have drifted or have been cleared out from the 2 km ROI, meaning we cannot identify them. Consequently, the temporal aspect of data availability for both the discharge and ArcticDEM/iceberg datasets are currently incompatible to yield any meaningful relationships.

5.4 **Conclusions**

For the first time, we have been able to assemble a comprehensive dataset of 1.3 million icebergs in the near-terminus region of Greenland's marine-terminating glaciers. These data have been used to infer iceberg dynamics and how they are distributed within the fjords around the ice sheet. We have found that icebergs exceeding 10000 m^3 dominate the total iceberg volume calved by the marine-terminating glaciers around the GrIS (57% to 97%). Consequently, glacier mass loss via iceberg calving alone is dominated by large calving events, rather than smaller events. However, these smaller calving events are responsible for the makeup of the near-terminus regions and are integral to the fjord dynamics, ecology and biogeochemistry around Greenland. Each sector of the ice sheet has similar iceberg probability distributions, meaning no sector is calving in a substantially different way, though significant differences exist when compared to single glacier sites, particularly in the larger iceberg size classes. At an ice sheet scale, no evidence of shifts in calving styles occurs from July to October when runoff conditions vary substantially. Single glacier sites may experience dynamic changes, but these are not identifiable with currently available data. We also cannot yet

translate a relationship between iceberg volumes, terminus depths and solid ice discharge. However, scope for such a research question may become possible if and when more automated iceberg detection workflows that can be applied to optical satellite data are developed.

Chapter 6: Do icebergs deteriorate via calving or melting in the near terminus region of Kangiata Nunaata Sermia

Connor J. Shiggins[1], James M. Lea[1], Stephen Brough[1,2].

[1]*Department of Geography and Planning, School of Environmental Sciences, University of Liverpool, Liverpool, L69 7ZT, United Kingdom.*

[2]*Central Teaching Laboratory, Faculty of Science and Engineering, University of Liverpool, United Kingdom.*

Author contributions: Connor Shiggins led the writing and conducted all of the analysis. James Lea and Stephen Brough provided conceptual advice and contributed towards the writing of the paper.

Paper in preparation for submission to the Journal of Glaciology.

Summary: This Chapter characterises the near-terminus fjord environment of Kangiata Nunaata Sermia (KNS) and the implications for both iceberg decay and calving behaviour (Objective 4). Findings from this Chapter provide insights into whether previously applied power laws are the most suitable descriptor of iceberg size distributions in close proximity to the glacier terminus. The use of three-dimensional iceberg data alongside environmental data reveal seasonal shifts in calving behaviour at KNS, and that the magnitude and frequency of calving events are sensitive to subglacial hydrological forcing (Objective 4).

Abstract. Iceberg distributions can provide insights into the calving dynamics of marine-terminating glaciers and ice shelves around the Greenland Ice Sheet (GrIS). Iceberg area and volume distributions remain an understudied part of the complex ice-ocean interface in many different fjord environments and have offered insights into the behaviour of calving fronts in a select few sites across Greenland. Here we present both annual and monthly iceberg distributions at Kangiata Nunaata Sermia (KNS), southwest Greenland, derived in Google Earth Engine (GEE) using high spatial resolution timestamped ArcticDEM (Arctic Digital Elevation Model) version 3 2-meter strip data. The workflow detected 35412 icebergs from 12 ArcticDEM scenes for analysis between 2013 and 2017. We find that it is not possible to distinguish between whether icebergs exhibit power law and lognormal distributions, suggesting that these approaches cannot be used to separate between iceberg fracture (power law) and melting (lognormal) processes at KNS. Despite observing icebergs in the near-terminus region of KNS, log-likelihood ratios suggest lognormal distributions are the most suitable candidate to describe the iceberg distribution in the fjord through time. Fewer icebergs are observed in August and tend to be smaller in area and volume size when compared to icebergs identified in September and October. The calving of these smaller icebergs occurred after peak runoff values in each year, and following a drop-in ice velocity likely associated with the evolution of a channelised subglacial drainage system. For each month, over 90% of the icebergs in the dataset are small (< 1000 m^2) and contribute significantly (43% to 61%) to the total iceberg volume in the fjord proximal to the ice front. This suggests that small icebergs, particularly in August have overarching importance for solid ice loss from KNS. These findings reveal: 1) power laws are not the best descriptor of iceberg distributions in the near-terminus region of KNS, rather lognormal are better suited and 2) a transitional phase of increasing iceberg sizes between August and October. These results have implications for both remote sensing and numerical modelling studies that suggest sole distributional fits should not be assumed to be the only appropriate candidate to describe iceberg size distributions in close proximity to an ice front.

6.0 **Introduction**

The GrIS lost 3800 gigatonnes of ice between 1992 and 2018, 48% of which was from marine-terminating glaciers (Shepherd et al., 2020) due to iceberg calving and submarine melting. By 2100, solid ice discharge could account for between 22 and 70% of the total mass loss from the GrIS (Choi et al., 2021), highlighting that the evolution of iceberg calving is poorly constrained. However, studies determining how icebergs are distributed in Greenland's fjords has become much more prominent in recent years because they offer insights into the behaviour of iceberg calving (e.g. Enderlin et al., 2016; Kirkham et al., 2017; Sulak et al., 2017; Scheick et al., 2019; Rezvanbehbahani et al., 2020; Åström et al., 2021; Cook et al., 2021; Chapters 4 and 5).

Understanding spatial and temporal changes in iceberg distributions can provide information into how calving regimes may evolve in the future and therefore improve our solid ice discharge predictions from the outlet glaciers which drain the ice sheet. For example, Sermeq Kujalleq's (also known as Jakobshavn Isbræ) summer calving regime transitioned from low energy calving events producing large and tabular icebergs (2000-2002), to higher energy calving events producing smaller icebergs (2013-2015) because of the frontal change from a year-round floating ice tongue to a seasonally grounded terminus (Scheick et al., 2019).

Icebergs deteriorate via two main processes: fracture and melting. Iceberg decay via fracture typically occurs when icebergs first calve from their parent glacier and have been described as fitting a power law distribution (Sulak et al., 2017). However, as icebergs begin to drift down fjord, they primarily melt and are described as following a lognormal distribution (Kirkham et al., 2017). Power law distributions have been effectively utilised to determine calving behaviour at a select few sites in Greenland, including: Sermilik Fjord (Enderlin et al., 2016; Sulak et al., 2017; Rezvanbehbahani et al., 2020), Disko Bay/Ilulissat (Enderlin et al., 2016; Scheick et al., 2019), Kangerlussuaq (Rezvanbehbahani et al., 2020), Kangerlussuup (Sulak et al., 2017) and Rink Isbræ (Sulak et al., 2017). A key metric obtained from these distributions is the power law slope value (or α exponent) which determines the iceberg characteristics present in the fjord at the time of data acquisition. Power law slope values for Greenlandic outlets have been observed to range from -1.23 to -2.89 in the previously mentioned studies (Table 3.2). More negative exponents are indicative of smaller icebergs in the distribution (e.g. -2.89), whereas less negative values (e.g. -1.23) suggest larger icebergs dominate the population (Chapters 4 and 5).

While a range of alpha values have been noted from Greenland's outlets, they are not necessarily directly comparable due to the definition of the x_{min}. This value removes iceberg sizes below a threshold value to allow the best fitting of a power law distribution. The x_{min} is therefore fundamental to the resultant power law slopes, however its definition is dependent on the size of glacier being studied and the spatial resolution of data being used to identify the target icebergs.

Iceberg size distributions are not only important for remote sensing and field-based studies, but also for model domain setup, inferring iceberg melting and the subsequent release of freshwater, such as Davison et al. (2020a) assuming power law slope values of -1.8 to -2.0 in an adapted Massachusetts Institute of Technology General Circulation Model. However, once icebergs begin to drift down fjord and out into the open ocean, they are considered to transition from power laws to lognormal to best describe their distribution (Kirkham et al., 2017). This distributional transition suggests icebergs predominately disintegrate through breakup close to the ice front, however melting becomes the dominant control as they exit the fjord mouth (continuous decay).

The characterisation of the number and size of icebergs within a fjord can be used to derive their potential freshwater budget (Enderlin et al., 2016; Moyer et al., 2019; Davison et al., 2020a). Iceberg meltwater fluxes can reduce ocean thermal forcing close to the fjord surface and direct heat fluxes towards the glacier calving front, enhancing submarine melt (Davison et al., 2020a). Only 9-14% of the icebergs calved from Helheim Glacier leave Sermilik Fjord as a solid ice flux, highlighting the substantial release of freshwater from melting and changing iceberg distributions through the fjord (Moyer et al., 2019). Ice mélange (matrix of sea ice and icebergs) water fluxes dominate the freshwater budget Illulissat Isfjord (678 – 1346 $m^3 s^{-1}$) and Sermilik Fjord (126 – 494 $m^3 s^{-1}$) (Enderlin et al., 2016).

There are 285 marine-terminating glaciers across the GrIS which are all dynamically different, however, only a handful of outlets have had their iceberg area and volume size distributions constrained from temporally limited snapshots. Consequently, to gain a comprehensive understanding of iceberg distributions at Greenland's outlets, more workflows are needed to identify a greater number of iceberg distributions across a wider range of glaciers, and covering a wider temporal range. These data are necessary for deriving glacier calving behaviour through satellite imagery (e.g. Scheick et al., 2019), but as well for model input to derive real-world simulations (e.g. Davison et al., 2020a). Here we therefore present annual and monthly

iceberg area and volume size distributions at Kangiata Nunaata Sermia (KNS), southwest Greenland between 2013 and 2017 to identify changes in the calving regime. We also aimed to determine whether iceberg degradation at the ice front was dominated by fracture (power law distribution) or melt (lognormal distribution) processes.

6.1 **Study site**

KNS is the largest marine-terminating glacier on the southwest coast of Greenland with a mean ice discharge (2010-2018) of 4.92 Gt yr^{-1} (Mankoff et al., 2020). The glacier has retreated significantly from its Little Ice Age maximum position (Lea et al., 2014a; Lea et al., 2014b), but has remained stable in the last decade (Davison et al., 2020b) with a grounding line depth of approximately 250 meters (Morlighem et al., 2017) (Figure 6.1). The evolution of KNS' seasonal velocities have been previously found to be sensitive to the development of an efficient hydrological system, rather than terminus position and/or the presence of ice mélange (Davison et al., 2020b). Subglacial hydrology at KNS' grounding line not only employs a strong control on velocity, rather it has been suggested to reduce the number of calving events in the summer following evolution to a channelised hydrological system and localised plume surfacing (Bunce et al., 2021).

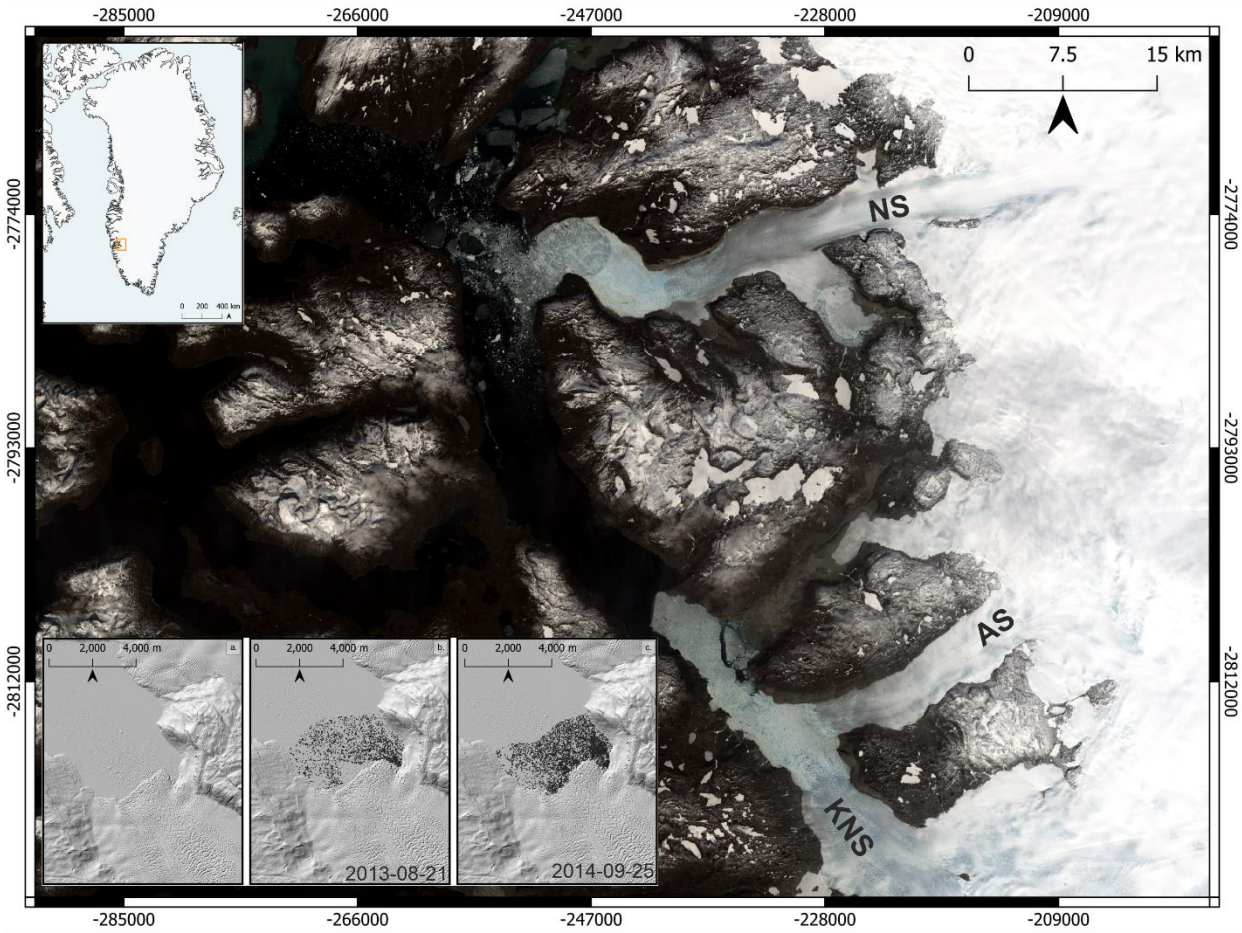

Figure 6.1. The location of Kangiata Nunaata Sermia (KNS) and Nuup Kangerlua. The base map is a Landsat 9 image acquired on 28th May 2023 with the insets showing that KNS lies in the southwest region of Greenland and the ArcticDEM mosaic in the near-terminus region (a). The subpanels (b) and (c) show the near-terminus region of KNS overlaid with identified icebergs from individual ArcticDEM scenes from 2013-08-21 and 2014-09-25. These subplots show the dynamic ROI and how it is able to identify icebergs in different sections of the fjord, depending on terminus position through both space and time.

6.2 **Methodology**

6.2.1 Iceberg detection

The icebergs identified at KNS were automatically delineated from a GEE workflow using ArcticDEM v3 strip data (Chapter 5 workflow). The DEMs available for analysis were limited to the summer months to avoid the presence of rigid mélange and the breakup of KNS' seasonal ice tongue which can influence the derivation of sea level and thus iceberg detection within the workflow. These filters resulted in DEMs being available in August, September and October at KNS. To maintain iceberg identification consistency at KNS, a detection threshold of 1.5 m above sea level was determined which ensured the smallest icebergs could be detected and is the value validated in Chapter 4 at KNS.

The icebergs delineated from the ArcticDEM scenes were detected 2 km proceeding KNS' terminus using the workflow described in Chapter 5 which automatically defines a ROI, using terminus observations from TermPicks (Goliber et al., 2022). The ice front of the glacier is relatively stable (Davison et al., 2020b), meaning the search window does not transition kilometres through the fjord, however the terminus has moved during the study period (~500 m to 1 km) (Figure 6.1). The ability of the workflow to adaptively adjust the ROI ensured the delineated icebergs were always within 2 km of the ice front, and captured icebergs that were the mostly likely to have been recently calved and not significantly modified through subsequent melt and/or fracture.

6.2.2 Iceberg distributions

As the ROI for the entire ArcticDEM collection was within 2 km of the ice front at the time of data acquisition, the icebergs were initially fitted to power law distributions. However, this study wanted to infer whether power laws were the best descriptor for the icebergs proximal to KNS, therefore we statistically compared them with a lognormal distribution. We also present iceberg sizes and iceberg counts as a cumulative percentage to identify how iceberg distributions vary temporally and reveal how different iceberg sizes can have importance to the fjords total volume and count.

6.2.2.1 Power law and lognormal distributions

Power laws are distributional fits and describe how a relative change in one parameter can affect another. At the time of calving and in the near-terminus region, it has previously been considered icebergs follow a power law distribution and transition into a lognormal distribution as they drift down-fjord and into the open ocean (Kirkham et al., 2017). The identified icebergs were fitted to both the heavy-tailed power law and lognormal distributions to infer which, if any is the best descriptor of iceberg distributions in Nuup Kangerlua (Figure 6.1).

To do this, we utilised the 'powerlaw' Python package developed by Alstott et al. (2014) which is capable of deriving and statistically comparing power law and lognormal distributions using log-likelihood ratio (R) tests. The comparisons between both heavy-tailed distributions using the R tests derives a comparative significance value that determines which distribution is most likely to best fit the icebergs in the fjord. If the significance value is not exceeded (p-value = < 0.05), it statistically determines only one candidate as suitable to best describe the iceberg distribution. If the p-value exceeds 0.05, the data cannot statistically discount a distribution as an inappropriate fit for the icebergs. When comparing the two distributions and a log-likelihood

ratio is derived with positive values, this indicates a power law is the better distributional fit, while negative values suggest lognormal is the most suitable candidate.

When fitting the icebergs to both distributions, an x_{min} value must be defined to filter icebergs under a certain area size threshold to allow temporal comparisons because of small icebergs following different distributions when compared to their larger counter parts. Scheick et al. (2019) determined an x_{min} value of 1800 m^2 for icebergs in Disko Bay, though as icebergs calved by KNS are much smaller than Sermeq Kujalleq, we defined the x_{min} at 1000 m^2 for data in each ArcticDEM scene and maintains consistency values used elsewhere in this thesis (Chapter 5). This ensures we remove small icebergs from the dataset which are more likely to be quickly impacted by melt-based processes and fit different distributions, but not setting a threshold too high which would remove the majority of the dataset and provides the most robust fit. Once the x_{min} value has been defined, the power law exponent (α) is calculated and used to determine the iceberg distribution, with more negative values indicative of a higher abundance of small icebergs.

6.2.3 Environmental parameters

We used data output from the regional climate model, Modèle Atmosphérique Régional (MAR) (15 km-v3-11) to derive daily runoff values that were clipped to the extent of KNS' catchment basin (Mouginot and Rignot, 2019). As the ArcticDEM scenes are only a snapshot of fjord conditions at the time of data acquisition, we cannot assume runoff on the same day of DEM capture would have influenced the calving style of KNS. Consequently, to ensure we captured the influence of runoff on iceberg size distributions, we summed the total runoff for the day of interest with values from eight-, nine- and ten-days preceding acquisition of the DEM.

The seasonal velocity at KNS is closely coupled with the amount of water in the subglacial system (e.g. higher runoff values = ice velocity increases) (Davison et al., 2020b). Consequently, we extracted ice velocities ~500 m from the ice front of KNS using data from the ITS_LIVE project (Gardner et al., 2019).

6.3 **Results**

The workflow for this study identified 12 ArcticDEM scenes of high quality for analysis. From these data, 35412 icebergs were detected in a 2 km search window proceeding the ice front between 2013 and 2017. Power laws describing iceberg distributions at KNS yielded relatively negative alpha values, ranging from -2.17 to -3.57 (Figure 6.2; Table 6.1). Power laws were derived by filtering icebergs which were smaller than or equal to 1000 m^2 (the x_{min} value) and

yielded the most negative alpha values in August when compared to September and October. For the entire August dataset, we identify no iceberg larger than 14000 m^2, explaining the extremely negative alpha values. While still relatively negative, September and October do consist of larger icebergs within their distributions and subsequently have more positive power law slope values.

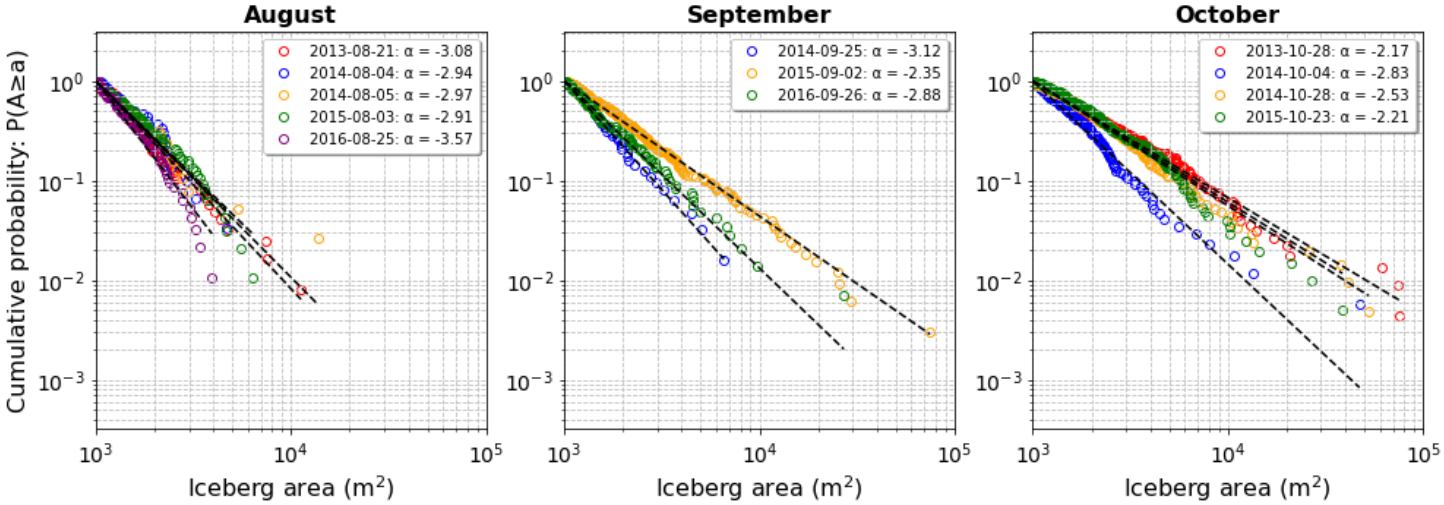

Figure 6.2. KNS's power law distributions for each DEM scene separated into their respective months. To compare each scene temporally, an x_{min} value of 1000 m^2 was defined. Grouping each DEM into one monthly distribution yields alpha values for August of -3.11, -2.54 for September and -2.31 for October. More negative alpha values provide a steeper gradient and suggest smaller icebergs dominate the distribution, whereas shallower gradients and more positive alpha values suggest larger icebergs dominate the distribution.

As distributions at KNS are dominated by small icebergs, we wanted to infer whether power laws were the only suitable candidate to describe their distribution at the ice front. When comparing power laws with lognormal distributions, it is suggested that the former is considered the best distributional descriptor for only 2 of the 12 ArcticDEM scenes in the dataset (Figure 6.3). The remaining ten scenes are more likely to be best described as fitting a lognormal distribution. However, no iceberg distribution can be statistically proven to reject either a power law or lognormal distribution (p values = > 0.05). This suggests the icebergs are unable to distinguish between both types of distributions, however lognormal is the more likely descriptor of the distribution.

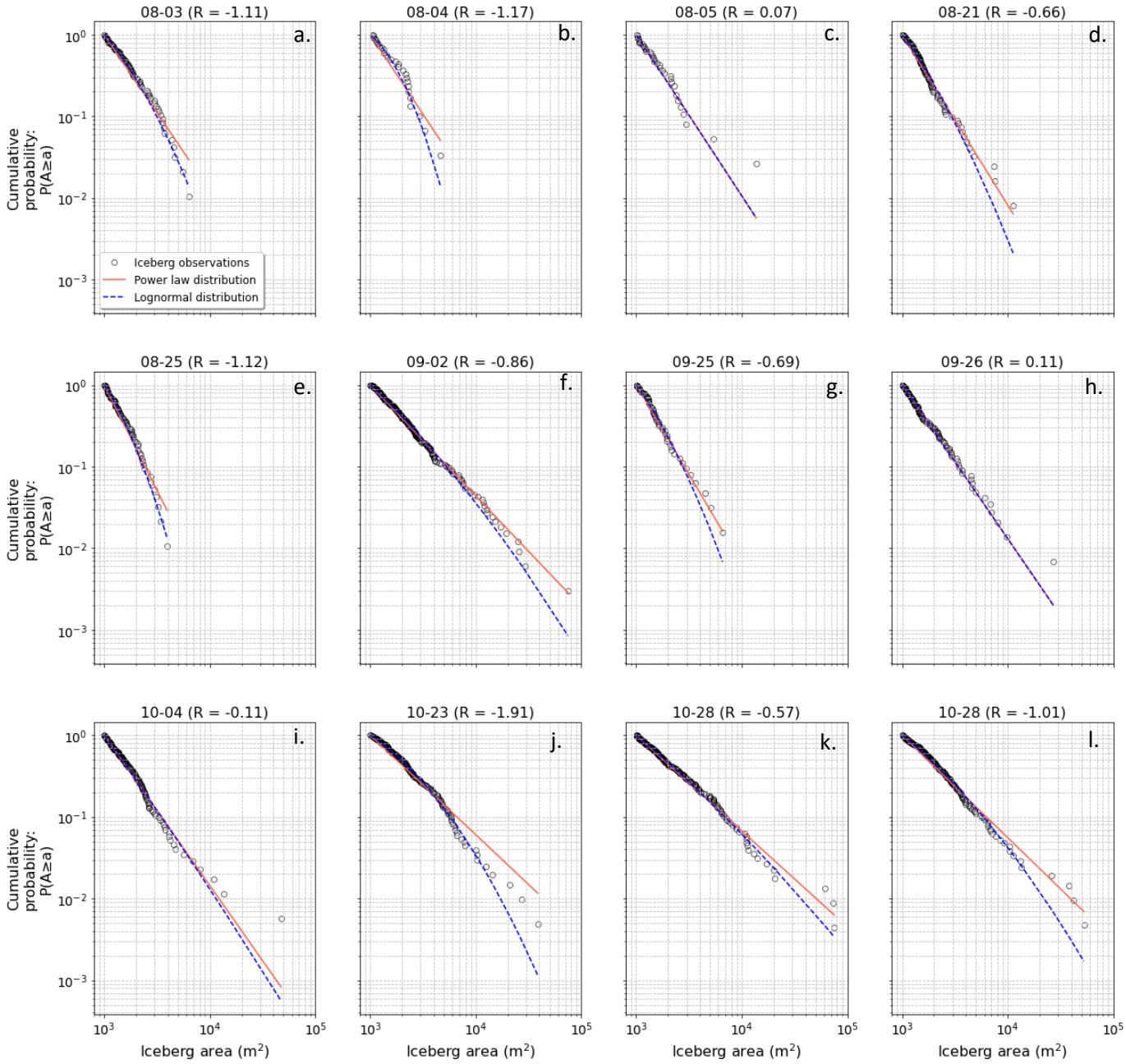

Figure 6.3. Power law vs lognormal distribution for each DEM scene with respective date with an x_{min} value of 1000 m^2 defined. The R value represents the log-likelihood ratio between the two distribution candidates. Positive R values (in the title) suggest the data is more likely to fit a power law distribution and negative values suggest the data is more likely to be described as lognormal. No DEM date has a significant p-value (< 0.05) to discount either distribution as inappropriate to describe the data. However, 10 out of the 12 DEMs suggest the data is best described as lognormal (although not statistically significant, p-values = > 0.05).

Similar to their planform surface area, iceberg volumes in August of each year are smaller than those in September and October (Figure 6.4). While the power law distributions vary by DEM (Figure 6.2), the median iceberg volume size remains relatively similar (~1000 to 1100 m^2) through all of the scenes. However, there is substantial variance in iceberg volumes when assessing the 100 largest icebergs in each ArcticDEM scene available. Boxplots reveal that the 100 largest icebergs in August of every year have smaller icebergs and that their volumes transitionally increase through August, September and October (Figure 6.4b).

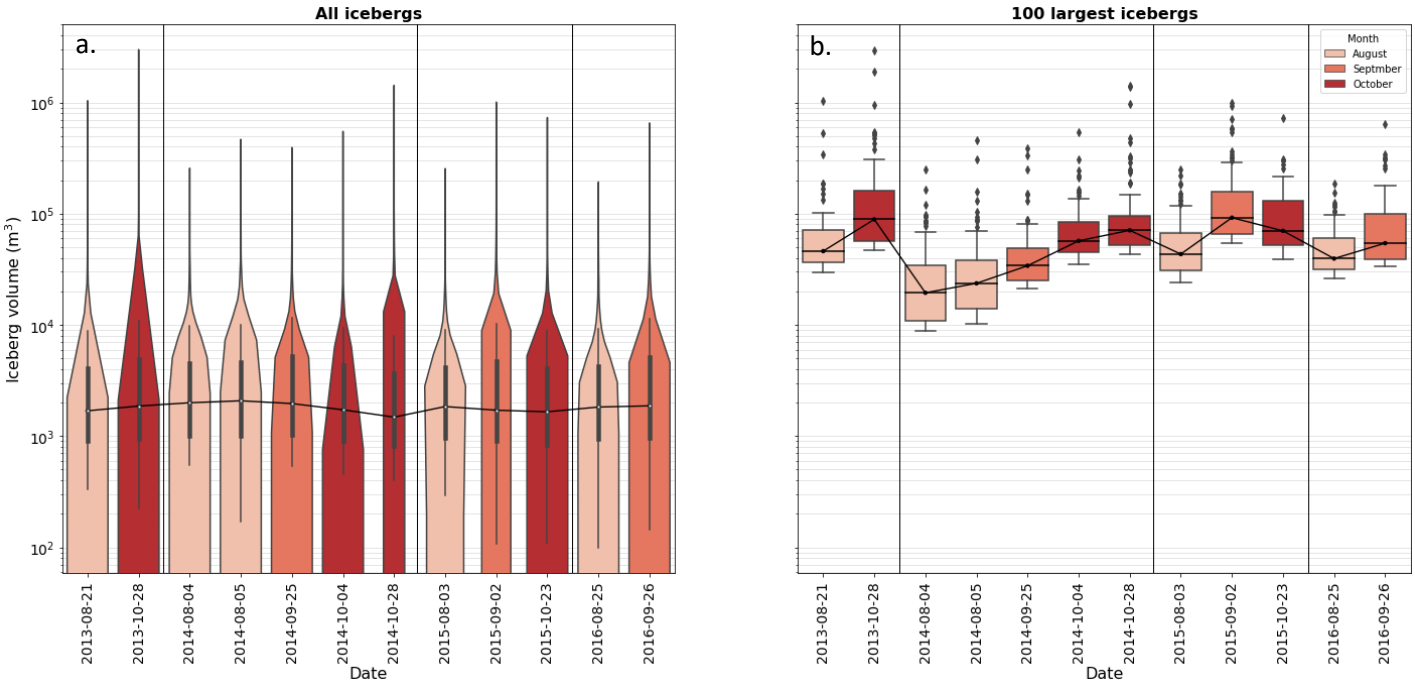

Figure 6.4. Violin plots for entire iceberg volume distributions for each ArcticDEM scene (a). The right hand-side subplot (b) shows boxplots for iceberg volume distributions for the largest 100 icebergs in each ArcticDEM scene at KNS. The change in year for each DEM (e.g. 2013 to 2014) is highlighted by a solid black line. Each subplot is colour coded by its respective month in which the DEM was acquired. The median values for both violin and boxplots are highlighted by the black lines. The median values for the entire dataset are similar temporally (within the 1000 to 2000 m^3 range), however there is a notable transition in increasing iceberg volumes from smaller volumes in August to larger volumes in October.

By taking the median values (both volume and area) of the largest 100 icebergs identified in each DEM, it is possible to infer the relationship between true iceberg sizes and derived power law slopes which are used to describe the iceberg distribution (Figure 6.5). We observe a strong and moderate relationship between iceberg (area and volume) median values for the largest 100 icebergs in each DEM and the respective alpha value derived for iceberg areas and volumes (r = 0.85 and 0.62). This reveals that while similar, iceberg area does not fully translate to an

iceberg volume and results in slightly varying differences in power law slopes and their relationship with median iceberg volumes for the largest 100 icebergs in each DEM.

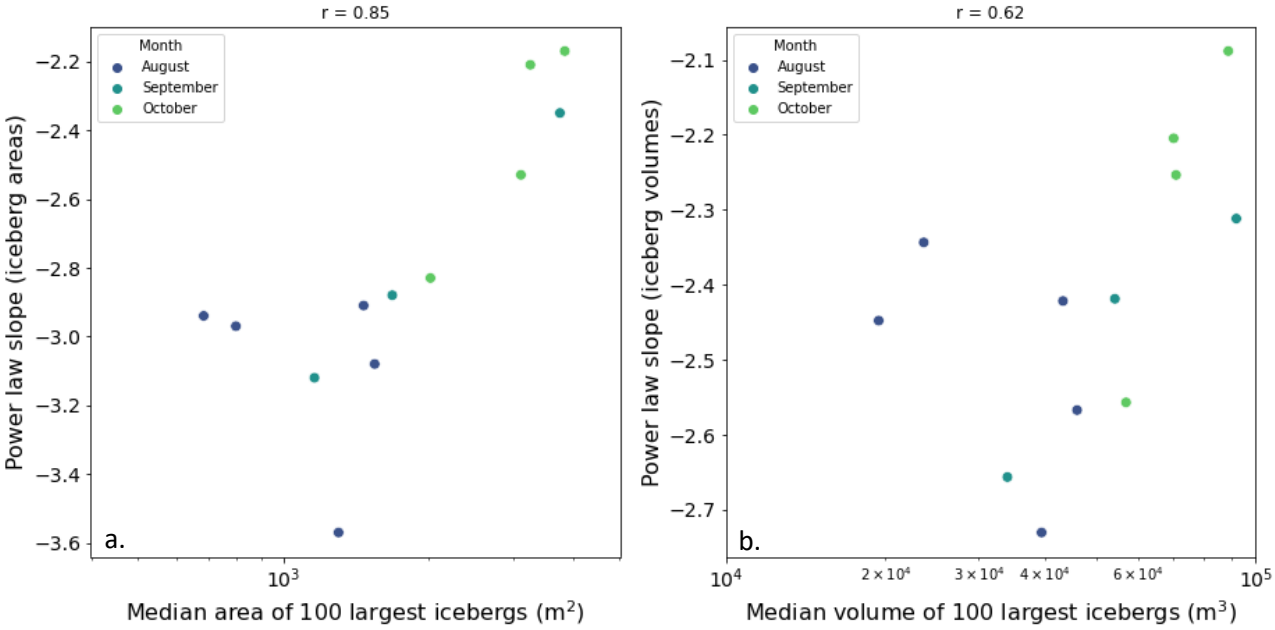

Figure 6.5. Power law slopes versus the median iceberg area (a) and volume (b) values for each DEM. The alpha values were derived both for iceberg area (x_{min} = 1000 m^2) and iceberg volume (x_{min} = 27900 m^3). The volume x_{min} was derived by converting the x_{min} used for the area (1000 m^2) using the conversion presented in Chapter 5 (equation 5.1). There is a strong relationship (Pearson's R = 0.85) between the median iceberg area for the 100 largest icebergs in each DEM and the respective area alpha value. The relationship is moderate (Pearson's R = 0.62) for median iceberg volume and the respective volume alpha value. Each point is colour coded by the month it was acquired in.

The total number of icebergs identified in August tend to be less than those delineated in September and October (Figure 6.6a). Overall, the iceberg observations made from the ArcticDEM scenes coincide with both subglacial runoff and ice velocity decreasing from its summer peak in late June (Figure 6.6b and 6.6c). Runoff values in every year are at their highest in August and begin to decline to their Autumn lows in September and October which coincide with reduced ice velocities at the terminus.

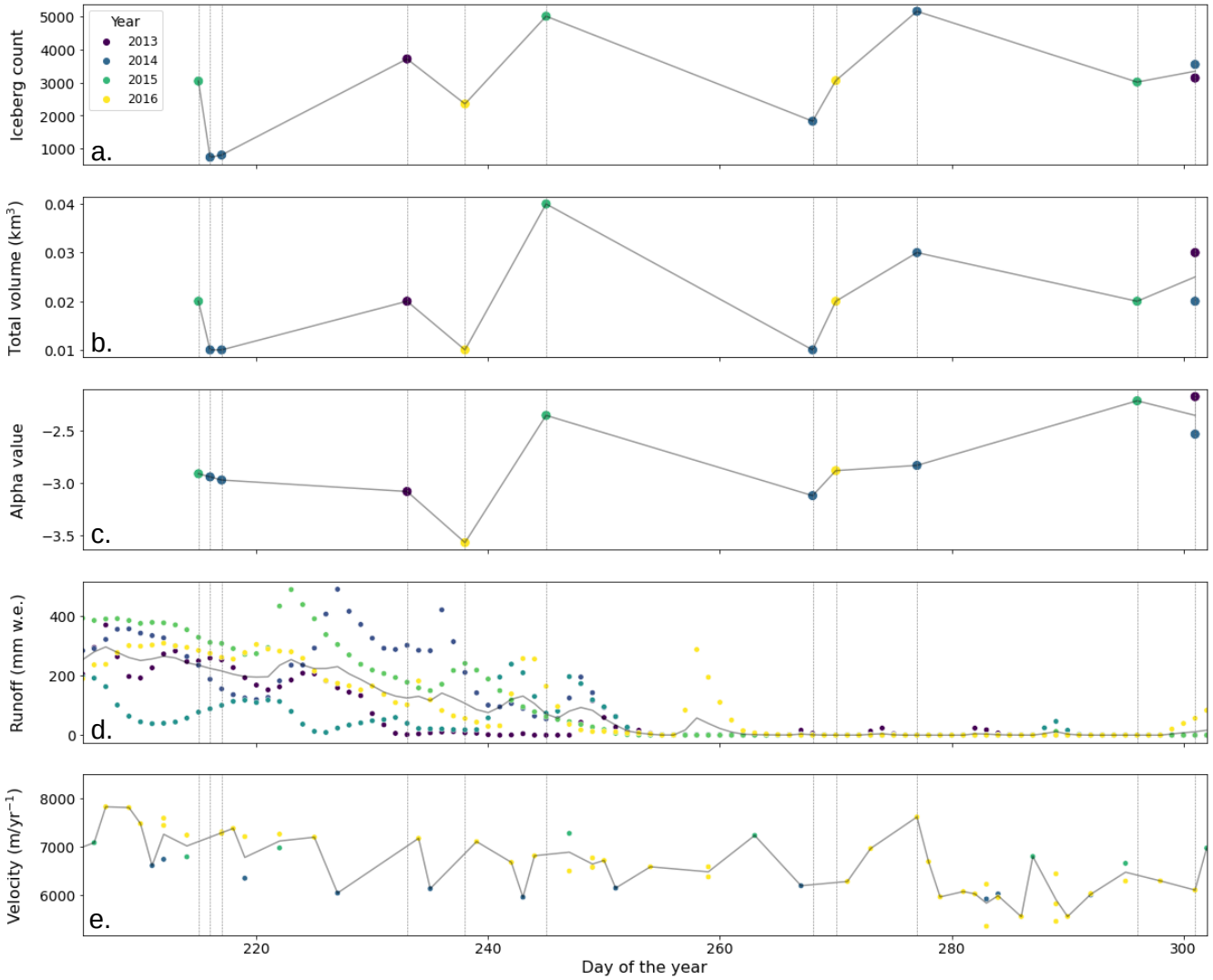

Figure 6.6. Time-series of KNS': a) iceberg count, b) total iceberg volume and c) alpha value for each ArcticDEM scene. The lower two subpanels show d) subglacial runoff values and e) ice velocity of KNS during the time of ArcticDEM observations. The x-axis represents the Julian day for the dataset, with each grey line on the subplots highlighting an ArcticDEM observation.

By looking at the amount of runoff in the subglacial system beneath KNS up to ten days prior to DEM acquisition, we observe a moderate, negative relationship between runoff values and median iceberg size for the 100 largest icebergs in each DEM (Figure 6.7). This indicates that higher runoff results in a reduction of iceberg size for the 100 largest icebergs calved by KNS.

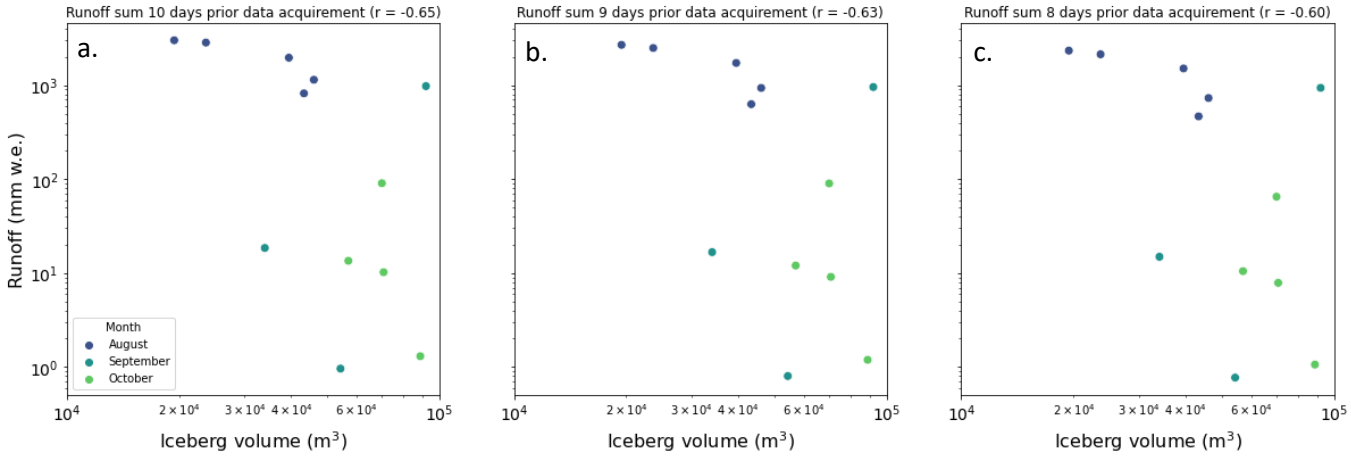

Figure 6.7. Median iceberg volume for the 100 largest icebergs in each DEM plotted against the runoff sum preceding the ArcticDEM observation (8 (a), 9 (b) and 10 (c) days). The Pearson's r value suggests a moderate, negative relationship between iceberg size and runoff (e.g. higher runoff results in smaller iceberg volumes).

Small icebergs (< 1000 m2) account for 90% of the total iceberg count in each month, but contribute to 61%, 48% and 43% of the total volume in August, September and October, respectively (Figure 6.8). Consequently, small icebergs are prominent through every summer month at KNS and have the most significance for total iceberg volume in August (60%). September and October have iceberg area sizes exceeding 70000 m^2 while the largest iceberg in August for each year is 13696 m^2. These findings suggest a transitional phase of small icebergs dominating the fjords total volume in August to larger icebergs accounting for a greater proportion of the total volume in September and October.

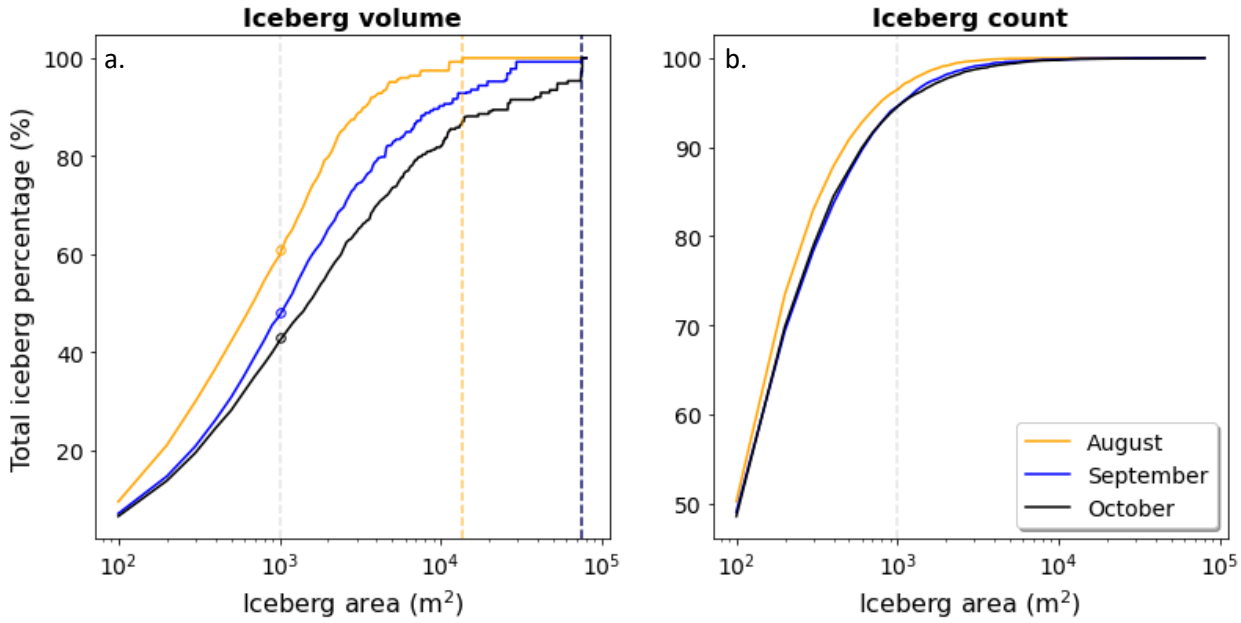

Figure 6.8. Cumulative iceberg volume (a) and count (b) plotted as percentages with their respective surface area for each month within the study period. The small iceberg threshold (1000 m^2) is defined by a dashed grey line on both plots. The circles on the volume plot represent how much of the total volume small icebergs account (< 1000 m^2) for. The dashed vertical line corresponds in colour to their month's maximum icebergs size (the blue and black lines overlap due to September and October having iceberg sizes of 74000 m^2 and 75000 m^2, respectively).

6.4 **Discussion**

6.4.1 Implications for iceberg distributions

Iceberg distributions in the near-terminus region of KNS cannot be distinguished statistically between power law and lognormal to best describe their distributions (Figure 6.3). Our findings reveal that 10 of the 12 available ArcticDEM scenes are more likely to be best suited to lognormal rather than the previously assumed power law distribution. While a statistical significance threshold of $p < 0.05$ is not reached for the scenes, most log-likelihood ratios (10 of 12) are negative and favour lognormal distributions.

Icebergs following both distributions, but being best described as lognormal is likely because KNS calves icebergs with small areas and volumes which will favour a disintegration from atmospheric and submarine melting, rather than breakup via fracturing. This is because lognormal describe continual distributions (e.g. melting through the fjord) and power laws are used to describe sudden changes in iceberg size (e.g. fracture and calving of an iceberg). This reveals that icebergs can be described as lognormal in close proximity to an ice front and do not require further modification down-fjord to be considered as a lognormal distribution.

These findings do not just have ramifications for the remote sensing, glacier dynamic and fjord hydrography communities when deriving iceberg distributions, but also the glacier and ocean numerical modelling communities which may define power law slope values in their domains. Numerical models (e.g. MITgcm IceBerg package) are currently designed to assume a power law slope (e.g. -2.1 for Ilulissat Icefjord: Kajanto et al., 2023) to derive iceberg freshwater fluxes. However, we have shown in the near-terminus regions that icebergs could be better suited to a different distribution and that power laws may not be the most appropriate. This could have implications for modelled freshwater fluxes which are derived from incorrectly assumed distributions that could have wider implications for the fjord and ocean systems. Therefore, it may be worth investigating whether such a finding has significant implications for how icebergs release their freshwater using such a distribution, and whether more time-evolving values are required to accurately describe iceberg distributions.

Power law slope values have been reported for Greenlandic iceberg sizes between -1.2 and -3.0 (Table 3.2; Sulak et al., 2017; Moyer et al. 2019; Scheick et al., 2019). While the majority of the alpha values derived from the ArcticDEM scenes reside within this range, three values are more negative than -3.0 (e.g. -3.08, -3.12, -3.57; Table 6.1). These values coincide with DEMs which contain no icebergs larger than 13696 m^2 and therefore results in particularly negative alpha values (Figure 6.2). By separating the data into individual ArcticDEM scenes to temporally compare iceberg distributions, the total iceberg count and the potential for large iceberg identification is much lower when compared to compiling all of the icebergs into one larger dataset, meaning we observe the most negative values observed to date from one of Greenland's outlets. These particularly negative alpha values could also be an artefact of the defined x_{min} (1000 m^2) as many icebergs are removed from the dataset and not considered in the power law distribution fitting. This may have a greater influence on our workflow compared to previously published research (Sulak et al., 2017; Scheick et al., 2019) as it can observe the smallest icebergs to date from satellite imagery due to the high spatial resolution of the DEMs, therefore the domination of smaller icebergs is more likely.

For the entire dataset we do not observe much variation in the iceberg size distributions proceeding KNS (Figure 35a), however the 100 largest icebergs in each DEM reveal heterogeneity in large iceberg sizes through the melt season (Figure 6.4b). We observe increases in sizes of the largest iceberg volumes from August when the melt season is still ongoing to October when surface runoff generation has ceased. When scaling power law slopes and median sizes for both iceberg areas and volumes, we note a strong (r = 0.85) and moderate

(r = 0.62) relationship, respectively. The strong relationship relates to the area power law slope and median iceberg area size for each DEM, whereas the relationship is weaker for the volumetric alpha value and median volume value for the largest 100 icebergs (Figure 6.7). These findings suggest that while a strong relationship exists between planform surface area and the respective alpha value (derived from area), the same relationship cannot be directly translated into an iceberg volume alpha value and median iceberg volume size. When studies are utilising two-dimensional imagery to detect icebergs and transform an area to a volume using an empirical convertor (e.g. Sulak et al., 2017; Chapter 4) these findings could be more pronounced (e.g. volume not having a strong relationship with alpha values) as the derived volumes will vary from the true iceberg volume because convertors cannot replicate the exact volume from a surface area.

It is worth noting our observations are limited to temporal snapshots of the fjord environment at the time of data acquisition and therefore higher temporal resolution data may be required (e.g. Cook et al., 2021) to infer time-evolving iceberg distributions. Nevertheless, the findings presented by Cook et al. (2021) indicate that power laws should not always be assumed to be the most appropriate distribution to describe icebergs which are in close proximity to the ice front. These conclusions were driven by their in-situ, high temporal resolution sampling (image every three minutes), however, even with less frequent data acquisition from ArcticDEM, observations reveal power laws may not be the best fit to describe iceberg distributions in the near terminus region.

The grounding line at KNS is approximately 250 m (Morlighem et al., 2017) and is comparatively shallow compared to previously studied glaciers for their iceberg distributions, e.g. Rink (850 m), Helheim (600 m) and Sermeq Kujalleq (800 m) (Carroll et al., 2016). Consequently, the icebergs in close proximity to the terminus of KNS may not fit power law distributions and are not directly comparable to these much deeper glaciers with different calving styles. However, between 2009 and 2018, 250 marine-terminating glaciers had mean terminus depths shallower than -250 m (according to BedMachine v5 and TermPicks data) and are similar to KNS with shallower terminus positions. Therefore, distributions may be overlooked as it is assumed lognormal is inappropriate close to the terminus. We have only been able to observe these findings at KNS because of the number of observations and this temporal frequency is not possible across the majority of the GrIS. Nevertheless, when more data becomes available (i.e. ArcticDEM v4) and there is sufficient temporal coverage, it will be possible to assess whether these findings from KNS are applicable elsewhere around the

GrIS. Whether these findings would be comparable to KNS is an open-ended question as the glacier flows relatively fast compared to other outlet glaciers of similar groundling line depths.

6.4.2 Implications for KNS

High values of subglacial runoff during the mid-to-late melt season has the capabilities of altering the iceberg sizes calved by KNS (Figure 6.4, 6.7 and 6.8). This is because subglacial plumes can upwell alongside the ice front and localise melting during the melt season (Bunce et al., 2021). We do not observe a dynamic shift in KNS' calving regime between August and October (e.g. serac failure producing small icebergs to full-thickness calving producing larger and more tabular icebergs). However, there is a clear transition between August and October where the same calving style is occurring, but smaller icebergs (< 1000 m^2) become less important volumetrically in the fjord (Figure 6.8).

These findings are evident as the structure of the curve in Figure 6.8 is similar for all of the months in the dataset, however the total volume made up of smaller icebergs is greater in August (61%) compared to September (48%) and October (43%). This suggests that KNS is calving icebergs primarily through serac failure, but during August, localised plume upwellings and subsequent melting is resulting in a higher percentage of the total volume being calved from smaller icebergs at only certain sections of the ice front. Once subglacial plumes disappear in the months of September and October because of lower runoff values, ice front wide calving will dominate with no localised calving hotspots, meaning the larger iceberg contribution to the fjord's total volume will become more important (cf. Bunce et al., 2021).

There is an evident, moderate relationship between cumulative runoff values and the reduced iceberg volume sizes of the 100 largest icebergs in each ArcticDEM observation (Figure 6.4). Consequently, the size of larger icebergs are lower in August when runoff is higher, particularly when compared to October when surface runoff is negligible as the melt season ends. These findings suggest runoff has at least some influence on the iceberg sizes being calved into Nuup Kangerlua from KNS. As runoff is projected to increase well into the 21st century under increased Greenland surface melting (MacFerrin et al., 2019), it is important to constrain the seasonal aspect of iceberg calving at tidewater glaciers. Associated uncertainty should also be considered as to whether increases in melt will result in an increase in melt season length or intensity. If the melt season was to become longer through the year, it is possible that there could be an increase in the amount of time that smaller icebergs will be calved and dominate the fjords total volume. Future studies should look to gauge higher temporal resolution datasets

which can cover the entire melt season to infer how iceberg sizes evolve in more detail, and at different glaciers to see if similar relationships are found elsewhere.

When runoff is at its highest in August, we observe particularly negative alpha values as a result of small icebergs dominating the distribution. When efficient, channelised subglacial systems form (Slater et al., 2015) during times of high runoff, the resultant subglacial upwellings are localised at the ice front and decrease the number of calving events at KNS (Bunce et al., 2021). Our results support these findings and note that the number of icebergs in the fjord are lower and the largest icebergs in the distributions are smaller, resulting in more negative power law slopes (Figure 6.2). Consequently, subglacial hydrology can have bearing on ice front calving, both in terms of magnitude and frequency. However, a greater amount of spatiotemporal data are needed to better constrain time-evolving, seasonal differences in iceberg calving as a result of increased runoff and melt under a warming Greenland.

Small icebergs dominate Nuup Kangerlua (90%) and are responsible for a significant proportion (40% to 60%) of the total solid mass loss from KNS' iceberg calving. For the stability of the glacier, be that in solid ice discharge or terminus position in the summer months, small icebergs allow KNS to remain a stable glacier which does not experience significant frontal fluctuations. If KNS was to dynamically transition to a different calving regime dominated by large summer calving events which produce tabular icebergs, the stability of the glacier could be in question, as could the delivery of ice and subsequent freshwater to the fjord system. In the near future it is unlikely KNS will undergo such dynamic changes given the shallow groundling line depth inhibiting the possibility of basal crevassing (Bassis and Walker, 2012).

6.5 **Conclusions**

For the first time using remote sensing techniques, it has been observed that icebergs in the near-terminus region are not best described as a power law. The icebergs identified in the ArcticDEM scenes are unable to statistically distinguish between power law and lognormal distributions, but rather log-likelihood ratios suggest 83% (10 of 12 observations) of the data are actually best suited to lognormal distributions. These findings have implications for both the remote sensing and numerical modelling communities within glaciology and fjord hydrography/oceanography when analysing icebergs in the near-terminus regions of Greenland's outlets given that previously assumed power laws may not always be the most suitable candidate.

We have shown a change in the size of the largest icebergs between August and October at KNS during the mid-late melt season. During August of each year (2013-2017), we find a reduction in the magnitude and frequency of iceberg size and count, respectively. These observations coincide with more negative power law exponents and high runoff within the subglacial system. These insights are therefore in agreement with previous findings that show higher runoff decreases terminus-wide calving activity at KNS (Bunce et al., 2021) as less icebergs are identified proceeding the ice front. Consequently, smaller icebergs in August become more important for the total solid ice discharge (60%) from KNS and emphasises the importance of these icebergs for the stability of the calving regime and position of the terminus.

These observations suggest that KNS may calve smaller icebergs for longer periods of time during the summer months under projected increases in surface runoff and melt across the GrIS into the 21st century. Whether similar findings are transferable across the ice sheet to glaciers with similar groundling line depths to KNS is currently unknown due to insufficient temporal resolution data at other Greenlandic outlet glaciers. Nonetheless, future data releases will provide opportunities for higher spatiotemporal analysis of iceberg distributions at an ice sheet scale to assess whether KNS is a 'typical' iceberg calving outlet glacier or whether key differences exist when compared to similar glaciers.

Chapter 7: Thesis discussion and significance

7.1 **Achieving thesis aim and objectives**

This thesis aimed to obtain iceberg data at glacier to ice sheet scale, providing insight into the controls on their size distributions. Four main objectives were set, namely:

1. *Generating automated workflows to detect icebergs using cloud computing and open-access digital elevation models (DEMs). [Chapters 4 and 5]*.
2. *Packaging the workflow into a graphical user interface (GUI) to provide an open-access tool for the iceberg/glaciological community to derive their own iceberg datasets. [Chapter 4]*.
3. *Adapt and apply this workflow to all the marine-terminating glaciers in Greenland to gain understanding of iceberg distributions at an ice-sheet scale. [Chapter 5]*.
4. *Explore glacier-specific, seasonal iceberg distribution variability and potential controls. [Chapter 6]*.

All of these objectives have been achieved and have been made possible by the high resolution ArcticDEM v3 strip data within Google Earth Engine (GEE).

The methodological advances of Chapter 4 were fundamental to the subsequent work presented in this thesis. It provides the foundations for the iceberg detection being scaled across the Greenland Ice Sheet (GrIS) and has been validated by a manual operator (Objective 1). The scientific advances made by Chapter 4 provides the first open-access GUI to automatically obtain large quantities of iceberg outlines across the Arctic in the near-terminus regions of marine-terminating glaciers (Objective 2). The workflow employs a highly automated approach that does not rely on user-classification of image suitability (Scheick et al., 2019) and iceberg identification (Sulak et al., 2017). It is not just the magnitude of iceberg observations which is unprecedented, rather the three-dimensional data provided by the workflow has allowed Chapters 4-6 to infer iceberg volume distributions which other research has not been able to address due to the previous use of two-dimensional imagery (e.g. Sulak et al., 2017; Schieck et al., 2019; Moyer et al., 2019).

In terms of significance to the wider iceberg community, the data derived in Chapter 4 presented new area-to-volume conversions based on 163,026 more observations than previously used for studies that require an iceberg volume conversion from two-dimensional imagery (e.g. Sulak et al., 2017, n = 712). Further to this, Chapter 4 identifies two distinct iceberg distributions which represent: 1) individual icebergs and 2) iceberg rafts. New approaches are presented on how different visualisations of expressing iceberg count versus

iceberg volume as a percentage are useful to infer the significance of different iceberg sizes on solid ice discharge and fjord dynamics. These visualisations provide an alternative approach to presenting iceberg distribution data, contrasting with the use of a single power law slope value (alpha value) that otherwise ignores the contribution of small icebergs (i.e. those with areas and volumes less than the defined x_{min}) to overall iceberg distributions.

Once the iceberg detection workflow was shown to be applicable at different glaciers with varying fjord conditions (Objective 1), it was determined that it could be upscaled to all marine-terminating glaciers where data was available around the GrIS (Objective 3). This provides data from 133 outlet glaciers with more than 1.3 million icebergs detected, derived from spatially and temporally dynamic ROIs (Chapter 5). It was also possible to automatically define these ROIs in a methodologically consistent manner that removed operator bias. It was found that Greenland's outlets calve similar iceberg sizes up to 10,000 m^3 and that larger icebergs are relatively rare in abundance, but for each glacier account for a disproportionate amount of the total volume in Greenland's fjords.

Chapter 6 presents iceberg distributions at KNS, the largest tidewater glacier on the southwest coast of Greenland which can calve large icebergs, resulting in a dynamic fjord environment proceeding the ice front (Objective 4). At the time of iceberg calving, it had been assumed that the resulting icebergs are best described to fit a power law distribution (Kirkham et al., 2017). However, it was found that icebergs proceeding the ice front of KNS (2 km) cannot statistically distinguish between power law and lognormal distributions. Further, the log-likelihood ratios indicate that lognormal is the preferred distribution to describe the icebergs, suggesting icebergs calved in KNS' fjord likely disintegrate through melt-based processes in close proximity to the ice front and do not need to drift down fjord to be considered lognormal (*contra* Sulak et al., 2017). It is also observed that iceberg distributions in August were dominated by smaller icebergs compared to September and October because of a channelised subglacial hydrological system that localises ice frontal melt through the upwelling of subglacial plumes. This supports findings from previous work (Bunce et al., 2021), though goes further in finding moderately strong inverse relationships between the median of the largest 100 iceberg sizes and runoff total from the previous eight to ten days.

This thesis been able to drastically increase the quantity and quality of iceberg outline data across the GrIS providing the potential to up-scale analysis across the Arctic. For the first time, this project has provided a fully automated approach for detecting icebergs with no manual

(e.g. Sulak et al., 2017; Crawford et al., 2018) or image (Scheick et al., 2019) classification required (Chapters 4 and 5; Objectives 1-3). It has therefore contributed to addressing significant data gaps and knowledge requirements outlined in Chapter 1 through the automation of iceberg detection from DEM data and comparison with environmental data (overall thesis Aim).

The remainder of this Chapter will discuss the wider significance of the thesis results and how they have each contributed knowledge and data to the iceberg community. A discussion will also be provided about the future direction of iceberg detection and analysis of their distributions, in addition to how iceberg observations could help provide further information into glacier dynamics and their societal implications.

7.2 **Chapter 4**

The results presented in Chapter 4 were able to achieve: 1) a new workflow to rapidly detect icebergs packaged within a GUI, 2) statistically validate the automated detection approach by comparing outlines to manual delineations, 3) identify two iceberg distributions at two of three tidewater glaciers analysed and 4) derive a new iceberg area-to-volume conversion for two-dimensional imagery from a large dataset (n = 163,738).

These data and subsequent results established that it was possible to automate iceberg detection using open-access DEMs at different marine-terminating glacier localities with varying calving dynamics and different fjord characteristics in Greenland. Once the workflow for iceberg detection had been successfully developed, this was placed within a GUI for operational use as a tool within GEE. This tool is the first of its kind with regards to iceberg identification and allows any ROI delineation in a fjord where data are available and thus providing large user flexibility. The steps in the GUI were specifically designed to allow users of any computational ability to generate their own iceberg dataset with no coding required. To ensure ease of use for subsequent analysis, data can be exported as a shapefile which is a commonly used and recognisable geospatial format, however GeoJSON and CSV export file formats are also available. As well as the iceberg outlines, key metadata is appended to each iceberg so area and/or volume distributions can be inferred easily and therefore reduces the amount of post-processing required of users. Alongside the development of the tool, a GitHub read.me page (https://github.com/ConnorShiggins/Google-Earth-Engine-and-icebergs) has also been provided for extra information and a step-by-step guide for users who are unfamiliar with the GEE interface and have not used a GUI before in the platform. All of the above have been built

to provide open-access data to the community, but also as a resource for undergraduate and postgraduate research projects that may wish to generate data across the Arctic at scale easily.

The resulting iceberg data can be used to analyse ice dynamics and to infer iceberg calving behaviour, but also for studies investigating iceberg freshwater flux, both for observations and as input for numerical models (e.g. Davison et al., 2020a). Outside of specific research requirements, the kind of approach presented in this thesis highlights the potential for the use of remote sensing in the cryosphere and how geospatial data can be made accessible (and the subsequent benefits). While the spatial extent of the ArcticDEM v3 strip data in GEE is limited to several kilometres in front of Greenland's outlets, the simplicity of the workflow has shown efficacy to generate large datasets which could be considered for optical and SAR satellite data, such as the Landsat and Sentinel satellite remote sensing programmes.

As with any automated approach, the resultant output should be validated by a manual operator to ensure the detection process and subsequent metadata is correct. In Chapter 4, this was achieved at three separate tidewater glaciers on the west coast of Greenland that were typified by different iceberg densities, yielding good comparisons between the automated and manual delineation methods. This provided validation for the tool to be upscaled to different study sites around the Arctic where data availability allows. The Pearson's r-values for the three glaciers (0.70 to 0.96) showed good to excellent agreement between manual and automated delineation methods, providing confidence that the resulting data can be used by operators elsewhere. A distinct advantage of the automated workflow over manual delineation is that it can provide a more consistent iceberg identification.

One of the primary benefits of using DEMs for this work rather than optical or SAR data (Sulak et al., 2017; Moyer et al., 2019; Scheick et al., 2019) is the ability to calculate an iceberg's volume directly, rather than having to rely on an empirically derived convertor to transform an area to a respective volume. Observing the iceberg characteristics and the relationship between their area and volume revealed the detection process was able to identify two distinct iceberg distributions existing in the fjord: 1) icebergs and 2) iceberg rafts (which can contain a matrix of multiple icebergs).

The large dataset (n = 163,738) generated from the automated workflow can calculate iceberg volumes and has been able to derive an updated iceberg area-to-volume conversion from the original power law relationship presented by Sulak et al. (2017). While good, the previous convertor (Sulak et al., 2017) could not replicate correct volumes for our iceberg dataset,

underestimating volume for smaller icebergs (<1,000 m^2), but overestimating the volume of larger icebergs (>1,000 m^2) (Figure 4.7). Also provided are convertors that give users the ability to calculate uncertainties on iceberg area-to-volume conversions for the first time. These new area to volume convertors presented in Chapter 4 (Equations 4.2-4.6) should be beneficial to remote sensing studies wishing to derive a volume from a planform surface area. A significant benefit of accurately converting iceberg area to volume is for oceanographic numerical modelling studies (e.g. Davison et al., 2020a) that require iceberg outline input to determine freshwater release from icebergs. By deriving a new convertor from a much larger number of iceberg observations with true volumes, it was possible to increase the certainty of correctly transforming iceberg areas from two-dimensional optical data to the three dimensions.

It is known iceberg distributions change through time depending on the boundary conditions of the glacier (Scheick et al., 2019). However, these studies are limited to only a few of Greenland's fjords. Much effort is going into the testing of realistic calving behaviour in numerical models (e.g. Amaral et al., 2020), but such simulations require validation to determine model success. At the same time, if iceberg observations are upscaled and boundary conditions are constrained (e.g. when an iceberg was calved, constraining the terminus depth and ice velocity), there remains scope to work backwards and determine the probability of what iceberg size distributions should be expected.

Chapter 4 brings together a new methodological application to automatically detecting icebergs using cloud computing within GEE. This approach has highlighted the ability to use simple but effective workflows into the remote sensing of icebergs to generate comprehensive datasets. The iceberg community will hopefully benefit from the derivation of the area-to-volume conversion that can output realistic iceberg volumes for determining freshwater release into fjord environments.

7.3 **Chapter 5**

This Chapter develops the iceberg detection pipeline from Chapter 4 to apply to all glaciers across the GrIS where ArcticDEM v3 strip data are available. To allow upscaling to 133 marine-terminating glaciers the workflow was significantly modified, providing a new approach to consistently define a search window for an ROI and appending of new metadata.

The new dynamic ROI automatically defines a search area 2 km down-fjord of each ice front for each glacier and allows full automation for the first time. This is a significant benefit from the first workflow which is reliant on an operator manually defining a fixed ROI. This was

achieved by uploading the TermPicks dataset (Goliber et al., 2022) to GEE and aligning both the terminus and ArcticDEM dates. By defining a consistent search window at every glacier across the ice sheet there was no operator bias associated with the definition of the ROI, while maintaining a small enough area to ensure ArcticDEM availability in the near-terminus region.

The key aspect of the dynamic ROI is that it allows the workflow to automatically track glacier calving fronts. The moving ROI which tracks terminus positions ensures all the icebergs identified through space and time are proximal to the ice front, providing the most relevant iceberg data to investigate calving dynamics.

The new workflow in Chapter 5 builds on that presented in Chapter 4, using terminus data from TermPicks to provide a greater range of contextual knowledge regarding the parent glacier which the icebergs calved from, e.g. the terminus width, terminus depth (mean, minimum, standard deviation), iceberg and open water cover and the iceberg's keel depth, as well as the glacier ID number which the icebergs calved from. This extra information saves time post-processing and provides extra glacier identification information that permits comparison with other glaciological datasets (e.g. Mankoff et al., 2020).

As the quantity of data is significant for this Chapter (i.e. 1.3 million observations), it was possible to assess whether the iceberg area-to-volume conversion presented in Chapter 4 was applicable to the dataset generated here, while at the same time updating a new convertor derived from a more comprehensive number of icebergs from 133 TWGs. The convertors presented in Chapter 4 and by Sulak et al. (2017) can reproduce observed iceberg volumes at the study sites. However, the conversion (Equation 5.1) presented in Chapter 5 should be used for those wishing to convert iceberg areas to volume in glacier proximal regions (< 2 km). The other convertors are derived from iceberg outlines situated in different sections of the fjord which will have lost mass from both melting and further calving. This highlights the possibility that it may not be possible to provide a universal iceberg area-to-volume converter.

The quantity and quality of data this thesis has generated is unprecedented at the time of writing, providing the most comprehensive iceberg dataset to exist. Hopefully with the release and probable ingestion of ArcticDEM v4 strip data into GEE, these datasets can be expanded even further to more glaciers over a longer time period, expanding the potential applications to iceberg, fjord and glacier research.

The sectors of the GrIS calve similar iceberg sizes with the most frequently identified at every glacier within the 1,000 to 2,000 m^3 size class. While similar iceberg size distributions are

observed across the ice sheet, differences exist between sectors and between single glacier sites, particularly in the larger iceberg size classes. These differences are most pronounced amongst the larger the iceberg size classes (Figure 5.4). For example, not all glaciers will be able to calve icebergs larger than 1,000,000 m^3 due to their grounded positions, while some will calve significantly more than the sector average, producing greater glacier to glacier variability for larger iceberg size ranges.

The relationship between solid ice discharge for each glacier (Mankoff et al., 2020) and iceberg size was explored with the aim of potentially predicting iceberg size distributions from easily available data. Such a relationship could not be found (Figure S4). A potential reason for this is that BedMachine bed topography data (Morlighem et al., 2017) possess significant uncertainty, meaning that attempts to derive a relationship could be undermined through the use of erroneous data. Also, not all the ice flowing through flux gates defined by Mankoff et al. (2020) will be lost via iceberg calving, with submarine melting accounting for extra mass loss at the ice front (Wood et al., 2021). Consequently, with the data available, it was not possible translate ice discharge into an iceberg volume, however with more continuous observations becoming available, this research question should be revisited as the potential impact of such an approach is high.

7.4 **Chapter 6**

The results presented in Chapter 6 reveal new insights into iceberg distributions and their evolution through time in the near-terminus region at a marine-terminating glacier on the southwest coast of Greenland. Results show that the assumption of icebergs being best described as following power laws (Sulak et al., 2017) at the ice front is not necessarily true in the case of KNS. However, these icebergs are more likely to be described as fitting a lognormal distribution, that was previously assumed to occur down-fjord (Kirkham et al., 2017). Evidence from both in-situ data (Cook et al., 2021) and results presented in Chapter 6 suggest that power laws can be used to describe an iceberg distribution, however other distributions (e.g. lognormal distributions) should also be investigated as they could be more appropriate, even in areas close to the glacier termini.

Small icebergs are found to account for up to, or over half of the ice total volume in the fjord (40 to 60%). In August of every year (between 2013 and 2017), KNS calved no iceberg larger than 14,000 m^2 with small icebergs being predominately responsible for the solid ice discharge from the glacier.

The icebergs which are calved in August of each year are not just smaller than in September and October, there is also a smaller number of total icebergs during this time. This is in part due to fewer calving events across the ice front when subglacial runoff is higher (Bunce et al., 2021). Also, because runoff is higher, it is possible that the icebergs are cleared out from the ice front due to subglacial plumes being more likely to surface and further enhance fjord circulation and iceberg mobility within the fjord. Further to this, an ice-marginal lake resides close to the ice front at KNS (Weidick et al., 2012) and periodically drains. Consequently, when such an event happens, the significant discharge of water can clear out icebergs at the front.

Understanding the future evolution of iceberg size distributions from KNS is not only important for both ice sheet mass balance of the sector and fjord dynamics, but also for the settlements in Nuuk down-fjord. Constraining how icebergs will continue to be discharged from this specific fjord is crucial to understanding future logistics for stakeholders and businesses. While not constrained here due to sporadic data coverage, such questions are raised because of varied solid ice discharge and iceberg size distributions varying on monthly scales. However, the workflows can identify when larger icebergs are calved and provide iceberg size ranges (Chapter 5) that could be useful for constraining the iceberg flux reaching fjord mouths.

Deriving a high temporal resolution time series using ArcticDEM v3 strip data is not possible due to limits of current data availability. Consequently, the identified icebergs represent only a snapshot of the fjord environment at the time of data acquisition. However, the future release of ArcticDEM v4 should significantly increase the spatial coverage and temporal resolution of the near-terminus environment of Greenland's outlets where more complete time-series can be derived.

7.5 **Iceberg detection and iceberg distributions moving forward**

Throughout this thesis it has been shown that automatically identifying icebergs at scale are useful approaches to determine their respective distributions and thus inferring how the glaciers are calving their icebergs. It is shown that developing relatively simple workflows represent efficient approaches for detecting icebergs automatically. While computationally expensive and difficult to construct algorithms like convolutional neural networks (e.g. Rezvanbehbahani et al., 2020) can be useful, they may not always be necessary depending on the research question being addressed.

The main challenge posed to all satellite derived imagery (optical/SAR/DEMs) is automatically identifying icebergs from winter to early summer when rigid sea ice/mélange dominates the fjords of Greenland. These conditions tend to occur in non-observable seasons using optical imagery due to cloud contamination and the polar night, however SAR can overcome such issues. While the spatial resolution of SAR data (notably Sentinel 1) is gridded as high as 5 m, the pixels are typically coarser than this, precluding the detection of smaller icebergs. To potentially circumvent such problems, approaches could begin looking at categorising iceberg cover through surface roughness (e.g. Nolin et al., 2002) characteristics which should distinguish to some extent sea ice and icebergs upon processing. This research is required as icebergs are important all year round and not just in the observable (for optical imagery) months of the summer as freshwater release from iceberg melt does not necessarily stop in the winter months. However, these approaches are not yet developed outside of the summer (and early autumn) months, and we know little about iceberg dynamics in the fjord during the winter. While icebergs maybe frozen in mélange during the winter in the fjord, they are still potentially mobile and sea ice / fjord cover will continually change with a warming Arctic (both in summer and winter) (Stroeve and Notz, 2018), therefore insights are needed on a year-round basis to begin to better understand icebergs at different times of year.

While power law distributions are useful (e.g. as shown by Sulak et al., 2017; Scheick et al., 2019), they are one-dimensional descriptors as they only provide a single alpha value for the entire iceberg distribution, providing a limited description of the overall iceberg distribution. These alpha values can only infer whether an iceberg distribution is dominated by small or large icebergs and whether that has changed through time (e.g., Scheick et al., 2019). The new approach presented in this thesis where iceberg count and volume are expressed as a percentage allows the entire dataset to be retained and provides insights into how different iceberg sizes are important for the fjord and mass loss from the glacier. When analysing the 100 largest icebergs in the distribution (those typically exceeding x_{min} values), there is substantial variability in the iceberg sizes which are much clearer than power laws.

The new descriptors used in this thesis are useful approaches for different research questions. Expressing iceberg count and volume as percentages allows the entire iceberg distribution to be analysed and characterised which power laws are unable to do so because of the removal of data through the x_{min}. Observing the 100 largest icebergs in the distribution offers an alternative to power law slope values as the sizes of these icebergs typically exceed the x_{min} values. However, analysing these 100 icebergs in different ways (e.g. their distribution) has provided

insights into the larger iceberg size classes at KNS (Chapter 6), whereas power laws only describe a single alpha value. As ArcticDEM v4 data become available (with greater time-coverage and temporal resolution) these new forms of analysis will provide greater insight than is currently possible, using results presented in this thesis from v3 data.

It is worth noting that while new approaches applied by this thesis has shown potentially new ways to express iceberg distributions, numerical models (e.g. MITgcm IceBerg package) are currently designed to assume a power law slope (e.g. -2.1 for Ilulissat Icefjord: Kajanto et al., 2023). Therefore, while this fixed alpha value is used as a descriptor for a dynamic iceberg distribution, it is currently considered as the standard practice. Work in this thesis has shown distributions in the 100 largest icebergs (which exceed x_{min} values that are included in power laws) can significantly evolve through time, which questions whether alpha values are robust enough to describe these changes. Whether other approaches are better suited in models is as yet untested, but it is worth exploring as to whether they may provide more accurate descriptors of freshwater fluxes from icebergs.

Iceberg distributions could be used to infer the impact of the subglacial hydrological system and subglacial plume upwellings on the style (Chapter 6) and frequency of calving (Chapter 6; Bunce et al., 2021) at outlets across Greenland. Distributed subglacial systems result in plume upwellings across the entire ice front, however channelised systems result in plumes only surfacing where the channels form beneath the glacier (Slater et al., 2015). These plume upwellings localise melt of the calving face and can consequently decrease terminus wide calving activity (Bunce et al., 2021). Having more frequent observations (e.g. ArcticDEM v4) could identify at glaciers across the ice sheets where the channels form and determine the impacts of subglacial hydrology on calving.

Chapter 5 shows that deriving a single alpha value for each month of the dataset (July to October) does not yield any distinct changes in calving styles across the ice sheet (Figure 5.7). However, Chapter 6 has been able to identify iceberg size changes throughout the melt season by looking at the characteristics of the 100 largest icebergs and suggest runoff can impact the size of larger icebergs being calved. The findings presented in Chapter 6 were only possible as more DEMs are available for analysis at KNS compared to the majority of glaciers across the ice sheet. When more frequent data become available it will be possible to infer the importance of runoff on the iceberg sizes being calved with greater confidence. Fundamentally, these findings are again reliant on data availability, nonetheless future studies looking to constrain

similar dynamics should look to capture iceberg sizes across the entire melt season to identify any evolutional change, as transitional increases in larger icebergs being calved through the melt season are observed.

This thesis has utilised basal topography to try and decipher any relationships with iceberg size distributions (Chapter 5). Deeper grounded glaciers are in a situation where basal crevasses can propagate and cause full-thickness calving events (Bassis and Walker, 2012). This style of calving results in larger icebergs being detached from the ice front (James et al., 2014). Shallower glaciers however, do not necessarily experience such calving events and will be dominated by serac failure which tend to produce smaller icebergs in the fjord (Bartholomaus et al., 2013). As presented in Chapter 5, some deeper glaciers (> 230 m) around the ice sheet have fjords dominated by larger icebergs, but this is not the case for all glaciers. While relationships may exist, it is currently hard to quantify these dynamics because of the high uncertainty of bed topography data underlaying Greenland's outlets.

The temporal resolution of ArcticDEM v3 means that it is impossible to quantify iceberg residence time, however there is potential for this to be derived with other, more frequently acquired satellite imagery (e.g. Moyer et al., 2019). If workflows could automatically identify and track icebergs through the fjord system, it will provide the community with a greater spatial understanding of fjord dynamics and iceberg trajectories (e.g. determining whether iceberg pathways are forced by wind or ocean). Such research could not only help quantify the number of icebergs leaving the fjord, but also the total quantity of ice (and subsequent freshwater) entering the seas and oceans around Greenland. These trajectories could be hugely important for determining where icebergs may ground in the fjord (e.g. an iceberg has a deeper keel depth than the fjord depth), but also for models trying to constrain how freshwater is released from melting and where that subsequent water travels to in the fjord.

7.6 **Societal implications**

As noted in the Chapter 3, the presence of icebergs in the polar regions have implications for an expanding Arctic economy and society. Such industries include: offshore infrastructure, commercial shipping, tourism, coastal communities, mining (rare earth elements) and fishing industries. These stakeholders all have interest in Greenland due to its natural environment and economic potential.

This thesis has shown that Greenland's fjords are dominated by the presence of small icebergs with their larger counterparts being comparatively rare in abundance (Chapter 5). For local

fisheries utilising the resources of these fjords, small icebergs can be problematic as it can choke the fjord environment, meaning it is challenging to navigate in. Larger icebergs on the other hand are relatively easy to manoeuvre around for small boats, but represent a hazard to larger shipping. Large icebergs also pose tsunami risks during calving and capsize events (Lüthi and Vieli, 2016), especially when in close proximity to harbours. These icebergs dominate the fjord's total iceberg volume and therefore the freshwater reserves which can impact fjord conditions and biogeochemistry (Meire et al., 2016) which is important for food chains and fishing. The future evolution of iceberg calving and subsequent iceberg distributions could have profound implications for these fishing industries, both logistically and for resilience and location of fishing grounds.

Little to no work has been conducted on the specific challenges of increased iceberg discharge and how they are interacting with current observed changes in fish habitats in Greenland's waters. An example of changes that have already occurred includes the fact that the seas and oceans surrounding Greenland are becoming warmer, meaning fish are migrating further north (Jansen et al., 2016). For example, the migration and intrusion of previously excluded predators due to environmental barriers has implications for native species, such as the coastal Arctic Char which is now at risk due to the threat of pink salmon, an invasive predator that has migrated into waters that they were previously unable to (Nielsen et al., 2020). Such considerations are imperative for fish stocks, communal livelihoods and the challenges faced by a warming Greenland climate. It is known that icebergs can impact fjord productivity and the biogeochemical cycle (Meire et al., 2016), but the impact of iceberg meltwater modified water on commercial fishing and invasive species is currently unconstrained.

Icebergs pose a significant risk to coastal communities, with villages and towns having to be evacuated if large icebergs drift close to the settlements and are likely to calve and create tsunami waves (The Guardian, 2018). Coastal infrastructure is constantly being developed and/or built around Greenland for continued economic growth and mining exploration (Taarup-Esbensen and Gudmestad., 2022). Approaches developed in this thesis will allow for easier quantification of these risks, both from DEM data and two-dimensional satellite imagery. This is especially of importance for assessing risk to crucial national infrastructure such as ports, harbours, mines, pipelines, communication cabling and hydropower installations.

A noted in Chapter 3, Wood-Donnelly (2022) suggest iceberg sovereignty has ignited considerations for the future of icebergs in the geopolitical realm. While the idea of iceberg

'ownership' could be called into question, which may easily happen with water security uncertainty in the future, the categorisation of icebergs would be critical to this conversation. Work in this thesis shown that smaller icebergs are hugely important for the fjord count, but ice sheet wide they do not significantly contribute to the total volume (Chapter 5). Consequently, if iceberg sovereignty was to be considered, these open research questions need answering:

1) What iceberg size could be classed as 'large enough' for ownership?
2) Do all icebergs have a sovereignty, or only those large enough to contain a certain amount of freshwater?
3) Do certain countries have access to all iceberg sizes, or just small icebergs?

These questions will need addressing, with data and methods presented in this thesis holding potential to add context to how these challenges will evolve.

Icebergs are a dynamic and integral part of the ice-ocean interface that have implications not just for glacier dynamics and fjord freshwater reservoirs, but for human livelihoods and settlements, stakeholder interest (e.g. commercial, mining, tourism) and geopolitical uncertainty currently and in the future. This thesis has provided the characterisation of the near-terminus fjord environment through the automated mapping at ice sheet scale for the first time.

7.7 **Outlook**

The two automated workflows presented in this thesis (Chapters 4 and 5) have provided a framework for other studies which seek to generate new ways to automatically identify icebergs. Using similar detection methods as presented in this thesis, future work should consider generating iceberg datasets from higher spatial and temporal satellite imagery (e.g. Landsat and Sentinel programmes). By doing so, more complete time series of iceberg distributions from multiple fjords can be derived and result in a better overall understanding of how these vary temporally.

A consideration after this PhD would be to repackage these workflows into an Earth Engine Python API (see: https://developers.google.com/earth-engine/tutorials/community/intro-to-python-api) where both pre-and post-processing can be performed. Currently, all the iceberg detection and subsequent assignation of metadata is performed in GEE, and once exported, Python is used post-processing and analysis. Bringing this analysis into a single scripting environment provides the opportunity for future workflow development and data visualisation.

ArcticDEM strip data is an underutilised resource that provides high spatial resolution data (2 m posting, 10 cm vertical accuracy) which is easily accessed in GEE. These data do not have to be analysed using cloud computing, however, having the DEMs ingested into GEE is a significant benefit. Throughout this thesis it has been mentioned ArcticDEM v3 strip data is limited temporally, meaning our analysis is only able to provide snapshot observations of the fjord at the time of data acquisition. The release of ArcticDEM v4 strip data (with data updated to 2021) in October 2022 has yet to be ingested into GEE, however if and when it does, the workflow will be updated (ensuring the metadata in consistent with v3) which will allow users of the GUI to attain a greater quantity of data which is much more up to date. If such ingestion occurs, another five years of data will be made available, meaning that up to a decade's worth of iceberg outline data could be extracted. Consequently, providing scope for a more continuous observational period and greater temporal detail when inferring iceberg distributions and calving dynamics. Finally, the workflows will also be maintained for any future releases of ArcticDEM data (e.g. v4 and onwards).

Chapter 8: Closing remarks

This thesis has presented new approaches to cloud computing, iceberg detection and iceberg distributions at marine-terminating glaciers around Greenland. By creating new tools that have allowed the generation of an unprecedented dataset of iceberg observations, it has provided advances in understanding of how icebergs sizes are distributed between the fjords of Greenland. These technical developments have allowed this thesis to constrain iceberg size ranges across Greenland and observe time-evolving iceberg distributions during the melt season at an individual glacier location.

The development of a graphical user interface (GUI) highlights the flexibility and accessibility of the workflow, reducing the barriers for operators to obtain their own data. The underlying workflow has been user validated and generated over 163,000 three-dimensional iceberg observations that has led to the derivation of new iceberg area-to-volume convertors with associated uncertainties for the first time. It has also been developed in a way to ensure future-proofing upon the release of continued ArcticDEM strip data. Once ArcticDEM v4 is ingested into Google Earth Engine, the workflow will be updated to ensure all temporally available DEMs are within the GUI, providing a decade worth of potential iceberg data across the Arctic.

The work presented in this thesis has provided a framework for automating the delineation of a ROI at multiple glaciers across the ice sheet that can be applied to other satellite imagery pipelines. Utilising open-access data (e.g. Goliber et al., 2022) and cloud computing has enabled spatiotemporal analysis of iceberg distributions at ice sheet scale. The resulting data have revealed while small icebergs (< 10,000 m^3) are abundant in Greenland's fjords, they contribute little to the overall volume (ice sheet median = 12%). Trying to constrain these distributions with glacier discharge (Mankoff et al., 2020) is not currently possible due to the temporal resolution of ArcticDEM v3, and that submarine melting is an influential component of frontal ablation (Wood et al., 2021) which is beyond scope of this thesis.

It has not been possible to quantify any significant relationship between the depth of the glacier and iceberg calving because of uncertainties within BedMachine basal topography data

(Morlighem et al., 2017). This is exemplified by some of our termini depths being incorrectly identified as above sea level when they are observably in a marine-terminating environment. Consequently, the relationship between terminus depth and iceberg sizes may exist, however observing such is still limited due to uncertainties in basal topography across the ice sheet.

However, when focussing to one glacier in detail (KNS), the decay of icebergs is controlled by both melt and fracture. The concept of icebergs traditionally being best described as fitting a power law distribution in the near-terminus region is found to not be the case at KNS. Instead, it is not possible to distinguish between power law or lognormal distributions to best describe their sizes, rather the majority of the data is more likely to fit lognormally, though power laws also provide statistically adequate fits. While power laws are a major component of describing distributions in iceberg modelling studies (e.g. Davison et al., 2020a; Kajanto et al., 2023), they are not capable of characterising the entire distribution because of the removal of data through the x_{min}. The data which exceed the x_{min} threshold value are then collapsed into one alpha value to describe the iceberg sizes of the entire distribution calved by a glacier. The new representations of iceberg size distributions and data analysis presented by this thesis show that distribution characteristics evolve on seasonal to annual timescales, and can vary substantially between fjords.

References

Allard, J.L., Hughes, P.D. and Woodward, J.C., 2021. Heinrich Stadial aridity forced Mediterranean-wide glacier retreat in the last cold stage. *Nature Geoscience*, 14(4), pp.197-205.

Alstott, J., Bullmore, E. and Plenz, D., 2014. powerlaw: a Python package for analysis of heavy-tailed distributions. *PloS one*, 9(1).

Amaral, T., Bartholomaus, T.C. and Enderlin, E.M., 2020. Evaluation of iceberg calving models against observations from Greenland outlet glaciers. *Journal of Geophysical Research: Earth Surface*, 125(6).

Amundson, J.M., Fahnestock, M., Truffer, M., Brown, J., Lüthi, M.P. and Motyka, R.J., 2010. Ice mélange dynamics and implications for terminus stability, Jakobshavn Isbræ, Greenland. *Journal of Geophysical Research: Earth Surface*, 115(F1).

Anchang, J.Y., Prihodko, L., Ji, W., Kumar, S.S., Ross, C.W., Yu, Q., Lind, B., Sarr, M.A., Diouf, A.A. and Hanan, N.P., 2020. Toward operational mapping of woody canopy cover in tropical savannas using Google Earth Engine. *Frontiers in Environmental Science*, 8, p.4.

Andrés, E.D., Slater, D.A., Straneo, F., Otero, J., Das, S. and Navarro, F., 2020. Surface emergence of glacial plumes determined by fjord stratification. *The Cryosphere*, 14(6), pp.1951-1969.

Andresen, C.S., Straneo, F., Ribergaard, M.H., Bjørk, A.A., Andersen, T.J., Kuijpers, A., Nørgaard-Pedersen, N., Kjær, K.H., Schjøth, F., Weckström, K. and Ahlstrøm, A.P., 2012. Rapid response of Helheim Glacier in Greenland to climate variability over the past century. *Nature Geoscience*, 5(1), p.37.

Ashmore, D.W., Mair, D.W., Higham, J.E., Brough, S., Lea, J.M. and Nias, I.J., 2022. Proper orthogonal decomposition of ice velocity identifies drivers of flow variability at Sermeq Kujalleq (Jakobshavn Isbræ). *The Cryosphere*, 16(1), pp.219-236.

Åström, J., Cook, S., Enderlin, E.M., Sutherland, D.A., Mazur, A. and Glasser, N., 2021. Fragmentation theory reveals processes controlling iceberg size distributions. *Journal of Glaciology*, 67(264), pp.603-612.

Åström, J.A., Riikilä, T.I., Tallinen, T., Zwinger, T., Benn, D., Moore, J.C. and Timonen, J., 2013. A particle based simulation model for glacier dynamics. *The Cryosphere*, 7(5), pp.1591-1602.

Åström, J.A., Vallot, D., Schäfer, M., Welty, E.Z., O'Neel, S., Bartholomaus, T.C., Liu, Y., Riikilä, T.I., Zwinger, T., Timonen, J. and Moore, J.C., 2014. Termini of calving glaciers as self-organized critical systems. *Nature Geoscience*, 7(12), pp.874-878.

B. Riffenburgh (ed.), Encyclopedia of the Antarctic. New York: Routledge (2007)

Bamber, J., Van Den Broeke, M., Ettema, J., Lenaerts, J. and Rignot, E., 2012. Recent large increases in freshwater fluxes from Greenland into the North Atlantic. *Geophysical Research Letters*, 39(19).

Bamber, J.L., Griggs, J.A., Hurkmans, R.T.W.L., Dowdeswell, J.A., Gogineni, S.P., Howat, I., Mouginot, J., Paden, J., Palmer, S., Rignot, E. and Steinhage, D., 2013. A new bed elevation dataset for Greenland. *The Cryosphere*, 7(2), pp.499-510.

Barr, I.D., Dokukin, M.D., Kougkoulos, I., Livingstone, S.J., Lovell, H., Małecki, J. and Muraviev, A.Y., 2018. Using ArcticDEM to analyse the dimensions and dynamics of debris-covered glaciers in Kamchatka, Russia. *Geosciences*, 8(6), p.216.

Bartholomaus, T.C., Larsen, C.F. and O'Neel, S., 2013. Does calving matter? Evidence for significant submarine melt. *Earth and Planetary Science Letters*, 380, pp.21-30.

Bartholomaus, T.C., Stearns, L.A., Sutherland, D.A., Shroyer, E.L., Nash, J.D., Walker, R.T., Catania, G., Felikson, D., Carroll, D., Fried, M.J. and Noël, B.P., 2016. Contrasts in the response of adjacent fjords and glaciers to ice-sheet surface melt in West Greenland. *Annals of Glaciology*, 57(73), pp.25-38.

Bartholomew, I., Nienow, P., Sole, A., Mair, D., Cowton, T., Palmer, S. and Wadham, J., 2011. Supraglacial forcing of subglacial drainage in the ablation zone of the Greenland ice sheet. *Geophysical Research Letters*, 38(8).

Bartov, Y., Goldstein, S.L., Stein, M. and Enzel, Y., 2003. Catastrophic arid episodes in the Eastern Mediterranean linked with the North Atlantic Heinrich events. *Geology*, 31(5), pp.439-442.

Bassis, J.N. and Walker, C.C., 2012. Upper and lower limits on the stability of calving glaciers from the yield strength envelope of ice. *Proceedings of the Royal Society A: Mathematical, Physical and Engineering Sciences*, 468(2140), pp.913-931.

Bendixen, M., Overeem, I., Rosing, M.T., Bjørk, A.A., Kjær, K.H., Kroon, A., Zeitz, G. and Iversen, L.L., 2019. Promises and perils of sand exploitation in Greenland. *Nature sustainability*, 2(2), pp.98-104.

Benedek, C.L. and Willis, I.C., 2021. Winter drainage of surface lakes on the Greenland Ice Sheet from Sentinel-1 SAR imagery. *The Cryosphere*, 15(3), pp.1587-1606.

Benn, D.I. and Åström, J.A., 2018. Calving glaciers and ice shelves. *Advances in Physics: X*, 3(1), p.1513819.

Benn, D.I., Hulton, N.R. and Mottram, R.H., 2007a. 'Calving laws', 'sliding laws' and the stability of tidewater glaciers. *Annals of glaciology*, 46, pp.123-130.

Benn, D.I., Warren, C.R. and Mottram, R.H., 2007b. Calving processes and the dynamics of calving glaciers. *Earth-Science Reviews*, 82(3-4), pp.143-179.

Bevan, S.L., Luckman, A.J., Benn, D.I., Cowton, T. and Todd, J., 2019. Impact of warming shelf waters on ice mélange and terminus retreat at a large SE Greenland glacier. *The Cryosphere*, 13(9), pp.2303-2315.

Bigg, G. and Billings, S., 2014. The iceberg risk in the Titanic year of 1912: Was it exceptional?. *Significance*, 11(3), pp.6-10.

Bigg, G.R., 2015. *Icebergs: their science and links to global change*. Cambridge University Press.

Bigg, G.R., Jutard, Q. and Marsh, R., 2021. Evidence for iceberg fertilization of the NW Atlantic. *Ocean Science Discussions*, pp.1-25.

Bigg, G.R., Wadley, M.R., Stevens, D.P. and Johnson, J.A., 1997. Modelling the dynamics and thermodynamics of icebergs. *Cold Regions Science and Technology*, 26(2), pp.113-135.

Bigg, G.R., Wei, H.L., Wilton, D.J., Zhao, Y., Billings, S.A., Hanna, E. and Kadirkamanathan, V., 2014. A century of variation in the dependence of Greenland iceberg calving on ice sheet surface mass balance and regional climate change. *Proceedings of the Royal Society A: Mathematical, Physical and Engineering Sciences*, 470(2166), p.20130662.

Bislev, A. and Smed, K., 2018. When will the iceberg melt? Narrating the Arctic among Chinese and Danish tourists aboard a cruise ship in Greenland. *China & the Arctic*, 2018, pp.29-42.

Bjørk, A.A., Kruse, L.M. and Michaelsen, P.B., 2015. Brief communication: Getting Greenland's glaciers right–a new data set of all official Greenlandic glacier names. *The Cryosphere*, 9(6), pp.2215-2218.

Bond, G., Heinrich, H., Broecker, W., Labeyrie, L., McManus, J., Andrews, J., Huon, S., Jantschik, R., Clasen, S., Simet, C. and Tedesco, K., 1992. Evidence for massive discharges of icebergs into the North Atlantic Ocean during the last glacial period. *Nature*, 360(6401), pp.245-249.

Böning, C.W., Behrens, E., Biastoch, A., Getzlaff, K. and Bamber, J.L., 2016. Emerging impact of Greenland meltwater on deepwater formation in the North Atlantic Ocean. *Nature Geoscience*, 9(7), pp.523-527.

Boothroyd, R.J., Williams, R.D., Hoey, T.B., Barrett, B. and Prasojo, O.A., 2021. Applications of Google Earth Engine in fluvial geomorphology for detecting river channel change. *Wiley Interdisciplinary Reviews: Water*, 8(1), p.e21496.

Bowling, J.S., Livingstone, S.J., Sole, A.J. and Chu, W., 2019. Distribution and dynamics of Greenland subglacial lakes. *Nature communications*, 10(1), p.2810.

Box, J.E., Fettweis, X., Stroeve, J.C., Tedesco, M., Hall, D.K. and Steffen, K., 2012. Greenland ice sheet albedo feedback: thermodynamics and atmospheric drivers. *The Cryosphere*, 6(4), pp.821-839.

Braakmann-Folgmann, A., Shepherd, A. and Ridout, A., 2021. Tracking changes in the area, thickness, and volume of the Thwaites tabular iceberg "B30" using satellite altimetry and imagery. *The Cryosphere*, 15(8), pp.3861-3876.

Braakmann-Folgmann, A., Shepherd, A., Gerrish, L., Izzard, J. and Ridout, A., 2022. Observing the disintegration of the A68A iceberg from space. *Remote Sensing of Environment*, 270, p.112855.

Brough, S., Carr, J.R., Ross, N. and Lea, J.M., 2019. Exceptional retreat of Kangerlussuaq Glacier, east Greenland, between 2016 and 2018. *Frontiers in Earth Science*, 7, p.123.

Brough, S., Carr, J.R., Ross, N. and Lea, J.M., 2023. Ocean-forcing and glacier-specific factors drive differing glacier response across the 69ºN boundary, east Greenland. *Journal of Geophysical Research: Earth Surface*, p.e2022JF006857.

Brown, C.S., Meier, M.F. and Post, A., 1982. *Calving speed of Alaska tidewater glaciers, with application to Columbia Glacier* (Vol. 1258, p. 13). US Government Printing Office.

Bunce, C., Carr, J.R., Nienow, P.W., Ross, N. and Killick, R., 2018. Ice front change of marine-terminating outlet glaciers in northwest and southeast Greenland during the 21st century. *Journal of Glaciology*, 64(246), pp.523-535.

Cape, M.R., Straneo, F., Beaird, N., Bundy, R.M. and Charette, M.A., 2019. Nutrient release to oceans from buoyancy-driven upwelling at Greenland tidewater glaciers. *Nature Geoscience*, 12(1), pp.34-39.

Carlson, D.F. and Rysgaard, S., 2018. Adapting open-source drone autopilots for real-time iceberg observations. *MethodsX*, 5, pp.1059-1072.

Carlson, D.F., Boone, W., Meire, L., Abermann, J. and Rysgaard, S., 2017. Bergy bit and melt water trajectories in Godthåbsfjord (SW Greenland) observed by the Expendable Ice Tracker. *Frontiers in Marine Science*, 4, p.276.

Carr, J.R., Stokes, C.R. and Vieli, A., 2013. Recent progress in understanding marine-terminating Arctic outlet glacier response to climatic and oceanic forcing: Twenty years of rapid change. *Progress in Physical Geography*, 37(4), pp.436-467.

Carroll, D., Sutherland, D.A., Hudson, B., Moon, T., Catania, G.A., Shroyer, E.L., Nash, J.D., Bartholomaus, T.C., Felikson, D., Stearns, L.A. and Noel, B.P., 2016. The impact of glacier geometry on meltwater plume structure and submarine melt in Greenland fjords. *Geophysical Research Letters*, 43(18), pp.9739-9748.

Cassotto, R., Fahnestock, M., Amundson, J.M., Truffer, M. and Joughin, I., 2015. Seasonal and interannual variations in ice melange and its impact on terminus stability, Jakobshavn Isbræ, Greenland. *Journal of Glaciology*, 61(225), pp.76-88.

Cassotto, R.K., Burton, J.C., Amundson, J.M., Fahnestock, M.A. and Truffer, M., 2021. Granular decoherence precedes ice mélange failure and glacier calving at Jakobshavn Isbræ. *Nature Geoscience*, 14(6), pp.417-422.

Catania, G.A., Stearns, L.A., Moon, T.A., Enderlin, E.M. and Jackson, R.H., 2020. Future evolution of Greenland's marine-terminating outlet glaciers. *Journal of Geophysical Research: Earth Surface*, 125(2), p.e2018JF004873.

Choi, Y., Morlighem, M., Rignot, E. and Wood, M., 2021. Ice dynamics will remain a primary driver of Greenland ice sheet mass loss over the next century. *Communications Earth & Environment*, 2(1), pp.1-9.

Choi, Y., Morlighem, M., Wood, M. and Bondzio, J.H., 2018. Comparison of four calving laws to model Greenland outlet glaciers. *The Cryosphere*, 12(12), pp.3735-3746.

Christiansen, F.G., 2022. Greenland mineral exploration history. *Mineral Economics*, pp.1-29.

Clauset, A., Shalizi, C.R. and Newman, M.E., 2009. Power-law distributions in empirical data. *SIAM review*, 51(4), pp.661-703.

Condron, A. and Hill, J.C., 2021. Timing of iceberg scours and massive ice-rafting events in the subtropical North Atlantic. *Nature Communications*, 12(1), pp.1-14.

Condron, A., 2023. Towing icebergs to arid regions to reduce water scarcity. *Scientific Reports*, 13(1), p.365.

Cook, J., Edwards, A., Takeuchi, N. and Irvine-Fynn, T., 2016. Cryoconite: the dark biological secret of the cryosphere. *Progress in Physical Geography*, 40(1), pp.66-111.

Cook, S., Rutt, I.C., Murray, T., Luckman, A., Zwinger, T., Selmes, N., Goldsack, A. and James, T.D., 2014. Modelling environmental influences on calving at Helheim Glacier in eastern Greenland. *The Cryosphere*, 8(3), pp.827-841.

Cook, S.J., Christoffersen, P., Truffer, M., Chudley, T.R. and Abellán, A., 2021. Calving of a large Greenlandic tidewater glacier has complex links to meltwater plumes and mélange. *Journal of Geophysical Research: Earth Surface*, 126(4), p.e2020JF006051.

Cooley, S.W. and Christoffersen, P., 2017. Observation bias correction reveals more rapidly draining lakes on the Greenland Ice Sheet. *Journal of Geophysical Research: Earth Surface*, 122(10), pp.1867-1881.

Cortijo, E., Labeyrie, L., Vidal, L., Vautravers, M., Chapman, M., Duplessy, J.C., Elliot, M., Arnold, M., Turon, J.L. and Auffret, G., 1997. Changes in sea surface hydrology associated with Heinrich event 4 in the North Atlantic Ocean between 40 and 60 N. *Earth and Planetary Science Letters*, 146(1-2), pp.29-45.

Crawford, A., Crocker, G., Mueller, D., Desjardins, L.U.C., Saper, R.O.N. and Carrieres, T.O.M., 2018. The canadian ice island drift, deterioration and detection (CI2D3) database. *Journal of Glaciology*, 64(245), pp.517-521.

Crawford, A.J., Mueller, D., Desjardins, L. and Myers, P.G., 2018. The aftermath of Petermann Glacier calving events (2008–2012): Ice island size distributions and meltwater dispersal. *Journal of Geophysical Research: Oceans*, 123(12), pp.8812-8827.

Dai, C. and Howat, I.M., 2017. Measuring lava flows with ArcticDEM: Application to the 2012–2013 eruption of Tolbachik, Kamchatka. *Geophysical Research Letters*, 44(24), pp.12-133.

Dansgaard, W., Johnsen, S.J., Clausen, H.B., Dahl-Jensen, D., Gundestrup, N.S., Hammer, C.U., Hvidberg, C.S., Steffensen, J.P., Sveinbjörnsdottir, A.E., Jouzel, J. and Bond, G., 1993. Evidence for general instability of past climate from a 250-kyr ice-core record. *nature*, 364(6434), pp.218-220.

Das, S.B., Joughin, I., Behn, M.D., Howat, I.M., King, M.A., Lizarralde, D. and Bhatia, M.P., 2008. Fracture propagation to the base of the Greenland Ice Sheet during supraglacial lake drainage. *Science*, 320(5877), pp.778-781.

Davison, B.J., Cowton, T.R., Cottier, F.R. and Sole, A.J., 2020a. Iceberg melting substantially modifies oceanic heat flux towards a major Greenlandic tidewater glacier. *Nature communications*, 11(1), pp.1-13.

Davison, B.J., Sole, A.J., Cowton, T.R., Lea, J.M., Slater, D.A., Fahrner, D. and Nienow, P.W., 2020b. Subglacial drainage evolution modulates seasonal ice flow variability of three tidewater glaciers in southwest Greenland. *Journal of Geophysical Research: Earth Surface*, 125(9), p.e2019JF005492.

DeConto, R.M. and Pollard, D., 2016. Contribution of Antarctica to past and future sea-level rise. *Nature*, 531(7596), pp.591-597.

Duprat, L.P., Bigg, G.R. and Wilton, D.J., 2016. Enhanced Southern Ocean marine productivity due to fertilization by giant icebergs. *Nature Geoscience*, 9(3), pp.219-221.

Durand, G., Gagliardini, O., Favier, L., Zwinger, T. and Le Meur, E., 2011. Impact of bedrock description on modeling ice sheet dynamics. *Geophysical Research Letters*, 38(20).

Edwards, T.L., Nowicki, S., Marzeion, B., Hock, R., Goelzer, H., Seroussi, H., Jourdain, N.C., Slater, D.A., Turner, F.E., Smith, C.J. and McKenna, C.M., 2021. Projected land ice contributions to twenty-first-century sea level rise. *Nature*, 593(7857), pp.74-82.

Eik, K. and Gudmestad, O.T., 2010. Iceberg management and impact on design of offshore structures. *Cold regions science and technology*, 63(1-2), pp.15-28.

Enderlin, E. M., & Hamilton, G. S. (2014). Estimates of iceberg submarine melting from high-resolution digital elevation models: Application to Sermilik Fjord, East Greenland. Journal of Glaciology, 60(224), 1084–1092.

Enderlin, E.M., Carrigan, C.J., Kochtitzky, W.H., Cuadros, A., Moon, T. and Hamilton, G.S., 2018. Greenland iceberg melt variability from high-resolution satellite observations. *The Cryosphere*, 12(2), pp.565-575.

Enderlin, E.M., Hamilton, G.S., Straneo, F. and Sutherland, D.A., 2016. Iceberg meltwater fluxes dominate the freshwater budget in Greenland's iceberg-congested glacial fjords. *Geophysical Research Letters*, 43(21), pp.11-287.

Enderlin, E.M., Howat, I.M., Jeong, S., Noh, M.J., Van Angelen, J.H. and Van Den Broeke, M.R., 2014. An improved mass budget for the Greenland ice sheet. *Geophysical Research Letters*, 41(3), pp.866-872.

England, M.R., Wagner, T.J. and Eisenman, I., 2020. Modeling the breakup of tabular icebergs. *Science advances*, 6(51), p.eabd1273.

Fahrner, D., Lea, J.M., Brough, S., Mair, D.W. and Abermann, J., 2021. Linear response of the Greenland ice sheet's tidewater glacier terminus positions to climate. *Journal of Glaciology*, 67(262), pp.193-203.

Fendrock, M., Condron, A. and McGee, D., 2022. Modeling Iceberg Longevity and Distribution During Heinrich Events. *Paleoceanography and Paleoclimatology*, 37(6), p.e2021PA004347.

Fried, M.J., Catania, G.A., Bartholomaus, T.C., Duncan, D., Davis, M., Stearns, L.A., Nash, J., Shroyer, E. and Sutherland, D., 2015. Distributed subglacial discharge drives significant submarine melt at a Greenland tidewater glacier. *Geophysical Research Letters*, 42(21), pp.9328-9336.

Fried, M.J., Catania, G.A., Stearns, L.A., Sutherland, D.A., Bartholomaus, T.C., Shroyer, E. and Nash, J., 2018. Reconciling drivers of seasonal terminus advance and retreat at 13 Central West Greenland tidewater glaciers. *Journal of Geophysical Research: Earth Surface*, 123(7), pp.1590-1607.

Gardner, A.S., Fahnestock M.A., and Scambos, T.A., 2022. ITS_LIVE Regional Glacier and Ice Sheet Surface Velocities. Data archived at National Snow and Ice Data Center; doi: 10.5067/6II6VW8LLWJ7.

Gladstone, R.M., Bigg, G.R. and Nicholls, K.W., 2001. Iceberg trajectory modeling and meltwater injection in the Southern Ocean. *Journal of Geophysical Research: Oceans*, 106(C9), pp.19903-19915.

Gledhill, L.A. and Williamson, A.G., 2018. Inland advance of supraglacial lakes in north-west Greenland under recent climatic warming. *Annals of Glaciology*, 59(76), pp.66-82.

Goff, J.A. and Austin Jr, J.A., 2009. Seismic and bathymetric evidence for four different episodes of iceberg scouring on the New Jersey outer shelf: Possible correlation to Heinrich events. *Marine Geology*, 266(1-4), pp.244-254.

Goliber, S., Black, T., Catania, G., Lea, J.M., Olsen, H., Cheng, D., Bevan, S., Bjørk, A., Bunce, C., Brough, S. and Carr, J.R., 2022. TermPicks: a century of Greenland glacier terminus data for use in scientific and machine learning applications. *The Cryosphere*, 16(8), pp.3215-3233.

Gorelick, N., Hancher, M., Dixon, M., Ilyushchenko, S., Thau, D. and Moore, R., 2017. Google Earth Engine: Planetary-scale geospatial analysis for everyone. *Remote sensing of Environment*, 202, pp.18-27.

Grousset, F.E., Labeyrie, L., Sinko, J.A., Cremer, M., Bond, G., Duprat, J., Cortijo, E. and Huon, S., 1993. Patterns of ice-rafted detritus in the glacial North Atlantic (40–55° N). *Paleoceanography*, 8(2), pp.175-192.

Grousset, F.E., Pujol, C., Labeyrie, L., Auffret, G. and Boelaert, A., 2000. Were the North Atlantic Heinrich events triggered by the behavior of the European ice sheets?. *Geology*, 28(2), pp.123-126.

Hanna, E., Fettweis, X., Mernild, S.H., Cappelen, J., Ribergaard, M.H., Shuman, C.A., Steffen, K., Wood, L. and Mote, T.L., 2014. Atmospheric and oceanic climate forcing of the

exceptional Greenland ice sheet surface melt in summer 2012. *International Journal of Climatology*, 34(4), pp.1022-1037.

Heinrich, H., 1988. Origin and consequences of cyclic ice rafting in the northeast Atlantic Ocean during the past 130,000 years. *Quaternary research*, 29(2), pp.142-152.

Hendry, K.R., Huvenne, V.A., Robinson, L.F., Annett, A., Badger, M., Jacobel, A.W., Ng, H.C., Opher, J., Pickering, R.A., Taylor, M.L. and Bates, S.L., 2019. The biogeochemical impact of glacial meltwater from Southwest Greenland. *Progress in oceanography*, 176, p.102126.

Hill, B., 2005. Ship collisions with iceberg database. Report to PERD: Trends and analysis. *NRC, TR-2005-17*.

Hill, E., Carr, J.R., Stokes, C. and Gudmundsson, H., 2018. Dynamic changes in outlet glaciers in northern Greenland from 1948 to 2015. *The Cryosphere*, 12(10), pp.3243-3263.

Hirt, C., 2018. Artefact detection in global digital elevation models (DEMs): The Maximum Slope Approach and its application for complete screening of the SRTM v4. 1 and MERIT DEMs. *Remote Sensing of Environment*, 207, pp.27-41.

Holland, M.M. and Bitz, C.M., 2003. Polar amplification of climate change in coupled models. *Climate dynamics*, 21(3-4), pp.221-232.

Holland, D.M., Thomas, R.H., De Young, B., Ribergaard, M.H. and Lyberth, B., 2008. Acceleration of Jakobshavn Isbræ triggered by warm subsurface ocean waters. *Nature geoscience*, 1(10), pp.659-664.

Hopwood, M.J., Bacon, S., Arendt, K., Connelly, D.P. and Statham, P.J., 2015. Glacial meltwater from Greenland is not likely to be an important source of Fe to the North Atlantic. *Biogeochemistry*, 124(1), pp.1-11.

Ignéczi, Á., Sole, A.J., Livingstone, S.J., Leeson, A.A., Fettweis, X., Selmes, N., Gourmelen, N. and Briggs, K., 2016. Northeast sector of the Greenland Ice Sheet to undergo the greatest inland expansion of supraglacial lakes during the 21st century. *Geophysical Research Letters*, 43(18), pp.9729-9738.

IPCC, 2022: *Climate Change 2022: Impacts, Adaptation, and Vulnerability.* Contribution of Working Group II to the Sixth Assessment Report of the Intergovernmental Panel on Climate Change [H.-O. Pörtner, D.C. Roberts, M. Tignor, E.S. Poloczanska, K.

Mintenbeck, A. Alegría, M. Craig, S. Langsdorf, S. Löschke, V. Möller, A. Okem, B. Rama (eds.)]. Cambridge University Press. Cambridge University Press, Cambridge, UK and New York, NY, USA, 3056 pp., doi:10.1017/9781009325844.

James, T.D., Murray, T., Selmes, N., Scharrer, K. and O'Leary, M., 2014. Buoyant flexure and basal crevassing in dynamic mass loss at Helheim Glacier. *Nature Geoscience*, 7(8), pp.593-596.

Jansen, T., Post, S., Kristiansen, T., Óskarsson, G.J., Boje, J., MacKenzie, B.R., Broberg, M. and Siegstad, H., 2016. Ocean warming expands habitat of a rich natural resource and benefits a national economy. *Ecological Applications*, 26(7), pp.2021-2032.

Jenkins, A., 2011. Convection-driven melting near the grounding lines of ice shelves and tidewater glaciers. *Journal of Physical Oceanography*, 41(12), pp.2279-2294.

Jennings, A.E., Andrews, J.T., Cofaigh, C.Ó., Onge, G.S., Sheldon, C., Belt, S.T., Cabedo-Sanz, P. and Hillaire-Marcel, C., 2017. Ocean forcing of Ice Sheet retreat in central west Greenland from LGM to the early Holocene. *Earth and Planetary Science Letters*, 472, pp.1-13.

Joughin, I., Das, S.B., Flowers, G.E., Behn, M.D., Alley, R.B., King, M.A., Smith, B.E., Bamber, J.L., van den Broeke, M.R. and Van Angelen, J.H., 2013. Influence of ice-sheet geometry and supraglacial lakes on seasonal ice-flow variability. *The Cryosphere*, 7(4), pp.1185-1192.

Jullien, E., Grousset, F.E., Hemming, S.R., Peck, V.L., Hall, I.R., Jeantet, C. and Billy, I., 2006. Contrasting conditions preceding MIS3 and MIS2 Heinrich events. *Global and Planetary Change*, 54(3-4), pp.225-238.

Kajanto, K., Seroussi, H., de Fleurian, B. and Nisancioglu, K.H., 2020. Present day Jakobshavn Isbræ (West Greenland) close to the Holocene minimum extent. *Quaternary Science Reviews*, 246.

Kajanto, K., Straneo, F. and Nisancioglu, K., 2023. Impact of icebergs on the seasonal submarine melt of Sermeq Kujalleq. *The Cryosphere*, 17(1), pp.371-390.

Kamb, B., 1987. Glacier surge mechanism based on linked cavity configuration of the basal water conduit system. *Journal of Geophysical Research: Solid Earth*, 92(B9), pp.9083-9100.

Kehrl, L.M., Joughin, I., Shean, D.E., Floricioiu, D. and Krieger, L., 2017. Seasonal and interannual variabilities in terminus position, glacier velocity, and surface elevation at Helheim and Kangerlussuaq Glaciers from 2008 to 2016. *Journal of Geophysical Research: Earth Surface*, 122(9), pp.1635-1652.

Khazendar, A., Fenty, I.G., Carroll, D., Gardner, A., Lee, C.M., Fukumori, I., Wang, O., Zhang, H., Seroussi, H., Moller, D. and Noël, B.P., 2019. Interruption of two decades of Jakobshavn Isbrae acceleration and thinning as regional ocean cools. *Nature Geoscience*, 12(4), pp.277-283.

King, M.D., Howat, I.M., Candela, S.G., Noh, M.J., Jeong, S., Noël, B.P., van den Broeke, M.R., Wouters, B. and Negrete, A., 2020. Dynamic ice loss from the Greenland Ice Sheet driven by sustained glacier retreat. *Communications Earth & Environment*, 1(1), pp.1-7.

Kirkham, J.D., Rosser, N.J., Wainwright, J., Jones, E.C.V., Dunning, S.A., Lane, V.S., Hawthorn, D.E., Strzelecki, M.C. and Szczuciński, W., 2017. Drift-dependent changes in iceberg size-frequency distributions. *Scientific reports*, 7(1), pp.1-10.

Koenig, L.S., Lampkin, D.J., Montgomery, L.N., Hamilton, S.L., Turrin, J.B., Joseph, C.A., Moutsafa, S.E., Panzer, B., Casey, K.A., Paden, J.D. and Leuschen, C., 2015. Wintertime storage of water in buried supraglacial lakes across the Greenland Ice Sheet. *The Cryosphere*, 9(4), pp.1333-1342.

Kolb, J., Keiding, J.K., Steenfelt, A., Secher, K., Keulen, N., Rosa, D. and Stensgaard, B.M., 2016. Metallogeny of Greenland. *Ore Geology Reviews*, 78, pp.493-555.

Koo, Y., Xie, H., Ackley, S.F., Mestas-Nuñez, A.M., Macdonald, G.J. and Hyun, C.U., 2021. Semi-automated tracking of iceberg B43 using Sentinel-1 SAR images via Google Earth Engine. *The Cryosphere*, 15(10), pp.4727-4744.

Laidre, K.L. and Stirling, I., 2020. Grounded icebergs as maternity denning habitat for polar bears (Ursus maritimus) in North and Northeast Greenland. *Polar Biology*, 43(7), pp.937-943.

Larsen, P.H., Hansen, M.O., Buus-Hinkler, J., Krane, K.H. and Sønderskov, C., 2015. Field tracking (GPS) of ten icebergs in eastern Baffin Bay, offshore Upernavik, northwest Greenland. *Journal of Glaciology*, 61(227), pp.421-437.

Lea, J.M., 2018. The Google Earth Engine Digitisation Tool (GEEDiT) and the Margin change Quantification Tool (MaQiT)–simple tools for the rapid mapping and quantification of changing Earth surface margins. *Earth Surface Dynamics*, 6(3), pp.551-561.

Lea, J.M., Mair, D.W., Nick, F.M., Rea, B.R., Weidick, A., Kjaer, K.H., Morlighem, M., Van As, D. and Schofield, J.E., 2014a. Terminus-driven retreat of a major southwest Greenland tidewater glacier during the early 19th century: insights from glacier reconstructions and numerical modelling. *Journal of Glaciology*, 60(220), pp.333-344.

Lea, J.M., Mair, D.W.F., Nick, F.M., Rea, B.R., Van As, D., Morlighem, M., Nienow, P.W. and Weidick, A., 2014b. Fluctuations of a Greenlandic tidewater glacier driven by changes in atmospheric forcing: observations and modelling of Kangiata Nunaata Sermia, 1859–present. *The Cryosphere*, 8(6), pp.2031-2045.

Leeson, A.A., Shepherd, A., Briggs, K., Howat, I., Fettweis, X., Morlighem, M. and Rignot, E., 2015. Supraglacial lakes on the Greenland ice sheet advance inland under warming climate. *Nature Climate Change*, 5(1), pp.51-55.

Legleiter, C.J., Tedesco, M., Smith, L.C., Behar, A.E. and Overstreet, B.T., 2014. Mapping the bathymetry of supraglacial lakes and streams on the Greenland ice sheet using field measurements and high-resolution satellite images. *The Cryosphere*, 8(1), pp.215-228.

Lenaerts, J.T., Le Bars, D., Van Kampenhout, L., Vizcaino, M., Enderlin, E.M. and Van Den Broeke, M.R., 2015. Representing Greenland ice sheet freshwater fluxes in climate models. *Geophysical Research Letters*, 42(15), pp.6373-6381.

Lenaerts, J.T., Medley, B., van den Broeke, M.R. and Wouters, B., 2019. Observing and modeling ice sheet surface mass balance. *Reviews of Geophysics*, 57(2), pp.376-420.

Leoni, M., 2019. *From Colonialism to Tourism: An Analysis of Cruise Ship Tourism in Ittoqqortoormiit, East Greenland* (Doctoral dissertation).

Levermann, A., Albrecht, T., Winkelmann, R., Martin, M.A., Haseloff, M. and Joughin, I., 2012. Kinematic first-order calving law implies potential for abrupt ice-shelf retreat. *The Cryosphere*, 6, pp.273-286.

Liang, Y.L., Colgan, W., Lv, Q., Steffen, K., Abdalati, W., Stroeve, J., Gallaher, D. and Bayou, N., 2012. A decadal investigation of supraglacial lakes in West Greenland using a fully

automatic detection and tracking algorithm. *Remote Sensing of Environment*, 123, pp.127-138.

Lichey, C. and Hellmer, H.H., 2001. Modeling giant-iceberg drift under the influence of sea ice in the Weddell Sea, Antarctica. *Journal of Glaciology*, 47(158), pp.452-460.

Lin, H., Rauschenberg, S., Hexel, C.R., Shaw, T.J. and Twining, B.S., 2011. Free-drifting icebergs as sources of iron to the Weddell Sea. *Deep Sea Research Part II: Topical Studies in Oceanography*, 58(11-12), pp.1392-1406.

Lopez-Lopez, L., Parmiggiani, F., Moctezuma-Flores, M. and Guerrieri, L., 2021. On the Detection and Long-Term Path Visualisation of A-68 Iceberg. *Remote Sensing*, 13(3), p.460.

Lu, X., Yang, K., Lu, Y., Gleason, C.J., Smith, L.C. and Li, M., 2020. Small Arctic rivers mapped from Sentinel-2 satellite imagery and ArcticDEM. *Journal of hydrology*, 584, p.124689.

Lüthi, M.P. and Vieli, A., 2016. Multi-method observation and analysis of a tsunami caused by glacier calving. *The Cryosphere*, 10(3), pp.995-1002.

Lüthje, M., Pedersen, L.T., Reeh, N. and Greuell, W., 2006. Modelling the evolution of supraglacial lakes on the West Greenland ice-sheet margin. *Journal of Glaciology*, 52(179), pp.608-618.

MacAyeal, D.R., 1993. Binge/purge oscillations of the Laurentide ice sheet as a cause of the North Atlantic's Heinrich events. *Paleoceanography*, 8(6), pp.775-784.

Macdonald, G.J., Banwell, A.F. and MacAYEAL, D.R., 2018. Seasonal evolution of supraglacial lakes on a floating ice tongue, Petermann Glacier, Greenland. *Annals of Glaciology*, 59(76), pp.56-65.

MacFerrin, M., Machguth, H., As, D.V., Charalampidis, C., Stevens, C.M., Heilig, A., Vandecrux, B., Langen, P.L., Mottram, R., Fettweis, X. and Van Den Broeke, M.R., 2019. Rapid expansion of Greenland's low-permeability ice slabs. *Nature*, 573(7774), pp.403-407.

MacKenzie, B.R., Payne, M.R., Boje, J., Høyer, J.L. and Siegstad, H., 2014. A cascade of warming impacts brings bluefin tuna to Greenland waters. *Global change biology*, 20(8), pp.2484-2491.

Mair, D., Nienow, P., Sharp, M., Wohlleben, T. and Willis, I., 2002. Influence of subglacial drainage system evolution on glacier surface motion: Haut Glacier d'Arolla, Switzerland. *Journal of Geophysical Research: Solid Earth*, 107(B8), pp.EPM-8.

Mair, D., Willis, I., Fischer, U.H., Hubbard, B., Nienow, P. and Hubbard, A., 2003. Hydrological controls on patterns of surface, internal and basal motion during three "spring events": Haut Glacier d'Arolla, Switzerland. *Journal of Glaciology*, 49(167), pp.555-567.

Mankoff, K.D., Colgan, W., Solgaard, A., Karlsson, N.B., Ahlstrøm, A.P., Van As, D., Box, J.E., Khan, S.A., Kjeldsen, K.K., Mouginot, J. and Fausto, R.S., 2020. Greenland Ice Sheet solid ice discharge from 1986 through 2017. *Earth System Science Data*, 11(2), pp.769-786.

Marsh, R., Ivchenko, V.O., Skliris, N., Alderson, S., Bigg, G.R., Madec, G., Blaker, A.T., Aksenov, Y., Sinha, B., Coward, A.C. and Sommer, J.L., 2015. NEMO–ICB (v1. 0): interactive icebergs in the NEMO ocean model globally configured at eddy-permitting resolution. *Geoscientific Model Development*, 8(5), pp.1547-1562.

Marson, J.M., Myers, P.G., Hu, X. and Le Sommer, J., 2018. Using vertically integrated ocean fields to characterize Greenland icebergs' distribution and lifetime. *Geophysical Research Letters*, 45(9), pp.4208-4217.

McManus, J.F., Francois, R., Gherardi, J.M., Keigwin, L.D. and Brown-Leger, S., 2004. Collapse and rapid resumption of Atlantic meridional circulation linked to deglacial climate changes. *Nature*, 428(6985), pp.834-837.

McMillan, M., Nienow, P., Shepherd, A., Benham, T. and Sole, A., 2007. Seasonal evolution of supra-glacial lakes on the Greenland Ice Sheet. *Earth and Planetary Science Letters*, 262(3-4), pp.484-492.

Meire, L., Meire, P., Struyf, E., Krawczyk, D.W., Arendt, K.E., Yde, J.C., Juul Pedersen, T., Hopwood, M.J., Rysgaard, S. and Meysman, F.J.R., 2016. High export of dissolved silica from the Greenland Ice Sheet. *Geophysical Research Letters*, 43(17), pp.9173-9182.

Meire, L., Mortensen, J., Meire, P., Juul-Pedersen, T., Sejr, M.K., Rysgaard, S., Nygaard, R., Huybrechts, P. and Meysman, F.J., 2017. Marine-terminating glaciers sustain high productivity in Greenland fjords. *Global Change Biology*, 23(12), pp.5344-5357.

Mendsonboaz., 2009. Tsunami Greenland - Tsunami Groelândia 1995. Online: https://www.youtube.com/watch?v=z8LWSOPwkn8. Last accessed: 21st September 2021.

Mercenier, R., Lüthi, M.P. and Vieli, A., 2018. Calving relation for tidewater glaciers based on detailed stress field analysis. *The Cryosphere*, 12(2), pp.721-739.

Mernild, S.H., Holland, D.M., Holland, D., Rosing-Asvid, A., Yde, J.C., Liston, G.E. and Steffen, K., 2015. Freshwater flux and spatiotemporal simulated runoff variability into Ilulissat Icefjord, West Greenland, linked to salinity and temperature observations near tidewater glacier margins obtained using instrumented ringed seals. *Journal of Physical Oceanography*, 45(5), pp.1426-1445.

Mernild, S.H., Howat, I.M., Ahn, Y., Liston, G.E., Steffen, K., Jakobsen, B.H., Hasholt, B., Fog, B. and As, D.V., 2010. Freshwater flux to Sermilik Fjord, SE Greenland. *The Cryosphere*, 4(4), pp.453-465.

Miles, K.E., Willis, I.C., Benedek, C.L., Williamson, A.G. and Tedesco, M., 2017. Toward monitoring surface and subsurface lakes on the Greenland ice sheet using Sentinel-1 SAR and Landsat-8 OLI imagery. *Frontiers in Earth Science*, 5, p.58.

Møller, P.R., Nielsen, J.G. and Fossen, I., 2003. Patagonian toothfish found off Greenland. *Nature*, 421(6923), pp.599-599.

Moon, T., Joughin, I. and Smith, B., 2015. Seasonal to multiyear variability of glacier surface velocity, terminus position, and sea ice/ice mélange in northwest Greenland. *Journal of Geophysical Research: Earth Surface*, 120(5), pp.818-833.

Moon, T., Joughin, I., Smith, B. and Howat, I., 2012. 21st-century evolution of Greenland outlet glacier velocities. *Science*, 336(6081), pp.576-578.

Moon, T., Joughin, I., Smith, B., Van Den Broeke, M.R., Van De Berg, W.J., Noël, B. and Usher, M., 2014. Distinct patterns of seasonal Greenland glacier velocity. *Geophysical research letters*, 41(20), pp.7209-7216.

Moon, T., Sutherland, D.A., Carroll, D., Felikson, D., Kehrl, L. and Straneo, F., 2018. Subsurface iceberg melt key to Greenland fjord freshwater budget. *Nature Geoscience*, 11(1), pp.49-54.

Morlighem, M., Bondzio, J., Seroussi, H., Rignot, E., Larour, E., Humbert, A. and Rebuffi, S., 2016. Modeling of Store Gletscher's calving dynamics, West Greenland, in response to ocean thermal forcing. *Geophysical Research Letters*, 43(6), pp.2659-2666.

Morlighem, M., Williams, C.N., Rignot, E., An, L., Arndt, J.E., Bamber, J.L., Catania, G., Chauché, N., Dowdeswell, J.A., Dorschel, B. and Fenty, I., 2017. BedMachine v3: Complete bed topography and ocean bathymetry mapping of Greenland from multibeam echo sounding combined with mass conservation. *Geophysical research letters*, 44(21), pp.11-051.

Mortensen, J., Rysgaard, S., Bendtsen, J., Lennert, K., Kanzow, T., Lund, H. and Meire, L., 2020. Subglacial discharge and its down-fjord transformation in West Greenland fjords with an ice mélange. *Journal of Geophysical Research: Oceans*, 125(9), p.e2020JC016301.

Motyka, R.J., Dryer, W.P., Amundson, J., Truffer, M. and Fahnestock, M., 2013. Rapid submarine melting driven by subglacial discharge, LeConte Glacier, Alaska. *Geophysical Research Letters*, 40(19), pp.5153-5158.

Motyka, R.J., Hunter, L., Echelmeyer, K.A. and Connor, C., 2003. Submarine melting at the terminus of a temperate tidewater glacier, LeConte Glacier, Alaska, USA. *Annals of Glaciology*, 36, pp.57-65.

Motyka, R.J., Truffer, M., Fahnestock, M., Mortensen, J., Rysgaard, S. and Howat, I., 2011. Submarine melting of the 1985 Jakobshavn Isbræ floating tongue and the triggering of the current retreat. *Journal of Geophysical Research: Earth Surface*, 116(F1).

Mouginot, J., Rignot, E., Bjørk, A.A., Van den Broeke, M., Millan, R., Morlighem, M., Noël, B., Scheuchl, B. and Wood, M., 2019. Forty-six years of Greenland Ice Sheet mass balance from 1972 to 2018. *Proceedings of the national academy of sciences*, 116(19), pp.9239-9244.

Mouginot, Jeremie; Rignot, Eric (2019), Glacier catchments/basins for the Greenland Ice Sheet, Dryad, Dataset, https://doi.org/10.7280/D1WT11

Moyer, A.N., Sutherland, D.A., Nienow, P.W. and Sole, A.J., 2019. Seasonal variations in iceberg freshwater flux in Sermilik Fjord, southeast Greenland from Sentinel-2 imagery. *Geophysical Research Letters*, 46(15), pp.8903-8912.

Nachtsheim, D.A., Joiris, C.R. and D'Hert, D., 2016. A gravel-covered iceberg provides an offshore breeding site for ivory gulls Pagophila eburnea off Northeast Greenland. *Polar Biology*, 39(4), pp.755-758.

Neff, W., Compo, G.P., Martin Ralph, F. and Shupe, M.D., 2014. Continental heat anomalies and the extreme melting of the Greenland ice surface in 2012 and 1889. *Journal of Geophysical Research: Atmospheres*, 119(11), pp.6520-6536.

Neuhaus, S.U., Tulaczyk, S.M. and Branecky Begeman, C., 2019. Spatiotemporal distributions of icebergs in a temperate fjord: Columbia Fjord, Alaska. *The Cryosphere*, 13(7), pp.1785-1799.

Nghiem, S.V., Hall, D.K., Mote, T.L., Tedesco, M., Albert, M.R., Keegan, K., Shuman, C.A., DiGirolamo, N.E. and Neumann, G., 2012. The extreme melt across the Greenland ice sheet in 2012. *Geophysical Research Letters*, 39(20).

Nick, F.M., Van der Veen, C.J., Vieli, A. and Benn, D.I., 2010. A physically based calving model applied to marine outlet glaciers and implications for the glacier dynamics. *Journal of Glaciology*, 56(199), pp.781-794.

Nick, F.M., Vieli, A., Howat, I.M. and Joughin, I., 2009. Large-scale changes in Greenland outlet glacier dynamics triggered at the terminus. *Nature Geoscience*, 2(2), pp.110-114.

Nielsen, J., Rosing-Asvid, A., Meire, L. and Nygaard, R., 2020. Widespread occurrence of pink salmon (Oncorhynchus gorbuscha) throughout Greenland coastal waters. *Journal of Fish Biology*, 96(6), pp.1505-1507.

Nolin, A.W., Fetterer, F.M. and Scambos, T.A., 2002. Surface roughness characterizations of sea ice and ice sheets: Case studies with MISR data. *IEEE transactions on Geoscience and Remote Sensing*, 40(7), pp.1605-1615.

Normandeau, A., MacKillop, K., Macquarrie, M., Richards, C., Bourgault, D., Campbell, D.C., Maselli, V., Philibert, G. and Clarke, J.H., 2021. Submarine landslides triggered by iceberg collision with the seafloor. *Nature Geoscience*, 14(8), pp.599-605.

Ohashi, Y., Aoki, S., Matsumura, Y., Sugiyama, S., Kanna, N. and Sakakibara, D., 2020. Vertical distribution of water mass properties under the influence of subglacial discharge in Bowdoin Fjord, northwestern Greenland. *Ocean Science*, 16(3), pp.545-564.

O'Leary, M. and Christoffersen, P., 2013. Calving on tidewater glaciers amplified by submarine frontal melting. *The Cryosphere*, 7(1), pp.119-128.

Pearce, D.M., Mair, D.W., Rea, B.R., Lea, J.M., Schofield, J.E., Kamenos, N. and Schoenrock, K., 2018. The glacial geomorphology of upper Godthåbsfjord (Nuup Kangerlua) in southwest Greenland. *Journal of Maps*, 14(2), pp.45-55.

Podolskiy, E.A., Murai, Y., Kanna, N. and Sugiyama, S., 2022. Glacial earthquake-generating iceberg calving in a narwhal summering ground: The loudest underwater sound in the Arctic?. *The Journal of the Acoustical Society of America*, 151(1), pp.6-16.

Pollard, R.T., Salter, I., Sanders, R.J., Lucas, M.I., Moore, C.M., Mills, R.A., Statham, P.J., Allen, J.T., Baker, A.R., Bakker, D.C. and Charette, M.A., 2009. Southern Ocean deep-water carbon export enhanced by natural iron fertilization. *Nature*, 457(7229), pp.577-580.

Pope, A., Scambos, T.A., Moussavi, M., Tedesco, M., Willis, M., Shean, D. and Grigsby, S., 2016. Estimating supraglacial lake depth in West Greenland using Landsat 8 and comparison with other multispectral methods. *The Cryosphere*, 10(1), pp.15-27.

Porter, Claire; Morin, Paul; Howat, Ian; Noh, Myoung-Jon; Bates, Brian; Peterman, Kenneth; Keesey, Scott; Schlenk, Matthew; Gardiner, Judith; Tomko, Karen; Willis, Michael; Kelleher, Cole; Cloutier, Michael; Husby, Eric; Foga, Steven; Nakamura, Hitomi; Platson, Melisa; Wethington, Michael, Jr.; Williamson, Cathleen; Bauer, Gregory; Enos, Jeremy; Arnold, Galen; Kramer, William; Becker, Peter; Doshi, Abhijit; D'Souza, Cristelle; Cummens, Pat; Laurier, Fabien; Bojesen, Mikkel. https://doi.org/10.7910/DVN/OHHUKH, Harvard Dataverse, V1, 2018.

Porter, D.F., Tinto, K.J., Boghosian, A., Cochran, J.R., Bell, R.E., Manizade, S.S. and Sonntag, J.G., 2014. Bathymetric control of tidewater glacier mass loss in northwest Greenland. *Earth and Planetary Science Letters*, 401, pp.40-46.

Puliti, S., Hauglin, M., Breidenbach, J., Montesano, P., Neigh, C.S.R., Rahlf, J., Solberg, S., Klingenberg, T.F. and Astrup, R., 2020. Modelling above-ground biomass stock over Norway using national forest inventory data with ArcticDEM and Sentinel-2 data. *Remote Sensing of Environment*, 236, p.111501.

Raiswell, R., Benning, L.G., Tranter, M. and Tulaczyk, S., 2008. Bioavailable iron in the Southern Ocean: the significance of the iceberg conveyor belt. *Geochemical transactions*, 9(1), pp.1-9.

Rezvanbehbahani, S., Stearns, L.A., Keramati, R., Shankar, S. and van der Veen, C.J., 2020. Significant contribution of small icebergs to the freshwater budget in Greenland fjords. *Communications earth & environment*, 1(1), pp.1-7.

Rhodes, R.H., Brook, E.J., Chiang, J.C., Blunier, T., Maselli, O.J., McConnell, J.R., Romanini, D. and Severinghaus, J.P., 2015. Enhanced tropical methane production in response to iceberg discharge in the North Atlantic. *Science*, 348(6238), pp.1016-1019.

Rignot, E., Fenty, I., Xu, Y., Cai, C. and Kemp, C., 2015. Undercutting of marine-terminating glaciers in West Greenland. *Geophysical Research Letters*, 42(14), pp.5909-5917.

Rignot, E., Koppes, M. and Velicogna, I., 2010. Rapid submarine melting of the calving faces of West Greenland glaciers. *Nature Geoscience*, 3(3), pp.187-191.

Rignot, E., Mouginot, J., Morlighem, M., Seroussi, H. and Scheuchl, B., 2014. Widespread, rapid grounding line retreat of Pine Island, Thwaites, Smith, and Kohler glaciers, West Antarctica, from 1992 to 2011. *Geophysical Research Letters*, 41(10), pp.3502-3509.

Robel, A.A., Pegler, S.S., Catania, G., Felikson, D. and Simkins, L.M., 2022. Ambiguous stability of glaciers at bed peaks. *Journal of Glaciology*, 68(272), pp.1177-1184.

Rosenau, R., Schwalbe, E., Maas, H.G., Baessler, M. and Dietrich, R., 2013. Grounding line migration and high-resolution calving dynamics of Jakobshavn Isbræ, West Greenland. *Journal of Geophysical Research: Earth Surface*, 118(2), pp.382-395.

Ryan, J.C., Hubbard, A.L., Box, J.E., Todd, J., Christoffersen, P., Carr, J.R., Holt, T.O. and Snooke, N., 2015. UAV photogrammetry and structure from motion to assess calving dynamics at Store Glacier, a large outlet draining the Greenland ice sheet. *The Cryosphere*, 9(1), pp.1-11.

Scaramuzza, P. and Barsi, J., 2005, October. Landsat 7 scan line corrector-off gap-filled product development. In *Proceeding of Pecora*, 16, pp. 23-27.

Scheick, J., Enderlin, E.M. and Hamilton, G., 2019. Semi-automated open water iceberg detection from Landsat applied to Disko Bay, West Greenland. *Journal of Glaciology*, 65(251), pp.468-480.

Schild, K.M., Sutherland, D.A., Elosegui, P. and Duncan, D., 2021. Measurements of iceberg melt rates using high-resolution GPS and iceberg surface scans. *Geophysical Research Letters*, 48(3), p.e2020GL089765.

Schild, K.M., Hawley, R.L. and Morriss, B.F., 2016. Subglacial hydrology at Rink Isbræ, West Greenland inferred from sediment plume appearance. *Annals of Glaciology*, 57(72), pp.118-127.

Schlemm, T. and Levermann, A., 2019. A simple stress-based cliff-calving law. *The Cryosphere*, 13(9), pp.2475-2488.

Schoof, C., 2007. Ice sheet grounding line dynamics: Steady states, stability, and hysteresis. *Journal of Geophysical Research: Earth Surface*, 112(F3).

Schröder, L., Neckel, N., Zindler, R. and Humbert, A., 2020. Perennial supraglacial lakes in Northeast Greenland observed by polarimetric SAR. *Remote Sensing*, 12(17), p.2798.

Seale, A., Christoffersen, P., Mugford, R.I. and O'Leary, M., 2011. Ocean forcing of the Greenland Ice Sheet: Calving fronts and patterns of retreat identified by automatic satellite monitoring of eastern outlet glaciers. *Journal of Geophysical Research: Earth Surface*, 116(F3).

Seifert, M., Hoppema, M., Burau, C., Elmer, C., Friedrichs, A., Geuer, J.K., John, U., Kanzow, T., Koch, B.P., Konrad, C. and Van der Jagt, H., 2019. Influence of glacial meltwater on summer biogeochemical cycles in Scoresby Sund, East Greenland. *Frontiers in Marine Science*, 6, p.412.

Sergienko, O.V., 2013. Glaciological twins: basally controlled subglacial and supraglacial lakes. *Journal of Glaciology*, 59(213), pp.3-8.

Seroussi, H., Nakayama, Y., Larour, E., Menemenlis, D., Morlighem, M., Rignot, E. and Khazendar, A., 2017. Continued retreat of Thwaites Glacier, West Antarctica, controlled by bed topography and ocean circulation. *Geophysical Research Letters*, 44(12), pp.6191-6199.

Shaw, T.J., Raiswell, R., Hexel, C.R., Vu, H.P., Moore, W.S., Dudgeon, R. and Smith Jr, K.L., 2011. Input, composition, and potential impact of terrigenous material from free-drifting icebergs in the Weddell Sea. *Deep Sea Research Part II: Topical Studies in Oceanography*, 58(11-12), pp.1376-1383.

Shepherd, A., Ivins, E., Rignot, E., Smith, B., Van Den Broeke, M., Velicogna, I., Whitehouse, P., Briggs, K., Joughin, I., Krinner, G. and Nowicki, S., 2020. Mass balance of the Greenland Ice Sheet from 1992 to 2018. *Nature*, 579(7798), pp.233-239.

Shiggins, C.J., Lea, J.M. and Brough, S., 2023. Automated ArcticDEM iceberg detection tool: insights into area and volume distributions, and their potential application to satellite imagery and modelling of glacier–iceberg–ocean systems. *The Cryosphere*, 17(1), pp.15-32.

Shugar, D.H., Burr, A., Haritashya, U.K., Kargel, J.S., Watson, C.S., Kennedy, M.C., Bevington, A.R., Betts, R.A., Harrison, S. and Strattman, K., 2020. Rapid worldwide growth of glacial lakes since 1990. *Nature Climate Change*, 10(10), pp.939-945.

Slater, D.A. and Straneo, F., 2022. Submarine melting of glaciers in Greenland amplified by atmospheric warming. *Nature Geoscience*, 15(10), pp.794-799.

Slater, D.A., Nienow, P.W., Cowton, T.R., Goldberg, D.N. and Sole, A.J., 2015. Effect of near-terminus subglacial hydrology on tidewater glacier submarine melt rates. *Geophysical Research Letters*, 42(8), pp.2861-2868.

Smith Jr, K.L., Sherman, A.D., Shaw, T.J. and Sprintall, J., 2013. Icebergs as unique Lagrangian ecosystems in polar seas. *Annual review of marine science*, 5, pp.269-287.

Smith, S.D., 1993. Hindcasting iceberg drift using current profiles and winds. *Cold regions science and technology*, 22(1), pp.33-45.

Smith, W.D., Dunning, S.A., Brough, S., Ross, N. and Telling, J., 2020. GERALDINE (Google Earth Engine supRaglAciaL Debris INput dEtector): a new tool for identifying and monitoring supraglacial landslide inputs. *Earth Surface Dynamics*, 8(4), pp.1053-1065.

Snoeckx, H., Grousset, F., Revel, M. and Boelaert, A., 1999. European contribution of ice-rafted sand to Heinrich layers H3 and H4. *Marine Geology*, 158(1-4), pp.197-208.

Soldal, I.H., Dierking, W., Korosov, A. and Marino, A., 2019. Automatic detection of small icebergs in fast ice using satellite wide-swath SAR images. *Remote Sensing*, 11(7), p.806.

Stern, A.A., Adcroft, A., Sergienko, O. and Marques, G., 2017. Modeling tabular icebergs submerged in the ocean. *Journal of Advances in Modeling Earth Systems*, 9(4), pp.1948-1972.

Straneo, F. and Heimbach, P., 2013. North Atlantic warming and the retreat of Greenland's outlet glaciers. *Nature*, 504(7478), pp.36-43.

Straneo, F., Slater, D.A., Bouchard, C., Cape, M.R., Carey, M., Ciannelli, L., Holte, J., Matrai, P., Laidre, K., Little, C. and Meire, L., 2022. An Interdisciplinary Perspective on Greenland's Changing Coastal Margins. *Oceanography*, 35(3/4), pp.106-117.

Straneo, F., Sutherland, D.A., Holland, D., Gladish, C., Hamilton, G.S., Johnson, H.L., Rignot, E., Xu, Y. and Koppes, M., 2012. Characteristics of ocean waters reaching Greenland's glaciers. *Annals of Glaciology*, 53(60), pp.202-210.

Stríkis, N.M., Cruz, F.W., Barreto, E.A., Naughton, F., Vuille, M., Cheng, H., Voelker, A.H., Zhang, H., Karmann, I., Edwards, R.L. and Auler, A.S., 2018. South American monsoon response to iceberg discharge in the North Atlantic. *Proceedings of the National Academy of Sciences*, 115(15), pp.3788-3793.

Stroeve, J. and Notz, D., 2018. Changing state of Arctic sea ice across all seasons. *Environmental Research Letters*, 13(10).

Stuecker, M.F., Bitz, C.M., Armour, K.C., Proistosescu, C., Kang, S.M., Xie, S.P., Kim, D., McGregor, S., Zhang, W., Zhao, S. and Cai, W., 2018. Polar amplification dominated by local forcing and feedbacks. *Nature Climate Change*, 8(12), pp.1076-1081.

Sugiyama, S., Kanna, N., Sakakibara, D., Ando, T., Asaji, I., Kondo, K., Wang, Y., Fujishi, Y., Fukumoto, S., Podolskiy, E. and Fukamachi, Y., 2021. Rapidly changing glaciers, ocean and coastal environments, and their impact on human society in the Qaanaaq region, northwestern Greenland. *Polar Science*, 27, p.100632.

Sulak, D.J., Sutherland, D.A., Enderlin, E.M., Stearns, L.A. and Hamilton, G.S., 2017. Iceberg properties and distributions in three Greenlandic fjords using satellite imagery. *Annals of Glaciology*, 58(74), pp.92-106.

Sundal, A.V., Shepherd, A., Nienow, P., Hanna, E., Palmer, S. and Huybrechts, P., 2009. Evolution of supra-glacial lakes across the Greenland Ice Sheet. *Remote Sensing of Environment*, 113(10), pp.2164-2171.

Sutherland, D.A., Jackson, R.H., Kienholz, C., Amundson, J.M., Dryer, W.P., Duncan, D., Eidam, E.F., Motyka, R.J. and Nash, J.D., 2019. Direct observations of submarine melt and subsurface geometry at a tidewater glacier. *Science*, 365(6451), pp.369-374.

Sutherland, D.A., Roth, G.E., Hamilton, G.S., Mernild, S.H., Stearns, L.A. and Straneo, F., 2014. Quantifying flow regimes in a Greenland glacial fjord using iceberg drifters. *Geophysical Research Letters*, 41(23), pp.8411-8420.

Taarup-Esbensen, J. and Gudmestad, O.T., 2022. Arctic supply chain reliability in Baffin Bay and Greenland. *Polar Geography*, 45(2), pp.77-100.

The Guardian., 2018. Huge iceberg threatens tiny Greenland village. Online: https://www.theguardian.com/world/2018/jul/14/huge-iceberg-threatens-village-in-greenland. Last accessed: 21st September 2021.

The IMBIE Team, 2020. Mass balance of the Greenland Ice Sheet from 1992 to 2018. *Nature*, 579(7798), pp.233-239.

Todd, J. and Christoffersen, P., 2014. Are seasonal calving dynamics forced by buttressing from ice mélange or undercutting by melting? Outcomes from full-Stokes simulations of Store Glacier, West Greenland. *The Cryosphere*, *8*(6), pp.2353-2365.

Tournadre, J., Bouhier, N., Girard-Ardhuin, F. and Rémy, F., 2016. Antarctic icebergs distributions 1992–2014. *Journal of Geophysical Research: Oceans*, 121(1), pp.327-349.

Van As, D., Andersen, M.L., Petersen, D., Fettweis, X., Van Angelen, J.H., Lenaerts, J.T., Van Den Broeke, M.R., Lea, J.M., Bøggild, C.E., Ahlstrøm, A.P. and Steffen, K., 2014. Increasing meltwater discharge from the Nuuk region of the Greenland ice sheet and implications for mass balance (1960–2012). *Journal of Glaciology*, 60(220), pp.314-322.

van den Broeke, M.R., Enderlin, E.M., Howat, I.M., Kuipers Munneke, P., Noël, B.P., Van De Berg, W.J., Van Meijgaard, E. and Wouters, B., 2016. On the recent contribution of the Greenland ice sheet to sea level change. *The Cryosphere*, 10(5), pp.1933-1946.

Van der Veen, C.J., 1996. Tidewater calving. *Journal of Glaciology*, 42(141), pp.375-385.

Vieli, A., Funk, M. and Blatter, H., 2001. Flow dynamics of tidewater glaciers: a numerical modelling approach. *Journal of Glaciology*, 47(159), pp.595-606.

Vos, K., Harley, M.D., Splinter, K.D., Simmons, J.A. and Turner, I.L., 2019. Sub-annual to multi-decadal shoreline variability from publicly available satellite imagery. *Coastal Engineering*, 150, pp.160-174.

Wagner, T.J., Stern, A.A., Dell, R.W. and Eisenman, I., 2017. On the representation of capsizing in iceberg models. *Ocean Modelling*, 117, pp.88-96.

Walter, F., Amundson, J.M., O'Neel, S., Truffer, M., Fahnestock, M. and Fricker, H.A., 2012. Analysis of low-frequency seismic signals generated during a multiple-iceberg calving event at Jakobshavn Isbræ, Greenland. *Journal of Geophysical Research: Earth Surface*, 117(F1).

Wang, X., Xiao, X., Zou, Z., Hou, L., Qin, Y., Dong, J., Doughty, R.B., Chen, B., Zhang, X., Chen, Y. and Ma, J., 2020. Mapping coastal wetlands of China using time series Landsat images in 2018 and Google Earth Engine. *ISPRS Journal of Photogrammetry and Remote Sensing*, 163, pp.312-326.

Weeks, W.F. and Mellor, M., 1978. Some elements of iceberg technology. In *Iceberg utilization* (pp. 45-98). Pergamon.

Wehrlé, A., Lüthi, M.P. and Vieli, A., 2023. The control of short-term ice mélange weakening episodes on calving activity at major Greenland outlet glaciers. *The Cryosphere*, 17(1), pp.309-326.

Weidick, A., Bennike, O., Citterio, M. and Nørgaard-Pedersen, N., 2012. Neoglacial and historical glacier changes around Kangersuneq fjord in southern West Greenland. *GEUS Bulletin*, 27, pp.1-68.

Wharton Jr, R.A., McKay, C.P., Simmons Jr, G.M. and Parker, B.C., 1985. Cryoconite holes on glaciers. *BioScience*, pp.499-503.

Williams, J.J., Gourmelen, N. and Nienow, P., 2021. Complex multi-decadal ice dynamical change inland of marine-terminating glaciers on the Greenland Ice Sheet. *Journal of Glaciology*, *67*(265), pp.833-846.

.

Wolper, J., Gao, M., Lüthi, M.P., Heller, V., Vieli, A., Jiang, C. and Gaume, J., 2021. A glacier–ocean interaction model for tsunami genesis due to iceberg calving. *Communications Earth & Environment*, 2(1), pp.1-10.

Wood, M., Rignot, E., Fenty, I., An, L., Bjørk, A., van den Broeke, M., Cai, C., Kane, E., Menemenlis, D., Millan, R. and Morlighem, M., 2021. Ocean forcing drives glacier retreat in Greenland. *Science advances*, 7(1).

Wood, M., Rignot, E., Fenty, I., Menemenlis, D., Millan, R., Morlighem, M., Mouginot, J. and Seroussi, H., 2018. Ocean-induced melt triggers glacier retreat in Northwest Greenland. *Geophysical Research Letters*, 45(16), pp.8334-8342.

Wood-Donnelly, C., 2022. Iceberg sovereignty. *Marine Policy*, *143*, p.105139.

Wu, S.Y. and Hou, S., 2017. Impact of icebergs on net primary productivity in the Southern Ocean. *The Cryosphere*, 11(2), pp.707-722.

Xu, Y., Rignot, E., Menemenlis, D. and Koppes, M., 2012. Numerical experiments on subaqueous melting of Greenland tidewater glaciers in response to ocean warming and enhanced subglacial discharge. *Annals of Glaciology*, 53(60), pp.229-234.

Yang, K., Smith, L.C., Cooper, M.G., Pitcher, L.H., Van As, D., Lu, Y., Lu, X. and Li, M., 2021. Seasonal evolution of supraglacial lakes and rivers on the southwest Greenland Ice Sheet. *Journal of Glaciology*, 67(264), pp.592-602.

Yulmetov, R., Marchenko, A. and Løset, S., 2016. Iceberg and sea ice drift tracking and analysis off north-east Greenland. *Ocean Engineering*, 123, pp.223-237.

Zakharov, M., Gadal, S., Kamičaitytė, J., Cherosov, M. and Troeva, E., 2022. Distribution and Structure Analysis of Mountain Permafrost Landscape in Orulgan Ridge (Northeast Siberia) Using Google Earth Engine. *Land*, 11(8), p.1187.

Zwally, H.J., Abdalati, W., Herring, T., Larson, K., Saba, J. and Steffen, K., 2002. Surface melt-induced acceleration of Greenland ice-sheet flow. *Science*, 297(5579), pp.218-222.

Appendices

Supplementary material for Chapter 4

Figure S1. Example of an automated histogram calculated within GEE of elevation pixel count in an ArcticDEM image at KNS (2013-07-04). The elevation with the highest pixel count is automatically selected as the sea level for that scene. In this example sea level would be 33.25 m.

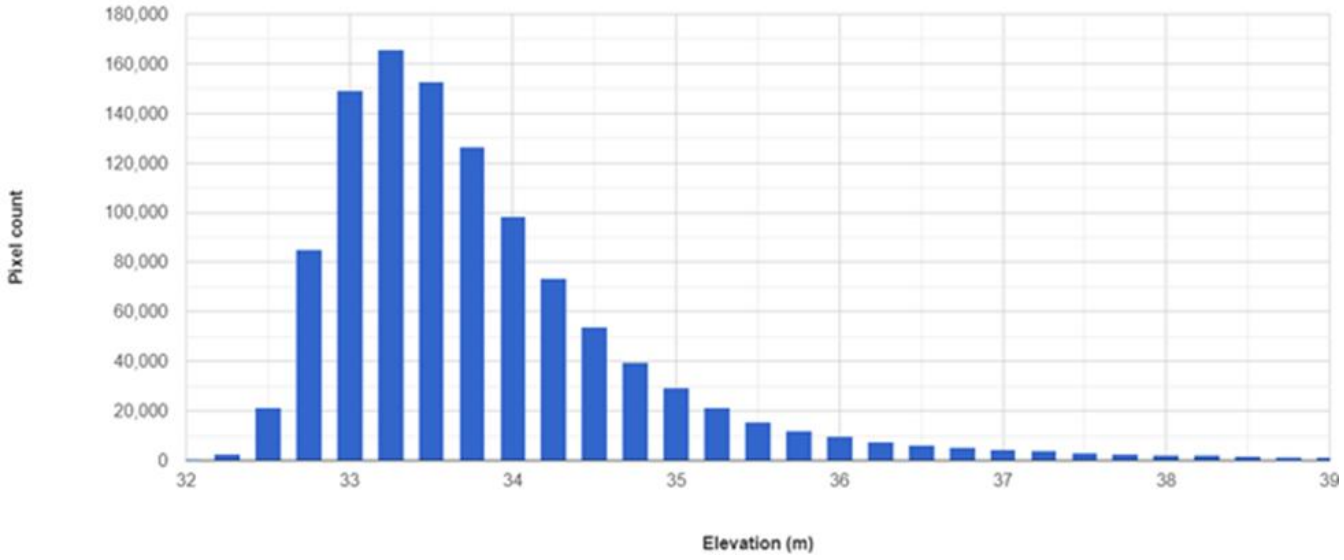

Figure S2. Google Earth Engine ArcticDEM v3 strip data availability (July-October) for Greenland's calving margins and all marine/lake/shelf terminating glaciers extent in the remainder of the Arctic.

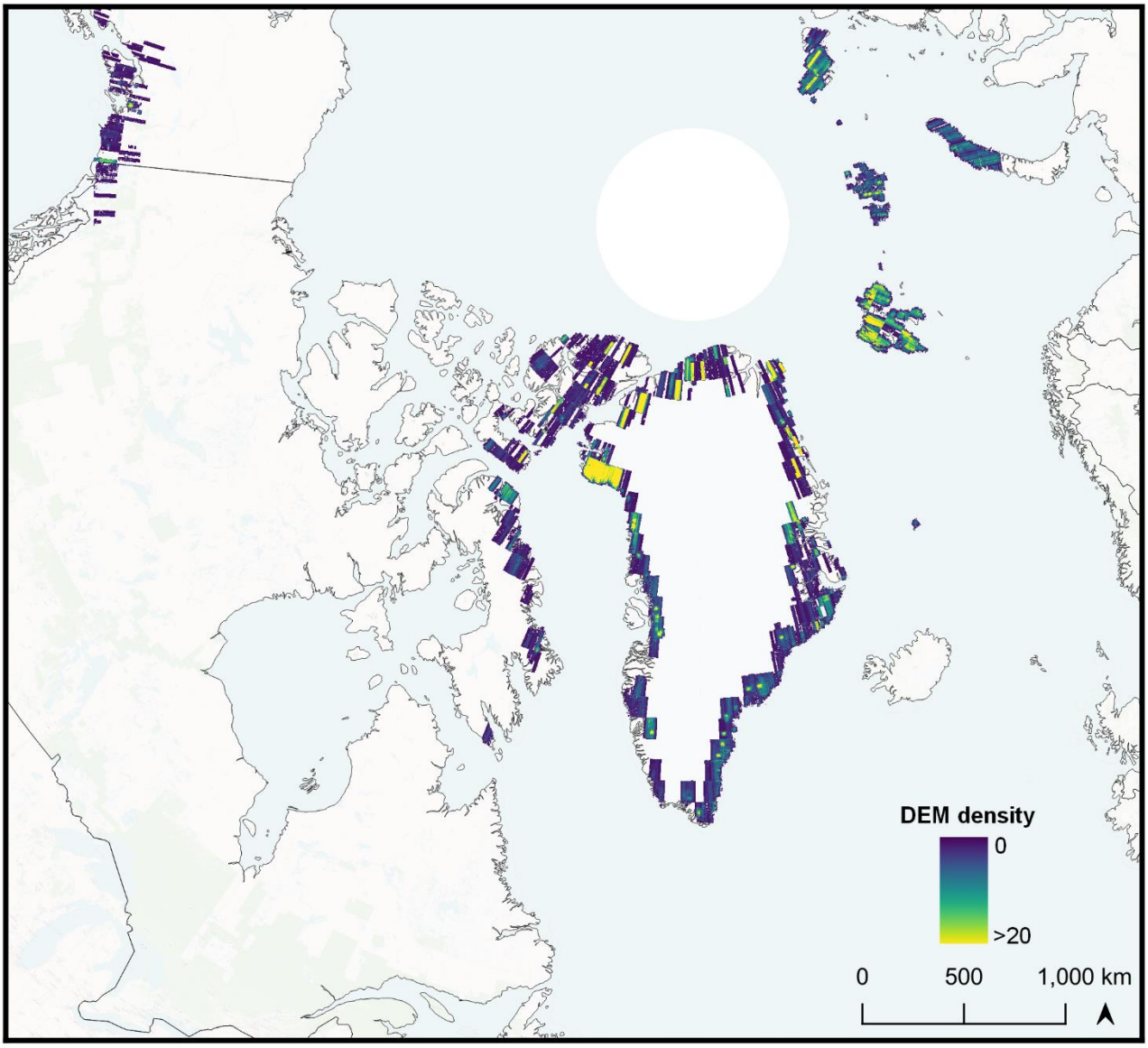

Supplementary material for Chapter 5

Figure S3. Example of the automated ROI construction with the filtering of the closest terminus trace by date (shown by the black line) overlaying the clipped ArcticDEM tile for automated iceberg detection at KNS.

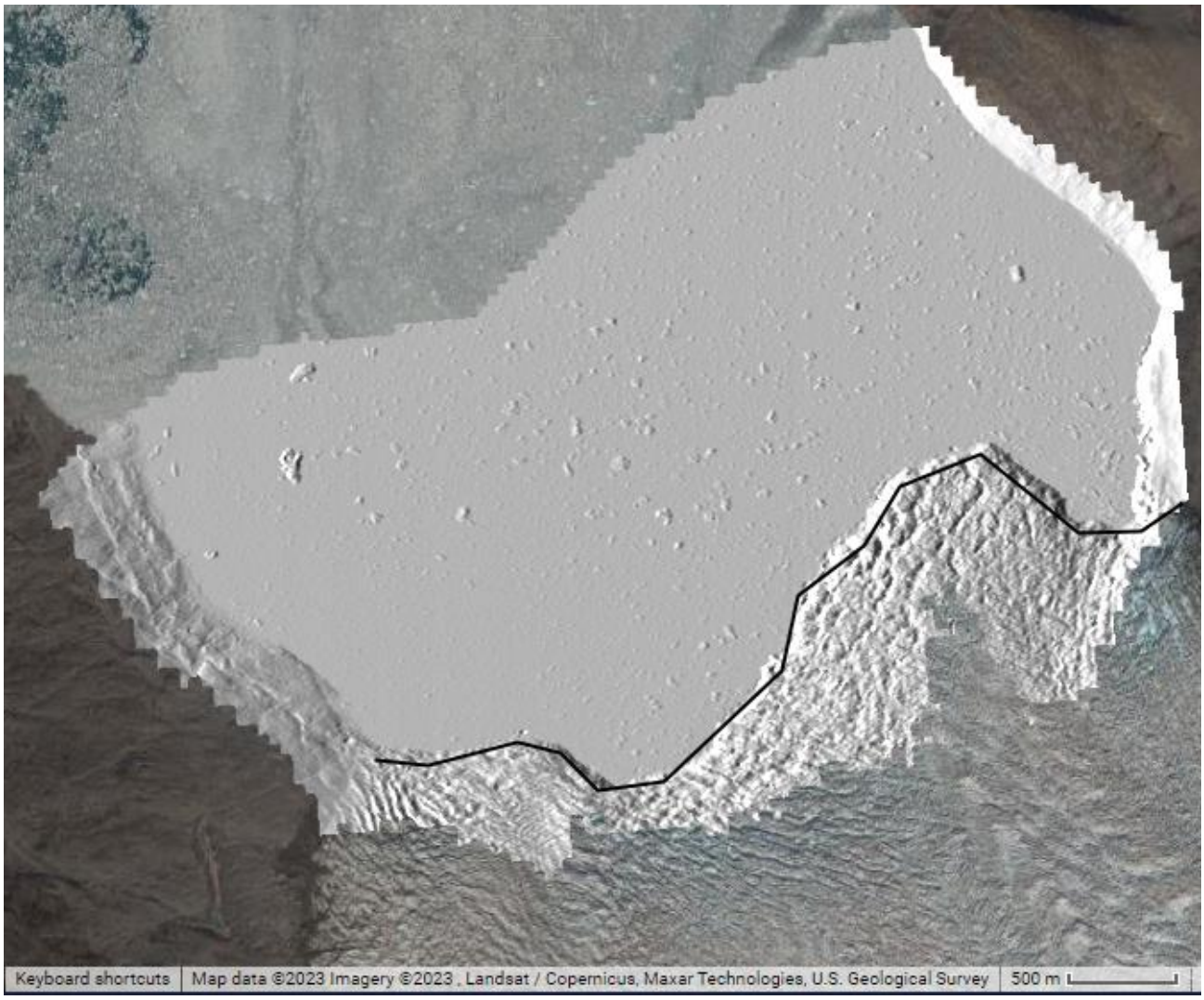

Figure S4. Total iceberg volume percentage for icebergs exceeding 10,000 m^3 for each glacier when compared to their respective mean discharge (Q), width (W) averaged Q, maximum terminus depth (D) averaged Q, mean D averaged Q and median D averaged Q.

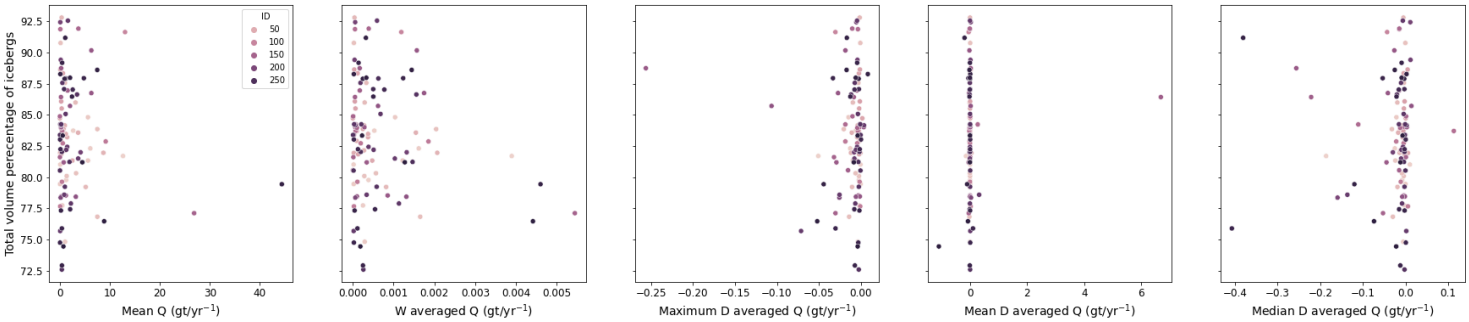

Figure S5. Total iceberg volume percentage for icebergs less than 10,000 m^3 for each glacier when compared to their respective mean discharge (Q), width (W) averaged Q, maximum terminus depth (D) averaged Q, mean D averaged Q and median D averaged Q.